Cold Spray Characteristics of Mixed 316L Stainless Steel and Commercial Purity Fe Powders

Xin Chu

Department of Mining and Materials Engineering,

McGill University, Montreal

December 2019

A thesis submitted to McGill University in partial fulfilment of the requirements of the degree of Doctor of Philosophy

Abstract

Some of the current trends in cold spray include the production of metal-metal composite coatings. Among the various strategies to prepare the composite feedstock, e.g. agglomerate-sintering, mechanically milling and coated/cladded feedstock, mixing metal powders (either by premixing or using dual feeder) is a straightforward method and is convenient to vary the mixture composition. However, it has been found to be difficult to predict the cold spray characteristics of mixed powders (e.g. deposition efficiency (DE), porosity and compositional yield) from those of the single component powders, which means that any new mixtures need to undergo extensive preliminary cold spray trials in order to optimize the process parameters. Thus, fundamentally, analyzing the cold spray characteristics of two metal powders will lead to accurate modeling of the process and minimize the cold spray trials required to optimize the process. This thesis aims to develop a better understanding of the effects of mixing powders on the cold spray characteristics of 316L/Fe mixed powders.

Single component 316L and Fe powders were deposited by cold spray, as well as the mixed 316L/Fe powders with a dual feeder setup. The as-sprayed coatings were also polished and single 316L and Fe particles were deposited on the as-polished coatings to form splats. To understand the splat deposition behavior of different impact scenarios (i.e. 316L on 316L, 316L on Fe, Fe on 316L, Fe on Fe), metrics of splat deformation, substrate deformation, splat adhesion strength/energy, and splat rebound were characterized. With a better understanding of the splat deposition behavior, efforts were made to explain the cold spray characteristics of bimodal size 316L/Fe powder mixtures. Since the finding suggests that the feedstock particle size could also be influential of the mixed powders deposition characteristics, different size combinations of 316L/Fe mixtures were deposited and studied.

Results show that the splat deposition behavior onto as-polished coatings is indicative of the feedstock deposition behavior during composite coating formation. In particular, the 316L on Fe impact scenario generates strong rebound/poor deposition; whereas the reverse scenario Fe on 316L leads to excellent deposition. The distinct deposition behaviors of different impact sequences between 316L and Fe were explained through the relative particle/substrate hardness, surface oxide thickness, and particle morphology. Besides, results also show the cold spray characteristics of bimodal size 316L/Fe mixtures exhibit unexpected variations with increasing feedstock Fe fractions, which reveals the contributions of various mechanisms during mixed powders deposition: mixed 316L/Fe impact interfaces, particle size difference, and tamping. Finally, the DEs of different sizes of 316L/Fe mixtures show different variations with increasing feedstock 316L fractions, which is due to particle-particle interactions (i.e. tamping and retention) only occur in small size feedstocks during cold spray.

Résumé

Dans le domaine de la projection à froid, certaines tendances actuelles incluent la production de revêtements de composites métal-métal. Parmi les diverses stratégies de préparation des poudres, comme par exemple l'agglomération et le frittage, le moulinage ou encore l'enrobage de poudres, le mélange de poudres métalliques (soit par mélangeage au préalable ou au moyen d'une double-alimentation) est un moyen simple et efficace pour faire varier la composition d'un mélange. Cependant, il est difficile de prédire les caractéristiques des revêtements obtenus par des mélanges de poudres lors de la projection à froid (par exemple, l'efficacité de la déposition (ED), la porosité et les fractions relatives de poudres dans le revêtement) comparées aux caractéristiques des revêtements obtenus par des poudres avec une seule composante. Ceci indique que chaque nouveau mélange de poudres doit être soumis à une étude préliminaire approfondie afin d'optimiser les paramètres du processus de projection à froid. Ainsi, fondamentalement, analyser les caractéristiques de déposition de deux poudres métalliques mènera à une modélisation précise du processus et minimisera le nombre d'essais requis pour optimiser les paramètres. Cette thèse vise à développer une meilleure compréhension des effets du mélange de poudres sur les caractéristiques de projection à froid du mélange de poudres 316L/Fe.

De l'acier 316L et du Fe purs ont été projetés à froid, ainsi que le mélange de poudres 316L/Fe au moyen d'une double-alimentation. Les revêtements bruts ont aussi été polis et des particules individuelles d'acier 316L et de Fe ont été déposées sur les revêtements polis pour former des « splats ». Afin de comprendre le comportement de déposition des splats dans différents scénarios d'impact (i.e. 316L sur 316L, 316L sur Fe, Fe sur 316L et Fe sur Fe), les métriques de la déformation des splats, la déformation du substrat, l'énergie ainsi que la force d'adhésion des

splats et le rebond des splats ont été caractérisés. Avec une meilleure compréhension du comportement des splats, il a été possible d'expliquer les caractéristiques de projection à froid de mélanges de poudres de 316L/Fe avec des distributions de taille bimodales. Puisque la découverte suggère que la taille des poudres de départ pourrait aussi influencer les caractéristiques de déposition du mélange, différentes combinaisons de tailles de poudres de 316L/Fe ont été étudiées.

Les résultats montrent que le comportement des splats sur des revêtements polis est indicatif du comportement des poudres initiales lors de la formation du revêtement composite. En particulier, le scénario d'impact du 316L sur Fe génère de forts rebonds/une faible déposition, tandis que le scénario inverse (Fe sur 316L) mène à une excellente déposition. Les différents comportements observés dans les différents scénarios d'impact entre le 316L et le Fe ont été expliqué par la dureté relative des particules et du substrat, par l'épaisseur de la couche d'oxide et par la morphologie des particules. En parallèle, les résultats mettent aussi en avant que les caractéristiques de projection à froid de mélanges de 316L/Fe bimodaux présentent des variations inattendues lors de l'augmentation de la proportion de Fe dans le mélange initial, ce qui révèle la contribution de divers mécanismes pendant la phase de revêtement : mélange d'interfaces d'impact de 316L/Fe, différence de tailles de particules et bourrage (« tamping »). Enfin, les ED de mélanges de différentes tailles de 316L/Fe montrent différentes variations avec une augmentation de la fraction de 316L, ce qui est dû à des interactions entre particules (i.e. bourrage et rétention), et ne surviennent qu'avec des petites distributions pendant la projection à froid.

Acknowledgements

I would like to sincerely thank my supervisor, Prof. Stephen Yue, who is a person with true wisdom. He brought me into the field of cold spray, provided me a great extent of freedom in research, and offered invaluable advice leading to the completion of this project. This thesis would not have been possible without his support and unique insights. I have learnt several great qualities from him, which lead me to be a better researcher and a better person.

I would like to offer sincere gratitude to Dr. Phuong Vo from the National Research Council of Canada, Boucherville, for his tremendous help in cold spray experiments, discussions and comments on my results. I would like to thank all the colleagues in my group and other groups of the department for the technical help of my research. I acknowledge Prof. Jolanta-Ewa Sapieha and Dr. Thomas Schmitt from Dept. of Engineering Physics, Polytechnique Montréal, for the access and training of the micro-combi microscratch tester. I thank Mr. Andre Liberati for the French translation of the thesis abstract.

I acknowledge the Natural Sciences and Engineering Research Council (NSERC) and McGill Engineering Doctoral Award (MEDA) program for the financial assistance.

I would like to express special gratitude to my parents, Mr. Zhibin Chu and Mrs. Lezhen Chen, for their open-mindedness and endless love, which allow me to concentrate on research without any distractions. I would like to thank my girlfriend, Ms. Chaoyi Teng, for her warm company.

Contribution of Authors

This thesis is organized using a manuscript-based format, as per the thesis preparation guidelines published by McGill University (http://www.mcgill.ca/gps/thesis/guidelines). The following journal articles are included as Chapters 3, 4, 5 and 6 in this thesis, respectively.

1. Xin Chu*, Hanqing Che, Phuong Vo, Rohan Chakrabarty, Binhan Sun, Jun Song, Stephen Yue, "*Understanding the cold spray deposition efficiencies of 316L/Fe mixed powders by performing splat tests onto as-polished coatings*", Surf. Coat. Technol. 324 (2017), 353-360.
2. Xin Chu*, Rohan Chakrabarty, Hanqing Che, Lihong Shang, Phuong Vo, Jun Song, Stephen Yue, "*Investigation of the feedstock deposition behavior in a cold sprayed 316L/Fe composite coating*", Surf. Coat. Technol. 337 (2018), 53-62.
3. Xin Chu, Hanqing Che*, Chaoyi Teng, Phuong Vo, Stephen Yue, "*A multiple particle arrangement model to understand cold spray characteristics of bimodal size 316L/Fe powder mixtures*", Surf. Coat. Technol., 2019. (Accepted)
4. Xin Chu, Hanqing Che*, Chaoyi Teng, Phuong Vo, Stephen Yue, "*Understanding particle-particle interactions from deposition efficiencies in cold spray of mixed Fe/316L powders with different particle size combinations*", J. Therm. Spray Technol., 2019. (Accepted)

Contribution of Authors: Xin Chu created and developed the experiments, performed most of the experiments, analyzed the results and wrote all the manuscripts. Prof. Stephen Yue defined

the project and actively supervised the research. Dr. Hanqing Che helped in the design of cold spray experiments and discussions of the results of all the manuscripts. Rohan Chakrabarty performed the finite element modeling of single particle impacts in the submitted version of **Article 1** and the final version of **Article 2** under the supervision of Prof. Jun Song. Dr. Binhan Sun helped in the discussion of the results and provided comments for **Article 1**. Dr. Lihong Shang assisted in EDS analyses for **Article 2**. Chaoyi Teng helped in the design of the experiments and discussions of the results for **Article 3-4**. Dr. Phuong Vo from National Research Council of Canada, Boucherville, provided assistance in cold spray experiments and comments of all the manuscripts.

One additional journal article prepared during the Ph.D. study is to be submitted. It is relevant to this research but is not included as the main chapters. The abstract is provided in Appendix B, and the title is shown below:

- Xin Chu*, Huseyin Aydin, Phuong Vo, Stephen Yue, "*Effects of powder characteristics and mixing powders on the cold sprayability and corrosion properties of tantalum coatings*", to be submitted.

Table of Contents

List of Figures

List of Tables

Chapter 1

-

Introduction

1.1 Background

Cold spray is an emerging coating deposition technique in which micron-sized (e.g. 10-45 μm) particles are accelerated to supersonic velocities via high pressure gas stream through a de-Laval converging-diverging nozzle and are impacted on the substrate in the solid state [1.1]. Due to the low process temperature and protective gas atmosphere which minimize the undesired oxidation and/or chemical degradation of the feedstock, cold spray has become an excellent alternative to the conventional thermal spray methods for producing thermal-sensitive and low oxide content coatings [1.1].

Some of the current trends in cold spray include the production of metal-metal composite coatings [1.1-1.3]. Compared with other strategies to prepare the composite feedstock, e.g. agglomerate-sintering, mechanical milling, and coated/cladded feedstock, mixing metal powders (by either pre-mixing and dual feeding) is a straightforward approach and is convenient to vary the feedstock mixing composition [1.1, 1.2]. Apart from the ease in producing novel composites, mixing metal powders has been found to lead to beneficial effects in cold spray, e.g. reduced porosity and improved deposition efficiency (DE) [1.4-1.6].

However, fundamentally, there is still a great lack in understanding the cold spray deposition process of mixed metal powders. For instance, it is still a challenge to predict the cold spray characteristics (e.g. DE, porosity, compositional yield) of mixed metal powders from those

of the single component powders. This means that any new powder mixtures must undergo extensive preliminary cold spray trials in order to optimize the process parameters. Therefore, analyzing the cold spray characteristics of two metal powders is of significant research interest as it will lead to accurate modeling of the process and minimize the cold spray trials required to optimize the process.

1.2 Research objectives

In this study, mixed 316L stainless steel and commercial purity Fe powders were investigated as part of an overall effort to fabricate bio-degradable composite stents with controlled galvanic corrosion rates [1.7]. The objective of this research is to develop a better understanding of the effects of mixing powders on the cold spray characteristics of mixed 316L/Fe powders. The study specifically focuses on the following aspects:

- The correlation between the splat deposition behavior onto as-polished coatings and feedstock deposition behavior during composite coating formation.
- The governing factors of the splat deposition behavior of a single 316L and Fe particle onto as-polished 316L and Fe coatings.
- Cold spray characteristics of bimodal size 316L/Fe powder mixtures and the associated deposition mechanisms.
- The effects of the feedstock particle size on the deposition characteristics of 316L/Fe powder mixtures.

1.3 Thesis layout

This thesis follows the manuscript-based structure and consists of 8 chapters. **Chapter 1** introduces the background and objectives of the research. An extensive literature review and the state of the knowledge on cold spray are presented in **Chapter 2**; this includes (a) process overview and generic characteristics of cold spray technology; (b) fundamentals of cold spray: bonding mechanisms and cold sprayability; (c) introduction of mixed powders cold spray: benefits and challenges; (d) reasons for studying mixed 316L/Fe powders. **Chapter 3** concerns the correlation of the splat deposition behavior onto as-polished coatings and feedstock deposition behavior during composite coating formation. **Chapter 4** presents a detailed investigation of the governing factors of the splat deposition behavior of a single 316L and Fe particle onto as-polished 316L and Fe coatings. **Chapters 3 and 4** develop a better understanding of mixed 316L/Fe interfaces in cold sprayed 316L/Fe composite coatings. **Chapter 5** focuses on understanding the deposition mechanisms associated with the cold spray of bimodal size 316L/Fe powder mixtures. The results in this chapter introduce a new perspective of understanding the mixed metal powders deposition process. **Chapter 6** focuses on the effects of the feedstock particle size on the deposition characteristics of mixed 316L/Fe powders in cold spray. The effects and characteristics of particle-particle interactions in cold spray of mixed 316L/Fe powders are proposed in this chapter. **Chapter 7** provides the major conclusions of the research and an outlook for future work is proposed. **Chapter 8** presents the contributions of this thesis to the original knowledge.

1.4 References

[1.1] S. Grigoriev, A. Okunkova, A. Sova, P. Bertrand, I. Smurov, Cold spraying: from process fundamentals towards advanced applications, Surf. Coat. Technol. 268 (2015) 77-84.

[1.2] A. Moridi, S.M. Hassani-Gangaraj, M. Guagliano, M. Dao, Cold spray coating: review of material systems and future perspectives, Surf. Eng. 30 (2014) 369-395.

[1.3] A. Sova, D. Pervushin, I. Smurov, Development of multimaterial coatings by cold spray and gas detonation spraying, Surf. Coat. Technol. 205 (2010) 1108-1114.

[1.4] S. Yue, W. Wong, H. Aydin, R. Mongrain, R. Barua, P. Vo, R. Dolbec, Improving cold sprayability: mixed metal powders, Proceedings of the International Thermal Spray Conference, USA, 2015, pp. 473-478.

[1.5] E. Irissou, J.-G. Legoux, B. Arsenault, C. Moreau, Investigation of Al-Al2O3 cold spray coating formation and properties, J. Therm. Spray Technol. 16 (2007) 661-668.

[1.6] H. Che, X. Chu, P. Vo, S. Yue, Cold spray of mixed metal powders on carbon fibre reinforced polymers, Surf. Coat. Technol. 329 (2017) 232-243.

[1.7] J. Frattolin, R. Barua, H. Aydin, S. Rajagopalan, L. Gottellini, R. Leask, S. Yue, D. Frost, O.F. Bertrand, R. Mongrain, Development of a novel biodegradable metallic stent based on microgalvanic effect, Ann. Biomed. Eng. 44 (2016) 404-418.

Chapter 2

-

Literature Review

2.1 Cold spray technology

Cold spray, or cold gas dynamic spray, was firstly discovered in mid-1980s by Dr. Anatolii Papyrin and his research group at the Institute of Theoretical and Applied Mechanics (Novosibirsk, Russia) [2.1]. While studying models related to supersonic two-phase flow (gas + solid particles) in a wind tunnel, scientists accidentally observed some aluminum particles were deposited [2.2]. Since then, this process has attracted increasing attention and efforts have been made to develop it into a practical industrial technology [2.2]. Cold spray has been used to produce coatings of a wide range of pure metals, metal alloys, and composite materials onto various substrates [2.3].

2.1.1 Process overview

A schematic diagram of the common high-pressure cold spray system is shown in Fig. 2.1. During cold spray, a high-pressure propellant gas is injected into the system: one stream is heated and then goes into the cold spray gun; the other stream goes towards the powder feeder and carries the feedstock into the high-pressure region of the cold spray gun [2.4]. Mixing of the high-pressure gas and the feedstock is realized in the gun, and after which the two-phase flow goes through the converging-diverging nozzle to obtain the supersonic velocity, and finally leaves the nozzle and impacts on the substrate to deposit a coating [2.4]. A de Laval type converging/diverging nozzle is almost always used in cold spray to generate the high-speed gas flow [2.5]. A supersonic velocity is produced in the nozzle throat and the nozzle diverging part [2.5]. Overall, cold spray looks like

a simple process, but still it has a few process parameters. The common process parameters, their working ranges, and effects on particle acceleration in cold spray are summarized in Table 2.1.

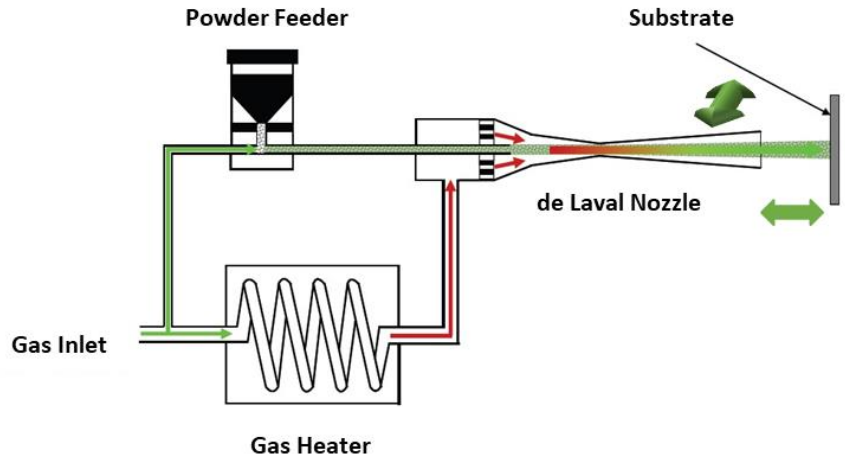

Fig. 2.1 Schematic diagram of the high-pressure cold spray process. (reproduced from Ref. [2.6] with permissions)

Table 2.1 Common process parameters, their working ranges, and effects on particle velocity (Vp) in cold spray. (reproduced from Ref. [2.7] with permissions)

Parameters	Working range	Vp
Particle size	< 100 μm	+/-
Powder morphology	Spherical (SP), irregular (IR)	SP < IR
Gas type	Air, N_2, He	Air < N_2 < He
Gas pressure	< 5 MPa	+
Gas temperature	< 1000 °C	+
Stand-off distance	5-100 mm	+/-
Gun travel speed	5-330 mm/s	N/A
Powder feed rate	< 150 g/min	N/A

2.1.2 Generic characteristics

In cold spray, the process temperature is well below the melting temperature of the spray materials; the particles remain in the solid state and the formation of coatings is due mainly to the kinetic energy of the impacting particles [2.8]. Compared with thermal spray, where the particles are in molten or semi-molten state, the solid-state particle deposition in cold spray exhibit various advantages [2.9] centered around the absence of high temperatures, which generates the least thermal input to the substrate, and permits flexible coating deposition between dissimilar materials (e.g. Al on Cu) without inducing thermal stresses or forming undesirable phases [2.10]. Cold spray is suitable to produce coatings of oxygen-sensitive (e.g. Al, Ti) or temperature-sensitive materials (e.g. amorphous, nanostructured powders) [2.1]. A high deposition efficiency (DE) (e.g. > 95% for Ti [2.11] and Cu [2.6]) and a high deposition rate (up to 14 kg/h for various metals [2.12]) have been reported, and dense and thick (up to several centimeters) coatings with wrought-like microstructure can be obtained [2.13]. Due to the low porosity and negligible oxides, coatings of high thermal and electrical conductivity (e.g. Cu [2.14]), as well as corrosion resistance (e.g. Ta [2.15], Al [2.16]) can be produced. Also, as feedstock powders have been heavily deformed, cold sprayed coatings generally exhibit high strength and hardness compared to the bulk material and the compressive residual stress generated during deposition can enhance coating fatigue properties [2.6]. Moreover, due to the relatively small (1-25 mm^2) and well-defined spray plume, cold spray can realize with reasonable precision and therefore minimizes the masking required [2.10, 2.17].

Despite all its advantages, cold spray has some disadvantages. For instance, cold spray requires at least one of the feedstock components to have certain capability to plastically deform, therefore, ceramics and very hard metals cannot be deposited alone; whereas almost all materials can be sprayed using thermal spray techniques [2.1, 2.4, 2.5]. Moreover, for some materials e.g.

Ti [2.18] and Ti6Al4V [2.19], in order to produce fully dense and high-quality coatings, expensive helium processing gas must be used to further accelerate the particle, which will incur substantial running cost [2.5]. In addition, although the mechanical properties can be improved via post heat treatment, cold sprayed coatings in their as-sprayed conditions have near-zero ductility [2.4].

2.2 Fundamentals of cold spray

2.2.1 Bonding mechanisms

In cold spray, the true bonding mechanisms of metal on metal deposition are still not clearly understood [2.10, 2.17, 2.20]. A variety of mechanisms have been proposed by different researchers through numerical simulations and/or experimental characterizations, and this include adiabatic shear instability (ASI) [2.8, 2.21], localized melting [2.22], diffusion [2.23], mechanical interlocking [2.24], interfacial amorphization [2.25], and oxide layer break-up [2.26]. Some of these mechanisms are not mutually exclusive, and it is considered that they can be mainly classified into two categories: metallurgical (or metallic) bonding and mechanical interlocking.

Metallurgical bonding can lead to strong adhesion strength [2.27, 2.28]. Since the surfaces of most metals are covered by native oxide films [2.29], the fundamentals of metallurgical bonding in cold spray are to fragment the surface oxides and bring two clean/fresh metallic surfaces into contact at the atomic level [2.30, 2.31]. The cross-section of a typical cold sprayed splat is shown in Fig. 2.2 (a). Non-uniform bonding is observed at the particle/substrate interface, where the center regions reveal obvious “gaps” (boxed) and the peripheral regions (arrowed) are in an intimate contact. The pull-off fracture surface (Fig. 2.2 (b)) and its auger electron spectroscopy mapping (Fig. 2.2 (c)) show the center regions are smooth and are covered by rich oxygen (dark areas); whereas the peripheral regions with few traces of oxygen (light areas) reveal dimple

structures (insets in Fig. 2.2 (b)), which are evidence of metallurgical bonding [2.27, 2.32-2.34]. Based on these observations, a schematic mechanism of metallurgical bonding formation in cold spray is proposed in Fig. 2.2 (d). It is considered that the impacts of highly kinetic particle would disrupt the interfacial oxide layer and induce intensive lateral deformation at interfaces to extrude fragmented oxides outwards, thus providing an intimate conformal contact under high pressure to permit bonding to occur [2.26].

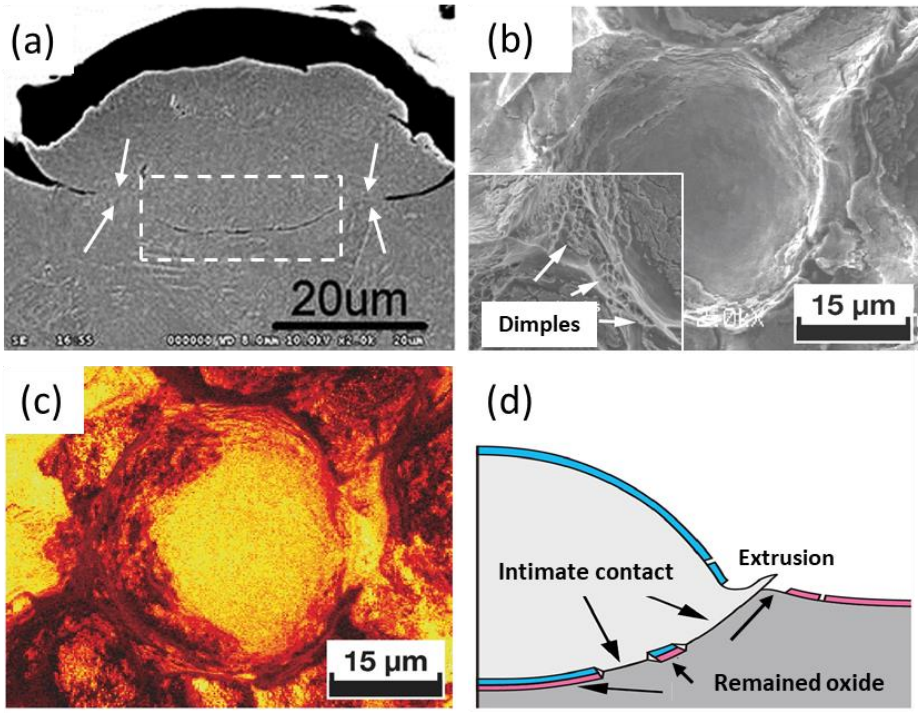

Fig. 2.2 (a) The cross-section of a typical cold sprayed splat [2.27]; (b) pull-off fracture surface of a deposited splat [2.35]; (c) auger electron spectroscopy mapping of oxygen (light areas) of (b) [2.35]; (d) schematic of the oxide layer break-up mechanism [2.36]. (reproduced from Refs. [2.27, 2.35, 2.36] with permissions)

Jetting, as shown in Fig. 2.3 (a), has been recently in-situ observed by Hassani-Gangaraj et al. [2.37] using a high-speed camera. Jetting is a type of intensive localized deformation behavior at interfaces which can effectively help to remove the broken oxide layer and provide clean

metallic contact [2.38]. Many researchers [2.27, 2.31, 2.38, 2.39] considered jetting (or remaining metal jets of a deposited splat) as evidence of metallurgical bonding formation in cold spray; however, it has also been reported that metallurgical bonding could occur without obvious jetting [2.30, 2.40]. Recently, there have been interesting debates over the generation of jetting in cold spray [2.30, 2.41, 2.42]. Assadi et al. [2.8], precursors of cold spray bonding mechanisms, considered that jetting is a result of adiabatic shear instability (ASI). They proposed that during particle impact, due to the localization of plastic strain and thermal softening effects, the temperature at interfaces would increase. When the temperature approaches melting temperature, the particles would lose their shear strength and the interfaces behave like viscous fluids and undergo excessive plastic deformation to form metal jets, as shown by the sudden rise of interfacial strain at a velocity of 580 m/s in Fig. 2.3 (b). Meanwhile, the excessive interfacial deformation of metal jets could also further induce the temperature rise of interfaces to reach partial melting [2.43]. Hassani-Gangaraj et al. [2.41] argued that adiabatic shear bands, as evidence of ASI formation, are not commonly observed at cold sprayed interfaces. They also removed the thermal softening capability of a material from numerical modeling and still observed jetting to occur at the same particle impact velocity. Therefore, instead, they proposed a shock pressure release mechanism as shown in Fig. 2.3 (c) and considered that the jetting in cold spray is formed due to the strong pressure waves interacting with the expanding edge of the particle and then fragmented under a spall-like process, similar to other natural hydrodynamic processes e.g. liquid droplet impact. They also considered that the localized melting at interfaces could induce erosion to the surface and impede particle deposition [2.44].

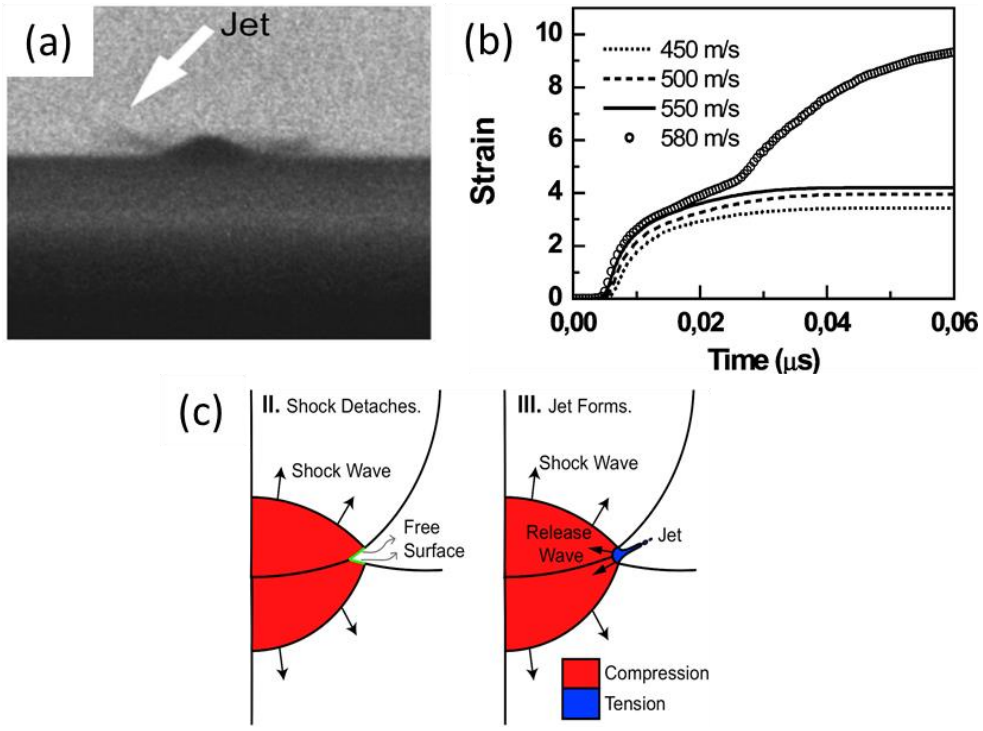

Fig. 2.3 (a) Jetting phenomenon in-situ observed by high-speed camera [2.37]; (b) simulated temporal evolution of interfacial strain upon impact: sudden increase at a velocity of 580 m/s due to adiabatic instability mechanism [2.8]; (c) schematic of jetting formation due to shock pressure release mechanism [2.41]. (reproduced from Refs. [2.8, 2.37, 2.41] with permissions)

The most common understanding of mechanical interlocking mechanisms in cold spray is the self-interlocking effects between two rough surfaces (particle/particle and particle/substrate), which can be generated by e.g. sandblasting the substrate, formation of interfacial jets (Fig. 2.4 (a)) [2.45] and using irregular morphology feedstocks. Mechanical interlocking can also form as the soft substrate material extrudes in between and envelopes the embedded hard particle, e.g. Cu on Al (boxed in Fig. 2.4 (b)) [2.38]. Moreover, Champagne et al. [2.46] observed another phenomenon in Cu on Al impacts called “interface mixing” when the heavily embedded particles cause the forced mixing of interface materials through the formation of interfacial waves, vortices,

and roll-ups (insets in Fig. 2.4 (b)) [2.46]. The interface mixing phenomenon is reported to be more obvious when the substrate is softer and particles have higher density [2.46].

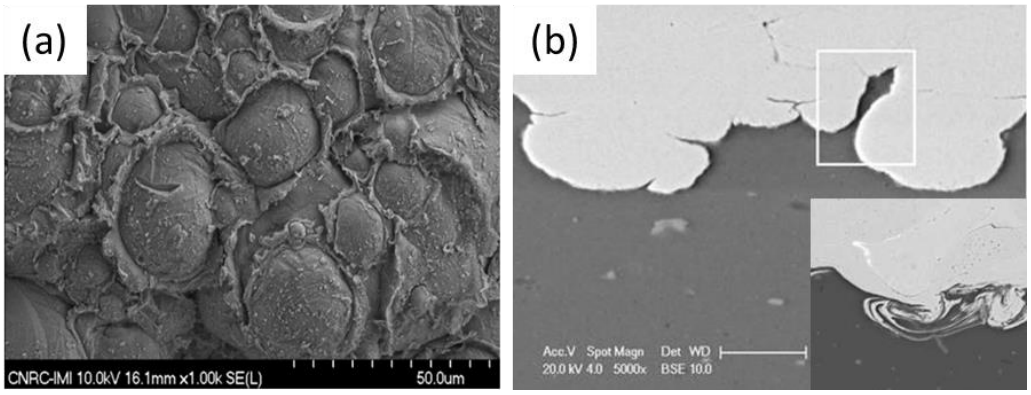

Fig. 2.4 SEM images of (a) metal jets on coating surface [2.45] and (b) Cu embedded in Al substrate [2.38] (insets are vortices formation at coating-substrate interface of Cu on Al [2.46]). (reproduced from Refs. [2.38, 2.45, 2.46] with permissions)

2.2.2 Cold sprayability

To evaluate the ease with which a powder can be deposited by cold spray, the term "cold sprayability" is introduced. This incorporates the critical velocity (Vcrit), deposition efficiency (DE), porosity, and mechanical properties (e.g. hardness and bond strength) [2.45, 2.47]. To maximize the cold sprayability, in general, a feedstock powder with the FCC crystal structure, low hardness, 10-45 μm in size, and spherical shape is preferred in cold spray, as compared with other powders with the BCC/HCP, high hardness, particle size either too large or too small and irregular shape [2.17, 2.48]. Also, increasing the intensity of cold spray process parameters (e.g. gas pressure and temperature) almost always benefits the cold spray outcomes of a feedstock.

2.2.2.1 Critical velocity

Critical velocity (Vcrit) is defined as the minimum particle impact velocity required for any deposition to occur [2.48]. As shown in Fig. 2.5, in the region below the critical velocity, no deposition can be achieved, and the particle impacts only result in the slight substrate erosion. If the particle velocity is higher than the critical velocity, deposition can be achieved.

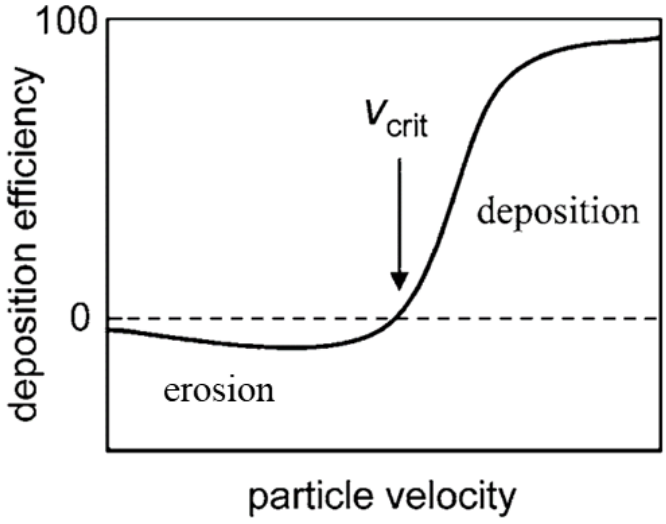

Fig. 2.5 Effect of particle impact velocity on deposition efficiency. (reproduced from Ref. [2.49] with permissions)

In cold spray literature, there have been many efforts to model the critical velocities of different metals [2.8, 2.41, 2.48]. Hassani-Gangaraj et al. [2.41] considered the critical velocity of a material is proportional to its bulk speed of sound. Assadi et al. [2.8] proposed a simple equation based on numerical simulations to calculate the critical velocity incorporating material properties:

$$V_{crit} = 667 - 0.014\rho + 0.08(T_m - T_R) + 10^{-7}\sigma_u - 0.4(T_i - T_R) \quad (2.1)$$

Where ρ is the particle density, T_m is the melting temperature, T_R is the reference temperature (293 K), σ_u is the ultimate tensile strength, and T_i is the impact temperature. It can be

seen that the critical velocity would increase with increasing material strength and melting temperature, and decrease with increasing density and particle temperature.

Schmidt et al. [2.48] proposed a modified equation to calculate the critical velocity using energy balance theories which exhibited a better approximation with the experimentally measured values, as shown in Eq. (2.2).

$$\mathrm{V}_{crit} = \sqrt{\frac{F_1 \cdot 4 \cdot \sigma_{TS} \cdot \left(1 - \frac{T_i - T_R}{T_m - T_R}\right)}{\rho} + F_2 \cdot c_P \cdot (T_m - T_i)} \tag{2.2}$$

Where σ_{TS} is the ultimate tensile strength, T_i is the impact temperature, T_R is the reference temperature (293 K), T_m is the melting temperature, ρ is the particle density, c_P is specific heat of the particle, and F_1, F_2 are the empirical factors. Based on Schmidt's equation, the critical velocities for 25 μm particles of different metals are calculated, as shown in Fig. 2.6. It can be seen that metals with relatively low melting points (e.g. tin, zinc, lead) usually have relatively low critical velocities; whereas metals that are naturally passivated by a dense oxide layer (e.g. aluminum, titanium) usually require high critical velocities [2.50].

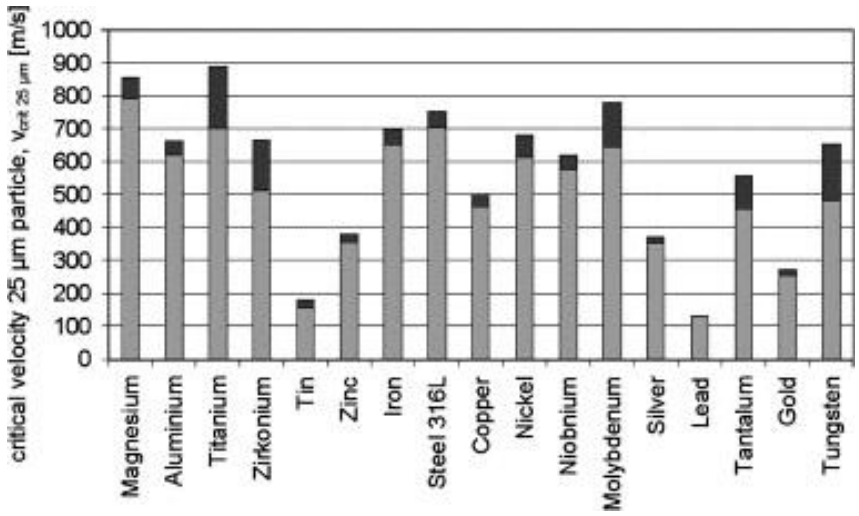

Fig. 2.6 Calculated critical velocity results for 25 µm particles of different materials. The dark part represents the uncertainty due to the available materials data. (reproduced from Ref. [2.48] with permissions)

2.2.2.2 Deposition efficiency

Deposition efficiency (DE) is often calculated as the mass change of a substrate over the total mass of spraying particles fed over the substrate [2.17]. As shown in Fig. 2.5, once the particle velocity exceeds the critical velocity, the DE would increase (sometimes to nearly 100%) with only a slight increase in the particle velocity, after which DE reaches a peak and might start to decrease due to erosion [2.17]. Since DE is a function of the particle velocity, increasing the cold spray intensity (i.e. gas temperature/pressure) almost always increases the DE.

The process of coating formation in cold spray is shown in Fig. 2.7. Generally, the coating deposition can be considered as a two-stage process: (i) particle adhesion on the substrate (formation of the first layer); (ii) particle-particle cohesion in the coating (coating build-up) [2.51]. At the first stage, incident particles shot peen and leave craters to the substrate surface, which activates the substrate surface by removing surface contaminations and help to bond the first

particle layer [2.6]. This stage is critical and largely depends on the material properties of the particle and substrate (e.g. hardness, oxide layer thickness), and the substrate conditions (e.g. preheating and roughness) [2.17]. Then at the second stage, the subsequent particles will adhere to the previously deposited layers, deform and realign, and particles start to form metallurgical bonding between each other [2.51]. After the coating is built up, the continuous peening effect leads to further densification and work-hardening of the coating [2.51]. Since the DE is the complex interplay of the two distinct processes, quantitative predictions of the DE of a powder at certain spray conditions are often difficult. But in the case that the particle and substrate materials have the similar deformability, Meng et al. [2.52] observed that a rate parameter R_{EQ}, determined from finite element simulations of single particle deposition as the equivalent plastic strain averaged over a particle ($\overline{PEEQ^2}$) over time, can correlate well with coating DE [2.53].

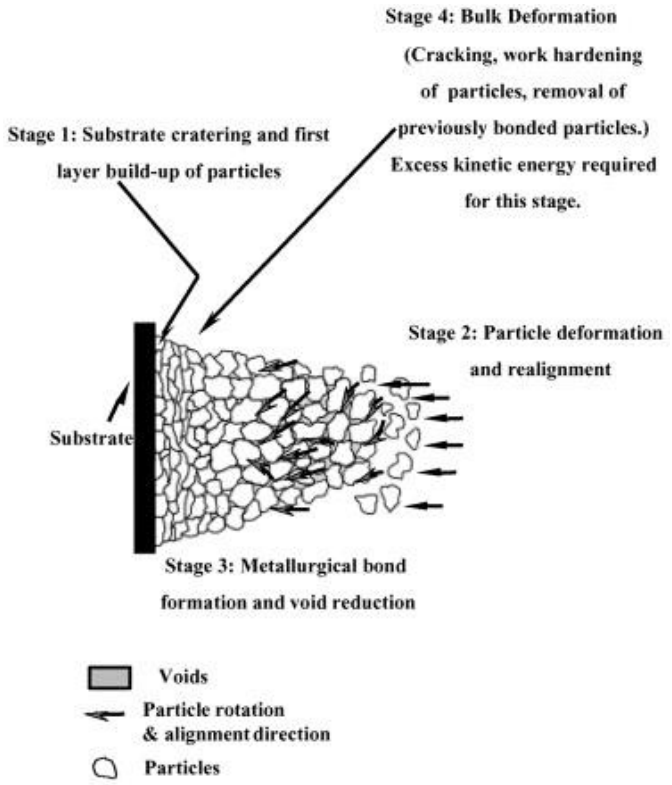

Fig. 2.7 Schematic diagram of the coating formation process in cold spray. (reproduced from Ref. [2.51] with permissions)

Individual particle impact tests (or splat tests) are often used in cold spray to understand the deposition/deformation behavior of a single particle [2.53-2.56]. As an indication of coating DE, the bond ratio (BR) metric is introduced to quantify the deposition behavior of a single particle. This is defined as the ratio of the number of bonded particles (splats) to the total impacting particles (splats + craters) per unit impact area, as shown in Fig. 2.8 (a) [2.57]. Fukumoto et al. [2.58] proposed a modified approach to calculate the BR as the ratio of the number of particles having metal jets to the total particles deposited over the substrate within the measured area. The obtained BR results were reported to exhibit a satisfactory consistency with coating DE [2.58]. Wu et al. [2.57] considered that the deposition of a single particle in cold spray is a competition between the adhesion energy (A) and rebound energy (R). It was observed that the difference between the

calculated adhesion energy and rebound energy (A-R) can well correlate with the BR results at different particle velocities, as shown in Fig. 2.8 (b). This approach provides a theoretical basis to explain and predict the deposition behavior of different metal powders onto various substrates [2.57]. However, some limitations of this model are that it fails to explain the plateau stage of DE and the erosion phenomenon, as shown in Fig. 2.5.

The equations to calculate the rebound energy (R) of an impacting particle can be denoted as below [2.59, 2.60]:

$$\mathrm{R} = \frac{1}{2} e_r m_p v_p^2 \tag{2.3}$$

$$e_r = 11.47\left(\frac{\bar{\sigma}_Y}{E^*}\right)\left(\frac{\rho_p v_p^2}{\bar{\sigma}_Y}\right)^{-\frac{1}{4}} \tag{2.4}$$

Where e_r is the recoil efficient, m_p, v_p, ρ_p are mass, velocity, and density of a particle, respectively; $\bar{\sigma}_Y$ is the effective yield stress calculated from finite element modeling during impact; E^* is the conventional elastic modulus of particle and substrate.

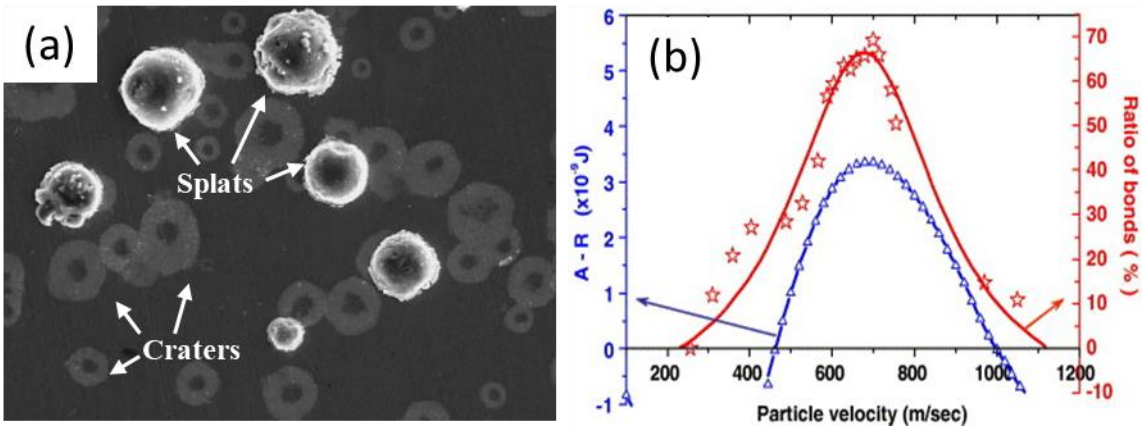

Fig. 2.8 (a) SEM image showing the splats and craters after individual particle impact tests; (b) correlation of bond ratio results to "adhesion energy-rebound energy (A-R)". (reproduced from Ref. [2.57] with permissions)

2.2.2.3 Porosity

Inadequate particle conformal deformation during deposition results in the presence of porosity in the coatings [2.51]. To evaluate the degree of particle bulk deformation during deposition, the flattening ratio (FR) is commonly used [2.61, 2.62]. One of the methods to calculate the flattening ratio is indicated in Fig. 2.9 (a) as the width to height ratio of a deformed particle [2.39, 2.63]. The porosity of cold sprayed coatings is commonly measured through image analyses [2.6] and is further characterized through methods such as Mercury Intrusion Porosimetry (MIP) [2.64] and Micro-CT [2.65]. Generally, a larger particle flattening would effectively close/fill the particle-particle gaps and leads to a denser coating [2.62, 2.63]. Coatings with lower porosity levels can often exhibit higher hardness, better corrosion resistance, and better thermal and electrical properties [2.3].

The porosity of a cold sprayed coating can vary from less than one to several tens of percents, depending on the types of the spray materials and the spray conditions [2.66]. For instance, cold sprayed Cu coatings are highly dense with less than 1% porosity due to its low yield strength and FCC structure which facilitates particle plastic deformation; whereas HCP Ti can exhibit the coating porosity as high as 20% when deposited with nitrogen gas [2.6, 2.67, 2.68]. The effect of cold spray conditions is generally that increasing the particle velocity increases the particle plastic deformation and decreases the porosity. However, Jenkins et al. [2.69] also observed an abnormal decrease in Al coating porosity when the DE and particle velocity are low, this observation reveals the contributions of the in-situ densification effect of impacted and rebounded particles to the previously deposited layers. Moreover, using helium instead of nitrogen as the propellant gas can elevate the particle acceleration and generate higher degree of particle

deformation and it is reported that Ti coating porosity can be reduced to 0.5% [2.18]. However, as shown in Fig. 2.9 (b), the porosity of cold sprayed Ti coatings is still observed to be typically non-uniform, with the top layers being porous and the bottom layers being dense due to the more intensive peening effect [2.70].

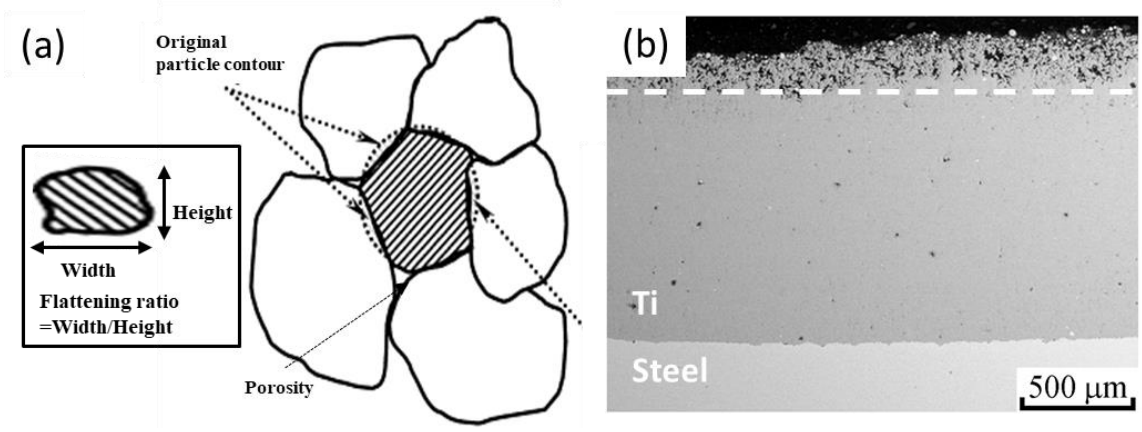

Fig. 2.9 (a) Schematic diagram of particle shape change during cold spray and the flattening ratio metric [2.51]; (b) typical porosity features in cold sprayed Ti coatings [2.70]. (reproduced from Refs. [2.51, 2.70] with permissions)

2.2.2.4 Mechanical properties

During cold spray, particles undergo intense deformation and are severely work hardened, therefore, the as-sprayed coatings normally possess higher hardness than their corresponding bulks [2.71, 2.72]. The coating hardness can also be affected by porosity or coating defects, and normally the higher the porosity (or coating defects), the lower the hardness [2.73, 2.74]. The hardness values within the cold sprayed coatings are not uniform. As reported by Zou et al. [2.75] in Fig. 2.10, higher hardness is presented at the particle-particle interface regions (particle periphery) which experiences intense deformation during deposition; whereas the center regions of a particle usually exhibit lower hardness due to the lower degree of deformation. Improving the hardness

uniformity in the cold sprayed coatings can be achieved by e.g. increasing the impact velocities to initiate more plastic deformation (especially the center regions) [2.5] and annealing to remove dislocations at the heavily deformed particle edges through recovery and recrystallization [2.76]. It is also noted that the hardness depth profile of cold sprayed coatings is relatively uniform except for the top porous layers possibly due to low thermal input to the substrate [2.77].

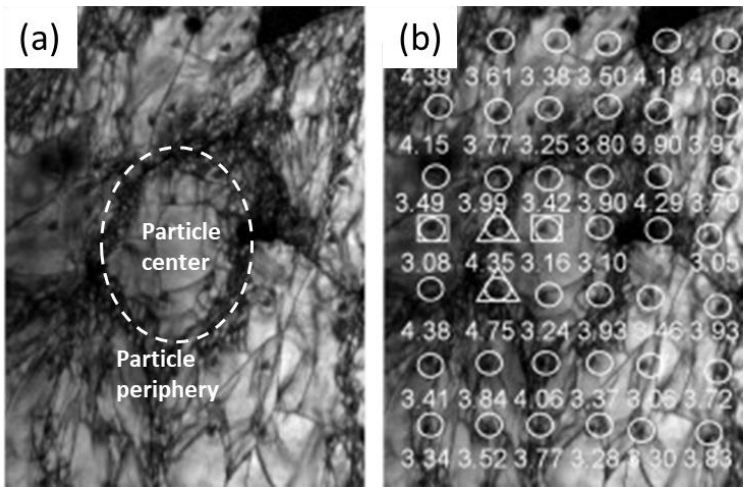

Fig. 2.10 EBSD maps of a cold sprayed Ni coating: (a) IQ map (dashed circle: peripheral areas of a particle); (b) corresponding nanohardness values. (reproduced from Ref. [2.75] with permissions)

The bond strength of cold sprayed coatings is evaluated by: (i) adhesive strength (separation from the base material) and (ii) cohesive strength (within each particle layer) [2.78]. The coating adhesive strength is often determined through pull-off tests according to ASTM C633, but is limited by the strength of epoxy adhesives (e.g. 70-80 MPa [2.79]). Higher coating adhesive strength can be alternately measured through e.g. laser shock tests [2.79] and shear tests [2.80]. Generally, cold sprayed metallic coatings on metallic substrates (e.g. Ti on mild steel > 85 MPa [2.22]) can exhibit acceptable adherence comparable to that of thermal sprayed coatings but still

much lower than the bulk strength [2.51]. The coating adhesive strength is also reported to be influenced by the coating thickness, with thicker coatings normally possessing lower adhesive strength due to higher residual stresses [2.45]. The coating cohesive strength can also be determined using above methods if particle/substrate interfaces exhibit higher adherence compared to particle-particle bonds, and this usually occurs when depositing on soft and low melting temperature substrates (e.g. Al) due to more metallurgical bonds and embedding effect [2.81]. Other indirect techniques such as scratch tests [2.82] and multi-scale indentation [2.73] can also generate results indicative of the coating cohesive strength. Chromik et al. [2.27, 2.83] developed a modified ball bond shear test to measure the adhesion strength/energy of a single deposited splat, as shown in Fig. 2.11. However, it is not clear how to correlate the splat adhesion value to the coating bond strength determined from e.g. traditional pull-off tests.

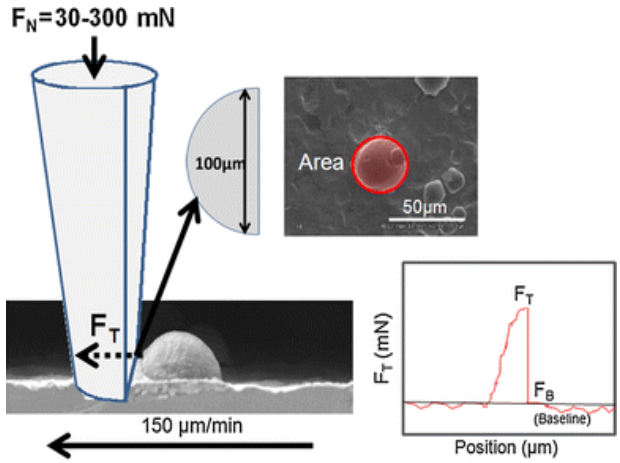

Fig. 2.11 Schematic diagram of the splat adhesion test. (reproduced from Ref. [2.27] with permissions)

2.3 Cold spray of mixed powders

Some of the current trends in cold spray involve the production of metal-metal composite coatings [2.10, 2.84, 2.85]. There are various strategies to deposit composite coatings by cold spray, as seen in Fig. 2.12, this includes using (i) powder mixtures; (ii) composite powders; (iii) cladded powders [2.10]. The latter two methods often produce coatings with well-defined and homogeneous structures [2.10]. However, using composite powders require feedstock pre-processing such as agglomerate-sintering or mechanical milling in order to bring bonding/mechanical constraints between particles, which might deteriorate the powder characteristics (e.g. work hardening, powder fragmentation) and/or surface chemistries (e.g. oxidation, contamination) [2.84]. With coated/cladded powders there are often issues due to the limited available supplies of various powder compositions [2.10]. Comparatively speaking, mixing powders (premixing or dual powder feeding) is a simple method and it is convenient in varying the feedstock mixing composition [2.10, 2.67, 2.84]. Moreover, it also allows interactions between the component powders during deposition, which is often reported to generate benefits in cold spray, e.g. improved deposition efficiency or reduced porosity [2.86-2.88]. However, there is a lack of understanding towards the deposition process of cold spraying mixed powders. For instance, it is still a challenge to predict the cold sprayability of the mixed powders from that of the single component powders and the composite coating compositional yield (i.e. the deposited composition vs the initial composition). This means that any new mixtures need to undergo extensive preliminary cold spray trials in order to optimize the process parameters. Thus, fundamentally, analyzing the cold spray characteristics of two metal powders is necessary as it will lead to accurate modeling of the process and minimize the cold spray trials required to optimize the process.

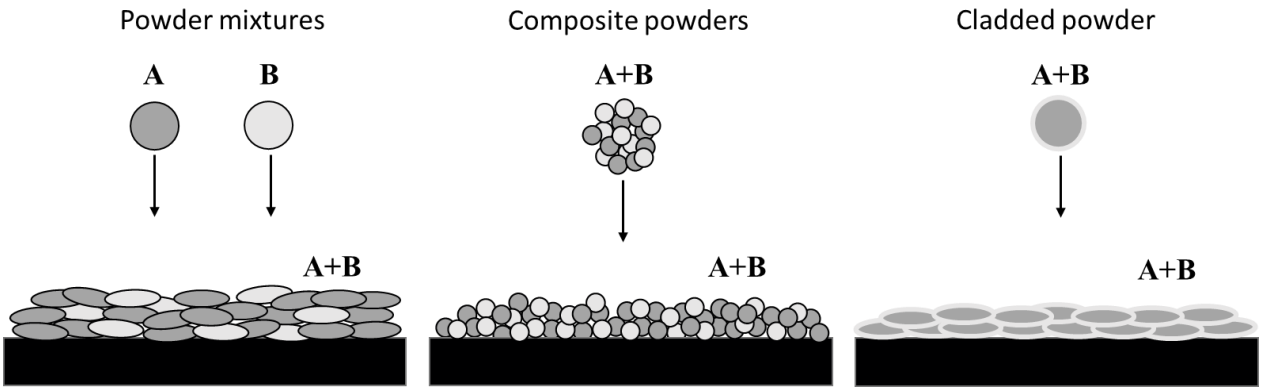

Fig. 2.12 Different strategies of composite coating deposition by cold spray. (Reproduced from Ref. [2.10] with permissions)

2.3.1 Mixed powders deposition

In cold spray literature, there are comparatively limited studies concerning the deposition process of mixed powders. The schematics of binary mixed powders deposition process are shown in Fig. 2.13. Compared with the deposition of single component powders, mixed powders deposition exhibits more complexities, e.g. it incorporates unknown impact scenarios of A on B and B on A. Sova et al. [2.89] proposed a simple mathematical model to interpret the DE of mixed powders. As shown in Fig. 2.13 (a), the fundamental aspect of this theory is to consider the depositing particles as mono-sized spheres and summarize the occurrence probability of all possible particle impact scenarios during deposition multiplied by its respective adhering probability to obtain the mixed powders DE. This model has been validated in cold spray of ternary Cu-316L-tribaloy powder mixtures. However, limitations of this model are that it only applies to mono-sized mixtures and does not incorporate effects of the potential particle-particle interactions.

Particle-particle interactions refer to the collisions between two moving particles. This could generally occur during three stages in cold spray: (i) powder feeding; (ii) powder in-flight;

(iii) upon impact or above the substrate. In this study, the third type of interaction is discussed since no evidence can be found in the literature reporting obvious effects of the first two types of interactions on the final cold spray outcome. As schematically shown in Fig. 2.13 (b), this type of particle-particle interactions occurs when the particle number density is high, and a summary from literature reveals two main scenarios. It is noted that such interactions are difficult to be directly experimentally visualized in cold spray; hence their existence is mainly speculative by the observations from DE characteristics and coating composition [2.90-2.93].

The first scenario (I in Fig. 2.13 (b)) refers to the interaction between the rebounding particles and subsequent incoming particles. King et al. [2.90] considered that, in order to retain/entrap a rebounding particle, its momentum must be overcome by the subsequent incoming particles, as given in Eq. (2.5).

$$\sum m_A v_A + \sum m_B v_B \geq m_r v_r \tag{2.5}$$

Where, m_A, m_B, m_r are the mass of particle A, B, and the rebounding particle, respectively; v_A, v_B, v_r are the velocity of particle A, B, and the rebounding particle, respectively. Since most of the kinetic energy of a rebounding particle is lost due to the plastic deformation and adhesive interactions with the substrate, its retention/entrapment is possible [2.91]. However, if there are high quantities of large/dense/heavy particles rebounding at the same time, this interaction might vice versa decelerate/deflect the later incoming impacting particles to impede their deposition [2.94-2.96].

The second scenario (II in Fig. 2.13 (b)) refers to the interaction between the subsequent incoming particles and depositing particles. This interaction is reported to be beneficial for deposition in the case that a hard particle impacts on a soft particle, i.e. tamping effect [2.87, 2.97].

Fernandez et al. [2.98] observed increases in the interfacial strain and temperature of the soft depositing particle when impacted by a hard particle through finite element simulations, which consequently benefit its deposition. However, in the literature, there are conflicting opinions towards the existence of this interaction in cold spray [2.92, 2.93, 2.98]. It is speculated that such a divergence might be due to the difference in the particle number density (e.g. as schematically shown in Figs. 2.13 (a) and (b)) resulted from the different process details and feedstock particle sizes used in different studies. Note that besides particle-particle interactions, there are also other "non-interaction" explanations of the beneficial effect of tamping on particle deposition: (i) hard particles embed in and "nail" the loosely bonded soft particles which could be otherwise eroded away by the impacts of another soft particle [2.88]; (ii) the impacts of hard particles fragment the oxide layers on the surfaces to facilitate the deposition of subsequent soft particles [2.99].

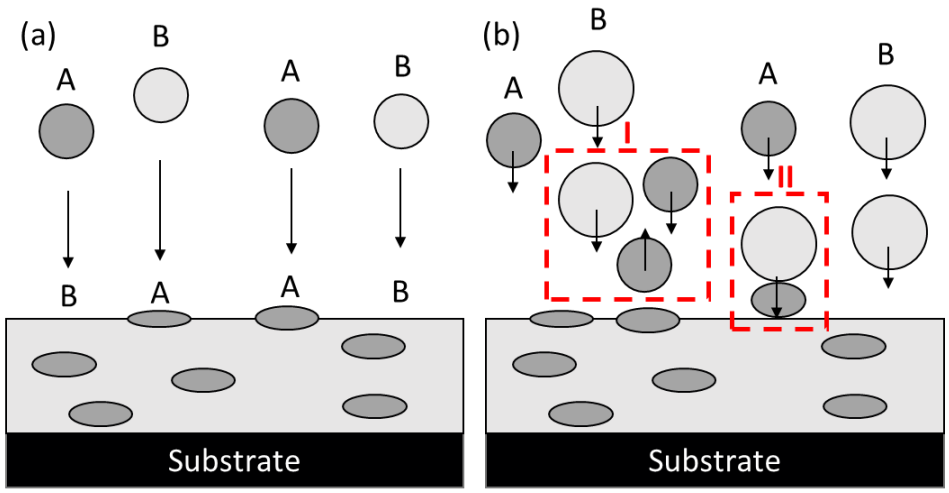

Fig. 2.13 Schematic diagrams of mixed powders deposition: (a) without particle-particle interactions; (b) with particle-particle interactions. (Constructed based on Refs. [2.89, 2.90, 2.98])

2.3.2 Effects of mixing powders

In the literature, the studies concerning the cold spray of mixed powders include mixing metals with non-metals (e.g. ceramics, intermetallics, and compounds) and another metals [2.84, 2.95]. Generally, these powder mixtures were prepared for two reasons: (i) to improve the feedstock cold sprayability; (ii) to fabricate novel metal matrix composites (MMC) or intermetallics. Regarding the first reason, Al_2O_3 is a commonly used ceramic that has been added to various metals for co-deposition, e.g. Al [2.87, 2.100], Cu [2.97], 316L [2.101] and Ni-20Cr [2.102]. Spraying a mixture of metal-ceramic instead of metal alone not only benefits the cold spray process since the hard ceramic can help to keep the nozzle clean and eliminate the clogging issue, but also the ceramic particles can activate the metal surfaces by removing oxide layers, contamination and impurities, consequently benefiting the subsequent metal deposition. Additions of irregular ceramic particle could also generate micro-asperities on the surfaces and favor the bonding/deposition of subsequent particles. The DE results of mixing angular Al_2O_3 with spherical Al powders are shown in Fig. 2.14 (a). It can be seen that the pure Al (0 wt.% Al_2O_3) cannot reach any deposition under the current conditions; whereas the addition of alumina lowers the critical velocity of Al and stimulates the DE of the mixture (solid lines) as well as the Al (dashed lines) [2.87]. The maximum mixture DE was observed at an Al_2O_3 content of about 30 wt.%, after which the DE started to decrease [2.87]. The use of metal-ceramic mixture can also lead to reduced coating porosity and improved coating bond strength due to the tamping of hard/brittle ceramic particles which induces further deformation of the deposited metal layers. Jodoin et al. [2.100] observed that when spherical morphology alumina instead of irregular morphology ones is added to the Al, there is no DE improvement but a further increase in adhesion strength of the composite coatings. It is also noted that despite the reduction in overall porosity of the composite coatings,

the interfaces between the metal and ceramic are not intimate and exhibit the presence of defects (e.g. porosity in Al-Al_2O_3 interfaces in Fig. 2.14 (b) [2.80]), which deteriorates the functionalities of the coatings, e.g. long-term corrosion barrier effects [2.87, 2.103]. Besides adding ceramics, it has been reported that mixing metal powders can also generate beneficial effects on the feedstock cold sprayability, and this is often accomplished by adding a relatively hard/dense/large metal powder to induce the tamping effect [2.74, 2.88]. Compared with ceramics, metals can exhibit more coherent interfaces with another metal and better characteristics e.g. electrical conductivity. Hanqing et al. [2.88] reported that the additions of small amount (e.g. 10 wt.%) of Cu or Zn powder to Sn could lead to the improved DE (arrow 1 in Fig. 2.14 (c)) and slight increase/no deterioration of the coating electrical conductivity; whereas too much additions (30-50 wt.%) of Cu or Zn otherwise reduce the DE (arrow 2 in Fig. 2.14 (c)). From the above examples, it can be concluded that the beneficial effects of mixing powders in cold spray are often limited to small amount additions (e.g. 10-30 wt.%) of second component (SC) powders.

Another reason to spray mixed powders is to fabricate MMC composites (e.g. metal-ceramic) utilizing the metal's plastic deformability. In this regard, there are often desires to include higher SC content in the coatings to enhance the functional performances [2.104]. However, since the SC powders (e.g. ceramics) often have the limited deformability and are thus difficult to deposit, there will be a significant loss of SC content in the deposited coatings compared with the initial feedstock, as shown in Fig. 2.14 (d) [2.87]. This requires a much higher SC content to be incorporated in the initial feedstock than the actual coating compositions expected, but this could also generate several issues. Firstly, for each specific mixture, there often exists a maximum SC content that can be entrapped e.g. 20-25 wt.% Al_2O_3 in Al in Fig. 2.14 (d) [2.87]. Further increases at high SC additions in fact mostly contribute to more impacts between the SC powders, which

does not effectively increase the deposited SC content (Fig. 2.14 (d)) but significantly reduces the mixture DE (Fig. 2.14 (a)). Secondly, the significant loss/rebounding of SC powders during deposition could generate interactions with subsequent in-flight particles to impede their deposition [2.95]. Al-Mangour et al. [2.105] observed in cold spraying mixed 316L/Co-Cr powders that 50 vol.% Co-Cr mixture would lead to much higher coating porosity of 4.5%; whereas the coating porosities from 20 and 33.3 vol.% Co-Cr mixtures are only 1%. Therefore, when there is a desire to increase the coating SC content, a compromise must be made between using higher feedstock SC content and the poor coating DE/quality.

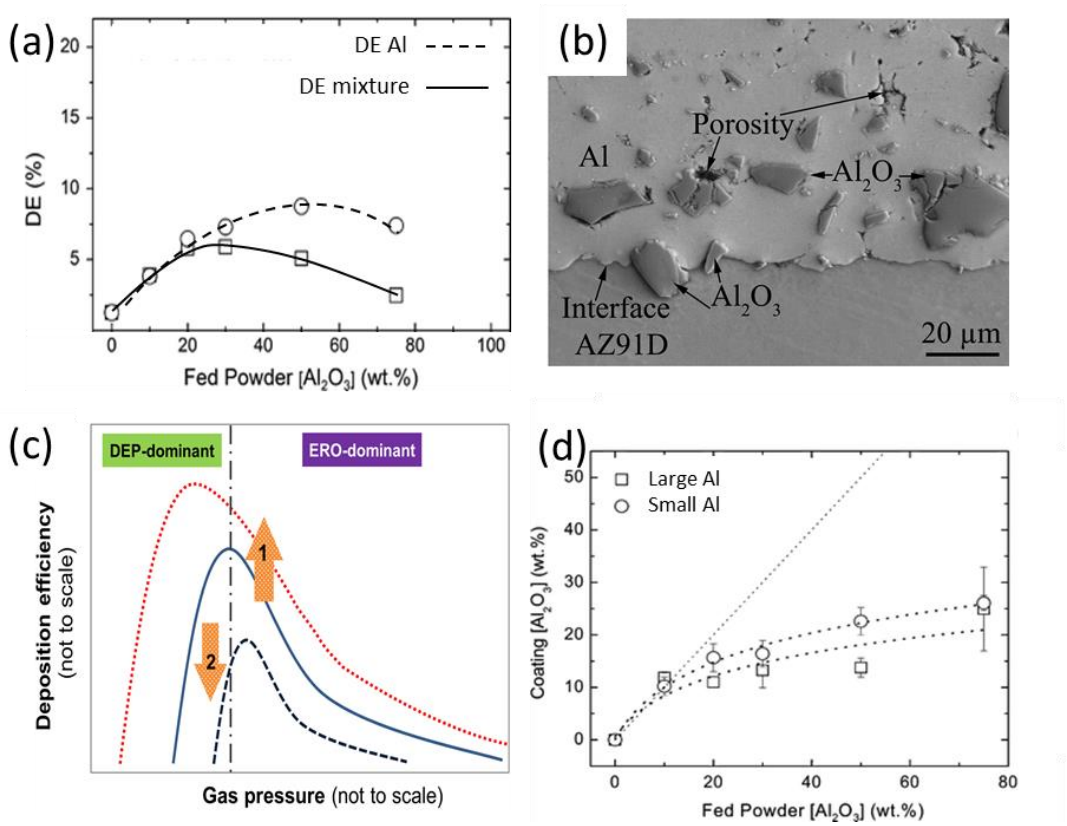

Fig. 2.14 (a) DE of Al-Al_2O_3 mixtures as a function of feedstock Al_2O_3 wt.% [2.87]; (b) cross-section of an Al-Al_2O_3 composite coating [2.80]; (c) DE of Sn by adding Cu or Zu as a function of gas pressure [2.88]; (d) coating composition of Al-Al_2O_3 mixtures as a function of feedstock

Al_2O_3 wt.% (the straight line has a slope of 1) [2.87]. (reproduced from Refs. [2.80, 2.87, 2.88] with permissions)

Mixing powders can also be applied to the same metals but of different characteristics (e.g. size and hardness). For instance, Spencer et al. [2.106] observed that the stainless steel 316L coating fabricated from the mixing of large/small 316L particles can exhibit comparable density and corrosion resistance to the coating from small particles; but without issues inherent in spraying small particles alone such as unstable powder feeding and nozzle fouling [2.106]. Besides the effect on porosity, DE-improving effects by mixing same specie powders having different properties have also been reported, e.g. soft Ta + hard Ta [2.86] and reclaimed Al (work-hardened) + original Al [2.92]. These findings show that simply creating a hardness difference among the feedstocks could benefit the cold sprayability and the practical guidance for cold spray is to mix powders from different batches or manufacturers when there is only a limited supply of one powder.

2.3.3 Studies of 316L/Fe mixed powders

In this study, mixtures of 316L stainless steel and commercial purity Fe powders were investigated as part of an overall effort to produce bio-degradable metal-metal composite stents [2.107]. Austenitic stainless steel 316L is considered as the reference material and it creates a galvanic couple with the less noble Fe [2.108]; when exposed to an electrolyte the reactive Fe anode corrodes and the more noble 316L cathode is protected. Both 316L and Fe are bio-compatible metals and the dissolved iron ions are useful for e.g. red blood cells, cytochromes, enzymes, hemoglobin and myoglobin [2.109]. Cold spray is a low temperature powder deposition process and allows for the manufacturing of materials with very fine grain size, resulting in improved mechanical properties and fatigue resistance. Moreover, mixing 316L/Fe powders for

cold spray has the convenience in varying the feedstock mixing composition, therefore the controlled degradation rates of the fabricated stents can be realized. Images of the fabricated stents after each post-processing step of grinding, electric discharge machining (EDM) to remove substrates, and final femto laser cutting can be seen in Fig. 2.15.

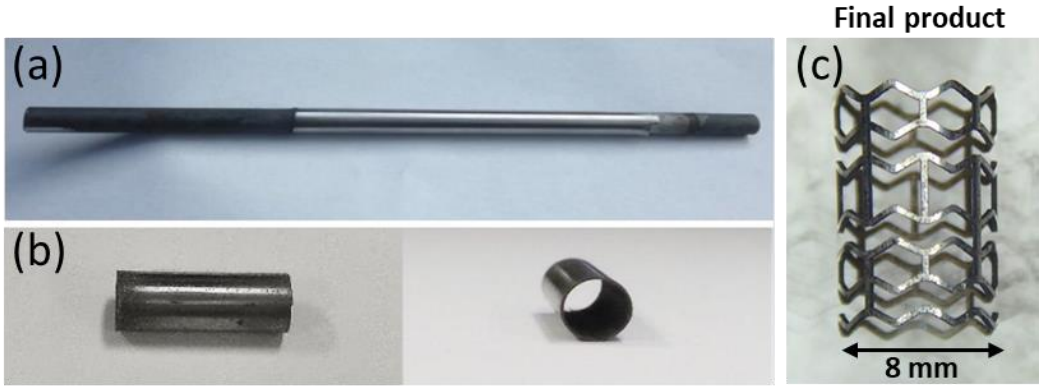

Fig. 2.15 The fabricated 316L/Fe composite metallic stent after each post-processing step of (a) grinding, (b) electric discharge machining (EDM) to remove substrates, (c) femto laser cutting. (reproduced from Ref. [2.107] with permissions)

In a previous PhD thesis, single component 316L, Fe, and three mixed 316L/Fe powders (316L-20 wt.%Fe (20Fe), 316L-50 wt.%Fe (50Fe), 316L-80 wt.%Fe (80Fe)) were cold spray deposited and interesting DE characteristics were observed [2.109]. As shown in Fig. 2.16, single component 316L powder has almost double the DE of the Fe; whereas the DE of mixed 316L/Fe powders increases with increasing the feedstock Fe fraction (poor DE component). The measured DE results of mixed 316L/Fe powders are totally different to the common predictions based on e.g. Rule of Mixtures (boxed column in Fig. 2.16). In particular, the DE of 80Fe is almost the same as single component 316L; 20Fe exhibits a DE close to single component Fe rather than single component 316L. These observations imply that there is a strong but “unpredictable” effect of

mixing on the DE of 316L/Fe powders. This current thesis is a continuing study of the DE characteristics of cold spraying mixed 316L and Fe powders. Since some difference between the two Fe-based alloys are hardness, surface oxide layer, and crystal structure [2.17], this thesis thus investigates how mixing powders of different characteristics could affect the cold sprayability.

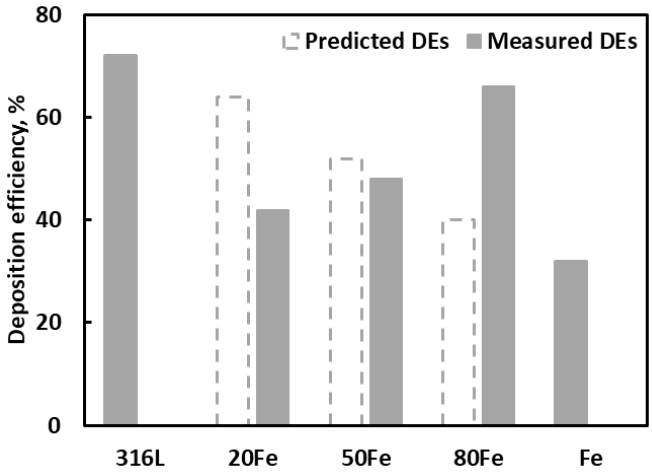

Fig. 2.16 DE results of single component 316L, Fe, and mixed 316L/Fe powders. Boxed columns: predicted DEs using Rule of Mixtures ($DE_{Mix} = DE_{316L} \times f_{316L} + DE_{Fe} \times f_{Fe}$). (reproduced from Ref. [2.109] with permissions)

2.4 References

[2.1] H. Singh, T.S. Sidhu, S.B.S. Kalsi, J. Karthikeyan, Development of cold spray from innovation to emerging future coating technology, J. Braz. Soc. Mech. Sci. Eng. 35 (2013) 231-245.

[2.2] A. Alkhimov, V. Kosarev, A. Papyrin, A method of cold gas-dynamic spraying, Doklady Akademii Nauk SSSR 315 (1990) 1062-1065.

[2.3] V.K. Champagne, The Cold Spray Materials Deposition Process: Fundamentals and Applications, Elsevier, 2007.

[2.4] A. Papyrin, V. Kosarev, S. Klinkov, A. Alkhimov, V.M. Fomin, Cold Spray Technology, Elsevier, 2006.

[2.5] H. Koivuluoto, Microstructural Characteristics and Corrosion Properties of Cold-Sprayed Coatings, PhD thesis, Tampere University of Technology, 2010.

[2.6] T. Hussain, Cold spraying of titanium: a review of bonding mechanisms, microstructure and properties, Key Eng. Mater. 533 (2012) 53-90.

[2.7] P. Vo, D. Goldbaum, W. Wong, E. Irissou, J.-G. Legoux, R.R. Chromik, S. Yue, Cold-Spray Processing of Titanium and Titanium Alloys, Titanium Powder Metallurgy, Butterworth-Heinemann, 2015.

[2.8] H. Assadi, F. Gärtner, T. Stoltenhoff, H. Kreye, Bonding mechanism in cold gas spraying, Acta Mater. 51 (2003) 4379-4394.

[2.9] J. Karthikeyan, The Advantages and Disadvantages of the Cold Spray Coating Process, The Cold Spray Materials Deposition Process, Woodhead Publishing, 2007.

[2.10] S. Grigoriev, A. Okunkova, A. Sova, P. Bertrand, I. Smurov, Cold spraying: from process fundamentals towards advanced applications, Surf. Coat. Technol. 268 (2015) 77-84.

[2.11] W. Wong, E. Irissou, A.N. Ryabinin, J.-G. Legoux, S. Yue, Influence of helium and nitrogen gases on the properties of cold gas dynamic sprayed pure titanium coatings, J. Therm. Spray Technol. 20 (2010) 213-226.

[2.12] J.R. Davis, Handbook of Thermal Spray Technology, ASM international, 2004.

[2.13] H. Singh, T. Sidhu, S. Kalsi, Cold spray technology: future of coating deposition processes, Frattura Integr. Strutt. 6 (2012) 69-84.

[2.14] C. Borchers, F. Gärtner, T. Stoltenhoff, H. Assadi, H. Kreye, Microstructural and macroscopic properties of cold sprayed copper coatings, J. Appl. Phys. 93 (2003) 10064-10070.

[2.15] H. Koivuluoto, J. Näkki, P. Vuoristo, Corrosion properties of cold-sprayed tantalum coatings, J. Therm. Spray Technol. 18 (2008) 75-82.
[2.16] K. Balani, T. Laha, A. Agarwal, J. Karthikeyan, N. Munroe, Effect of carrier gases on microstructural and electrochemical behavior of cold-sprayed 1100 aluminum coating, Surf. Coat. Technol. 195 (2005) 272-279.
[2.17] R. Ghelichi, M. Guagliano, Coating by the cold spray process: a state of the art, Frattura Integr. Strutt. 3 (2009) 30-44.
[2.18] S.H. Zahiri, C.I. Antonio, M. Jahedi, Elimination of porosity in directly fabricated titanium via cold gas dynamic spraying, J. Mater. Process. Technol. 209 (2009) 922-929.
[2.19] P. Vo, E. Irissou, J.G. Legoux, S. Yue, Mechanical and microstructural characterization of cold-sprayed Ti-6Al-4V after heat treatment, J. Therm. Spray Technol. 22 (2013) 954-964.
[2.20] Y. Xiong, G. Bae, X. Xiong, C. Lee, The effects of successive impacts and cold welds on the deposition onset of cold spray coatings, J. Therm. Spray Technol. 19 (2009) 575-585.
[2.21] M. Grujicic, C.L. Zhao, W.S. DeRosset, D. Helfritch, Adiabatic shear instability based mechanism for particles/substrate bonding in the cold-gas dynamic-spray process, Mater. Des. 25 (2004) 681-688.
[2.22] G. Bae, S. Kumar, S. Yoon, K. Kang, H. Na, H.-J. Kim, C. Lee, Bonding features and associated mechanisms in kinetic sprayed titanium coatings, Acta Mater. 57 (2009) 5654-5666.
[2.23] S. Guetta, M.H. Berger, F. Borit, V. Guipont, M. Jeandin, M. Boustie, Y. Ichikawa, K. Sakaguchi, K. Ogawa, Influence of particle velocity on adhesion of cold-sprayed splats, J. Therm. Spray Technol. 18 (2009) 331-342.
[2.24] M. Grujicic, J.R. Saylor, D.E. Beasley, W.S. DeRosset, D. Helfritch, Computational analysis of the interfacial bonding between feed-powder particles and the substrate in the cold-gas dynamic-spray process, Appl. Surf. Sci. 219 (2003) 211-227.
[2.25] K.H. Ko, J.O. Choi, H. Lee, Y.K. Seo, S.P. Jung, S.S. Yu, Cold spray induced amorphization at the interface between Fe coatings and Al substrate, Mater. Lett. 149 (2015) 40-42.
[2.26] W.-Y. Li, C.-J. Li, H. Liao, Significant influence of particle surface oxidation on deposition efficiency, interface microstructure and adhesive strength of cold-sprayed copper coatings, Appl. Surf. Sci. 256 (2010) 4953-4958.

[2.27] D. Goldbaum, J.M. Shockley, R.R. Chromik, A. Rezaeian, S. Yue, J.-G. Legoux, E. Irissou, The effect of deposition conditions on adhesion strength of Ti and Ti6Al4V cold spray splats, J. Therm. Spray Technol. 21 (2011) 288-303.
[2.28] R. Huang, W. Ma, H. Fukanuma, Development of ultra-strong adhesive strength coatings using cold spray, Surf. Coat. Technol. 258 (2014) 832-841.
[2.29] K. Kim, S. Kuroda, Amorphous oxide film formed by dynamic oxidation during kinetic spraying of titanium at high temperature and its role in subsequent coating formation, Scr. Mater. 63 (2010) 215-218.
[2.30] H. Assadi, F. Gärtner, T. Klassen, H. Kreye, Comment on 'adiabatic shear instability is not necessary for adhesion in cold spray', Scr. Mater. 162 (2019) 512-514.
[2.31] H. Assadi, H. Kreye, F. Gärtner, T. Klassen, Cold spraying - a materials perspective, Acta Mater. 116 (2016) 382-407.
[2.32] W.-Y. Li, C. Zhang, X. Guo, C.-J. Li, H. Liao, C. Coddet, Study on impact fusion at particle interfaces and its effect on coating microstructure in cold spraying, Appl. Surf. Sci. 254 (2007) 517-526.
[2.33] C. Chen, Y. Xie, S. Yin, M.-P. Planche, S. Deng, R. Lupoi, H. Liao, Evaluation of the interfacial bonding between particles and substrate in angular cold spray, Mater. Lett. 173 (2016) 76-79.
[2.34] G. Bae, J.-i. Jang, C. Lee, Correlation of particle impact conditions with bonding, nanocrystal formation and mechanical properties in kinetic sprayed nickel, Acta Mater. 60 (2012) 3524-3535.
[2.35] Y. Ichikawa, R. Tokoro, M. Tanno, K. Ogawa, Elucidation of cold-spray deposition mechanism by auger electron spectroscopic evaluation of bonding interface oxide film, Acta Mater. 164 (2019) 39-49.
[2.36] W.-Y. Li, W. Gao, Some aspects on 3D numerical modeling of high velocity impact of particles in cold spraying by explicit finite element analysis, Appl. Surf. Sci. 255 (2009) 7878-7892.
[2.37] M. Hassani-Gangaraj, D. Veysset, K.A. Nelson, C.A. Schuh, In-situ observations of single micro-particle impact bonding, Scr. Mater. 145 (2018) 9-13.

[2.38] T. Hussain, D.G. McCartney, P.H. Shipway, D. Zhang, Bonding mechanisms in cold spraying: the contributions of metallurgical and mechanical components, J. Therm. Spray Technol. 18 (2009) 364-379.
[2.39] D. Goldbaum, R.R. Chromik, S. Yue, E. Irissou, J.-G. Legoux, Mechanical property mapping of cold sprayed Ti splats and coatings, J. Therm. Spray Technol. 20 (2010) 486-496.
[2.40] Y. Xie, S. Yin, C. Chen, M.-P. Planche, H. Liao, R. Lupoi, New insights into the coating/substrate interfacial bonding mechanism in cold spray, Scr. Mater. 125 (2016) 1-4.
[2.41] M. Hassani-Gangaraj, D. Veysset, V.K. Champagne, K.A. Nelson, C.A. Schuh, Adiabatic shear instability is not necessary for adhesion in cold spray, Acta Mater. 158 (2018) 430-439.
[2.42] M. Hassani-Gangaraj, D. Veysset, V.K. Champagne, K.A. Nelson, C.A. Schuh, Response to Comment on "adiabatic shear instability is not necessary for adhesion in cold spray", Scr. Mater. 162 (2019) 515-519.
[2.43] W.-Y. Li, C.-J. Li, G.-J. Yang, Effect of impact-induced melting on interface microstructure and bonding of cold-sprayed zinc coating, Appl. Surf. Sci. 257 (2010) 1516-1523.
[2.44] M. Hassani-Gangaraj, D. Veysset, K.A. Nelson, C.A. Schuh, Melt-driven erosion in microparticle impact, Nat. Commun. 9 (2018) 5077.
[2.45] W. Wong, Understanding the Effects of Process Parameters on the Properties of Cold Gas Dynamic Sprayed Pure Titanium Coatings, Department of Mining and Materials Engineering, McGill University, 2012.
[2.46] V.K. Champagne, D. Helfritch, P. Leyman, S. Grendahl, B. Klotz, Interface material mixing formed by the deposition of copper on aluminum by means of the cold spray process, J. Therm. Spray Technol. 14 (2005) 330-334.
[2.47] J. Villafuerte, Modern Cold Spray: Materials, Process, and Applications, Springer, 2015.
[2.48] T. Schmidt, F. Gärtner, H. Assadi, H. Kreye, Development of a generalized parameter window for cold spray deposition, Acta Mater. 54 (2006) 729-742.
[2.49] T. Schmidt, H. Assadi, F. Gärtner, H. Richter, T. Stoltenhoff, H. Kreye, T. Klassen, From particle acceleration to impact and bonding in cold spraying, J. Therm. Spray Technol. 18 (2009) 794-808.
[2.50] H. Che, Cold Spray onto Carbon Fibre Reinforced Polymer for Lightning Strike Protection, Department of Mining and Materials Engineering, McGill University, 2016.

[2.51] T. Van Steenkiste, J. Smith, R. Teets, Aluminum coatings via kinetic spray with relatively large powder particles, Surf. Coat. Technol. 154 (2002) 237-252.
[2.52] F. Meng, S. Yue, J. Song, Quantitative prediction of critical velocity and deposition efficiency in cold-spray: a finite-element study, Scr. Mater. 107 (2015) 83-87.
[2.53] Y. Zhang, N. Brodusch, S. Descartes, J.M. Shockley, R. Gauvin, R.R. Chromik, The effect of submicron second-phase particles on the rate of grain refinement in a copper-oxygen alloy during cold spray, J. Therm. Spray Technol. 26 (2017) 1509-1516.
[2.54] R. Drehmann, T. Grund, T. Lampke, B. Wielage, K. Manygoats, T. Schucknecht, D. Rafaja, Splat formation and adhesion mechanisms of cold gas-sprayed Al coatings on Al2O3 substrates, J. Therm. Spray Technol. 23 (2013) 68-75.
[2.55] H. Che, P. Vo, S. Yue, Investigation of cold spray on polymers by single particle impact experiments, J. Therm. Spray Technol. 28 (2018) 135-143.
[2.56] S.I. Imbriglio, N. Brodusch, M. Aghasibeig, R. Gauvin, R.R. Chromik, Influence of substrate characteristics on single Ti splat bonding to ceramic substrates by cold spray, J. Therm. Spray Technol. 27 (2018) 1011-1024.
[2.57] J. Wu, H. Fang, S. Yoon, H. Kim, C. Lee, The rebound phenomenon in kinetic spraying deposition, Scr. Mater. 54 (2006) 665-669.
[2.58] M. Fukumoto, M. Mashiko, M. Yamada, E. Yamaguchi, Deposition behavior of copper fine particles onto flat substrate surface in cold spraying, J. Therm. Spray Technol. 19 (2009) 89-94.
[2.59] R.B. Clough, S.C. Webb, R.W. Armstrong, Dynamic hardness measurements using a dropped ball: with application to 1018 steel, Mater. Sci. Eng. A 360 (2003) 396-407.
[2.60] W. Kohlhöfe, R.K. Penny, Dynamic hardness testing of metals, Int. J. Pres. Ves. Pip. 61 (1995) 65-75.
[2.61] P.C. King, M. Jahedi, Relationship between particle size and deformation in the cold spray process, Appl. Surf. Sci. 256 (2010) 1735-1738.
[2.62] S.-L. Fu, C.-X. Li, Y.-K. Wei, X.-T. Luo, G.-J. Yang, C.-J. Li, J.-L. Li, Novel method of aluminum to copper bonding by cold spray, J. Therm. Spray Technol. 27 (2018) 624-640.
[2.63] W. Wong, P. Vo, E. Irissou, A.N. Ryabinin, J.G. Legoux, S. Yue, Effect of particle morphology and size distribution on cold-sprayed pure titanium coatings, J. Therm. Spray Technol. 22 (2013) 1140-1153.

[2.64] T. Hussain, D.G. McCartney, P.H. Shipway, T. Marrocco, Corrosion behavior of cold sprayed titanium coatings and free standing deposits, J. Therm. Spray Technol. 20 (2010) 260-274.
[2.65] C. Chen, X. Yan, Y. Xie, R. Huang, M. Kuang, W. Ma, R. Zhao, J. Wang, M. Liu, Z. Ren, H. Liao, Microstructure evolution and mechanical properties of maraging steel 300 fabricated by cold spraying, Mater. Sci. Eng. A 743 (2019) 482-493.
[2.66] A. Sova, S. Grigoriev, A. Okunkova, I. Smurov, Potential of cold gas dynamic spray as additive manufacturing technology, Int. J. Adv. Manuf. Technol. 69 (2013) 2269-2278.
[2.67] R. Lima, A. Kucuk, C. Berndt, J. Karthikeyan, C. Kay, J. Lindemann, Deposition efficiency, mechanical properties and coating roughness in cold-sprayed titanium, J. Mater. Sci. Lett. 21 (2002) 1687-1689.
[2.68] T. Marrocco, D. McCartney, P. Shipway, A. Sturgeon, Production of titanium deposits by cold-gas dynamic spray: numerical modeling and experimental characterization, J. Therm. Spray Technol. 15 (2006) 263-272.
[2.69] R. Jenkins, S. Yin, B. Aldwell, M. Meyer, R. Lupoi, New insights into the in-process densification mechanism of cold spray Al coatings: low deposition efficiency induced densification, J. Mater. Sci. Technol. 35 (2019) 427-431.
[2.70] X.-T. Luo, Y.-K. Wei, Y. Wang, C.-J. Li, Microstructure and mechanical property of Ti and Ti6Al4V prepared by an in-situ shot peening assisted cold spraying, Mater. Des. 85 (2015) 527-533.
[2.71] W.D. Callister, D.G. Rethwisch, Materials Science and Engineering: an Introduction, Wiley New York, 2007.
[2.72] E. Calla, D. McCartney, P. Shipway, Deposition of copper by cold gas dynamic spraying: an investigation of dependence of microstructure and properties of the deposits on the spraying conditions, Proceedings of the International Thermal Spray Conference, Japan, 2004, pp. 20-30.
[2.73] D. Goldbaum, J. Ajaja, R.R. Chromik, W. Wong, S. Yue, E. Irissou, J.-G. Legoux, Mechanical behavior of Ti cold spray coatings determined by a multi-scale indentation method, Mater. Sci. Eng. A 530 (2011) 253-265.
[2.74] H. Aydin, M. Alomair, W. Wong, P. Vo, S. Yue, Cold sprayability of mixed commercial purity Ti plus Ti6Al4V metal powders, J. Therm. Spray Technol. 26 (2017) 1-11.

[2.75] Y. Zou, D. Goldbaum, J.A. Szpunar, S. Yue, Microstructure and nanohardness of cold-sprayed coatings: electron backscattered diffraction and nanoindentation studies, Scr. Mater. 62 (2010) 395-398.
[2.76] E. Calla, D. McCartney, P. Shipway, Effect of heat treatment on the structure and properties of cold sprayed copper, Proceeding of the International Thermal Spray Conference, Switzerland, 2005, pp. 170-176.
[2.77] R. Ghelichi, S. Bagherifard, D. Mac Donald, M. Brochu, H. Jahed, B. Jodoin, M. Guagliano, Fatigue strength of Al alloy cold sprayed with nanocrystalline powders, Int. J. Fatigue 65 (2014) 51-57.
[2.78] Accepted practice to test bond strength of thermal spray coatings, J. Therm. Spray Technol. 22 (2013) 1263-1266.
[2.79] M. Perton, S. Costil, W. Wong, D. Poirier, E. Irissou, J.G. Legoux, A. Blouin, S. Yue, Effect of pulsed laser ablation and continuous laser heating on the adhesion and cohesion of cold sprayed Ti-6Al-4V coatings, J. Therm. Spray Technol. 21 (2012) 1322-1333.
[2.80] Q. Wang, K. Spencer, N. Birbilis, M.-X. Zhang, The influence of ceramic particles on bond strength of cold spray composite coatings on AZ91 alloy substrate, Surf. Coat. Technol. 205 (2010) 50-56.
[2.81] T. Stoltenhoff, C. Borchers, F. Gärtner, H. Kreye, Microstructures and key properties of cold-sprayed and thermally sprayed copper coatings, Surf. Coat. Technol. 200 (2006) 4947-4960.
[2.82] G. Sundararajan, N.M. Chavan, G. Sivakumar, P. Sudharshan Phani, Evaluation of parameters for assessment of inter-splat bond strength in cold-sprayed coatings, J. Therm. Spray Technol. 19 (2010) 1255-1266.
[2.83] R.R. Chromik, D. Goldbaum, J.M. Shockley, S. Yue, E. Irissou, J.-G. Legoux, N.X. Randall, Modified ball bond shear test for determination of adhesion strength of cold spray splats, Surf. Coat. Technol. 205 (2010) 1409-1414.
[2.84] A. Moridi, S.M. Hassani-Gangaraj, M. Guagliano, M. Dao, Cold spray coating: review of material systems and future perspectives, Surf. Eng. 30 (2014) 369-395.
[2.85] A. Sova, D. Pervushin, I. Smurov, Development of multimaterial coatings by cold spray and gas detonation spraying, Surf. Coat. Technol. 205 (2010) 1108-1114.

[2.86] S. Yue, W. Wong, H. Aydin, R. Mongrain, R. Barua, P. Vo, R. Dolbec, Improving cold sprayability: mixed metal powders, Proceedings of the International Thermal Spray Conference, USA, 2015, pp. 473-478.
[2.87] E. Irissou, J.-G. Legoux, B. Arsenault, C. Moreau, Investigation of Al-Al2O3 cold spray coating formation and properties, J. Therm. Spray Technol. 16 (2007) 661-668.
[2.88] H. Che, X. Chu, P. Vo, S. Yue, Cold spray of mixed metal powders on carbon fibre reinforced polymers, Surf. Coat. Technol. 329 (2017) 232-243.
[2.89] A. Sova, R. Maestracci, M. Jeandin, P. Bertrand, I. Smurov, Kinetics of composite coating formation process in cold spray: modelling and experimental validation, Surf. Coat. Technol. 318 (2017) 309-314.
[2.90] P.C. King, S.H. Zahiri, M.Z. Jahedi, Rare earth/metal composite formation by cold spray, J. Therm. Spray Technol. 17 (2007) 221-227.
[2.91] S. Ahmad Alidokht, P. Vo, S. Yue, R.R. Chromik, Erosive wear behavior of cold-sprayed Ni-WC composite coating, Wear 376-377 (2017) 566-577.
[2.92] J. Perry, P. Richer, B. Jodoin, E. Matte, Pin fin array heat sinks by cold spray additive manufacturing: economics of powder recycling, J. Therm. Spray Technol. 28 (2018) 144-160.
[2.93] K. Ito, Y. Ichikawa, Microstructure control of cold-sprayed pure iron coatings formed using mechanically milled powder, Surf. Coat. Technol. 357 (2019) 129-139.
[2.94] R.G. Maev, V. Leshchynsky, Air gas dynamic spraying of powder mixtures: theory and application, J. Therm. Spray Technol. 15 (2006) 198-205.
[2.95] S.M. Hassani-Gangaraj, A. Moridi, M. Guagliano, Critical review of corrosion protection by cold spray coatings, Surf. Eng. 31 (2015) 803-815.
[2.96] G. Huang, H. Wang, X. Li, L. Xing, J. Zhou, Deposition efficiency of low pressure cold sprayed aluminum coating, Mater. Manuf. Process 33 (2017) 1100-1106.
[2.97] H. Koivuluoto, P. Vuoristo, Effect of powder type and composition on structure and mechanical properties of Cu + Al2O3 coatings prepared by using low-pressure cold spray process, J. Therm. Spray Technol. 19 (2010) 1081-1092.
[2.98] R. Fernandez, B. Jodoin, Cold spray aluminum-alumina cermet coatings: effect of alumina content, J. Therm. Spray Technol. 27 (2018) 603-623.

[2.99] X.-T. Luo, M.-L. Yao, N. Ma, M. Takahashi, C.-J. Li, Deposition behavior, microstructure and mechanical properties of an in-situ micro-forging assisted cold spray enabled additively manufactured Inconel 718 alloy, Mater. Des. 155 (2018) 384-395.
[2.100] R. Fernandez, B. Jodoin, Cold spray aluminum-alumina cermet coatings: effect of alumina morphology, J. Therm. Spray Technol. 28 (2019) 737-755.
[2.101] K. Spencer, D.M. Fabijanic, M.X. Zhang, The influence of Al2O3 reinforcement on the properties of stainless steel cold spray coatings, Surf. Coat. Technol. 206 (2012) 3275-3282.
[2.102] H. Koivuluoto, P. Vuoristo, Effect of ceramic particles on properties of cold-sprayed Ni-20Cr+Al2O3 coatings, J. Therm. Spray Technol. 18 (2009) 555-562.
[2.103] H. Bu, M. Yandouzi, C. Lu, D. MacDonald, B. Jodoin, Cold spray blended Al+Mg17Al12 coating for corrosion protection of AZ91D magnesium alloy, Surf. Coat. Technol. 207 (2012) 155-162.
[2.104] S.A. Alidokht, P. Manimunda, P. Vo, S. Yue, R.R. Chromik, Cold spray deposition of a Ni-WC composite coating and its dry sliding wear behavior, Surf. Coat. Technol. 308 (2016) 424-434.
[2.105] B. Al-Mangour, R. Mongrain, E. Irissou, S. Yue, Improving the strength and corrosion resistance of 316L stainless steel for biomedical applications using cold spray, Surf. Coat. Technol. 216 (2013) 297-307.
[2.106] K. Spencer, M.X. Zhang, Optimisation of stainless steel cold spray coatings using mixed particle size distributions, Surf. Coat. Technol. 205 (2011) 5135-5140.
[2.107] J. Frattolin, R. Barua, H. Aydin, S. Rajagopalan, L. Gottellini, R. Leask, S. Yue, D. Frost, O.F. Bertrand, R. Mongrain, Development of a novel biodegradable metallic stent based on microgalvanic effect, Ann. Biomed. Eng. 44 (2016) 404-418.
[2.108] S.V. Verstraeten, L. Aimo, P.I. Oteiza, Aluminium and lead: molecular mechanisms of brain toxicity, Arch. Toxicol. 82 (2008) 789-802.
[2.109] R. Barua, Study of the Structural Properties and Control of Degradation Rate for Biodegradable Metallic Stents Using Cold Spray, PhD thesis, Department of Mechanical Engineering, McGill University, 2015.

Chapter 3

-

Understanding the Cold Spray Deposition Efficiencies of 316L/Fe Mixed Powders by Performing Splat Tests onto As-Polished Coatings

Understanding the cold spray deposition efficiencies (DEs) of mixed metal powders requires knowledge of the deposition behavior of a single particle. In this chapter, we sprayed single 316L or Fe particles (splats) onto as-polished (mirror-polished) coatings. Results show that the splat deposition behavior onto as-polished coatings correlates well with the coating DE, and the orders of impact play a significant role on the splat deposition behavior (i.e. 316L on Fe, Fe on 316L). Interesting effects of the splat deposition behavior onto as-polished composite 316L/Fe coatings were also observed but currently there is no explanations of these phenomena.

This chapter has been published as:

- Xin Chu*, Hanqing Che, Phuong Vo, Rohan Chakrabarty, Binhan Sun, Jun Song, Stephen Yue, "*Understanding the cold spray deposition efficiencies of 316L/Fe mixed powders by performing splat tests onto as-polished coatings*", Surf. Coat. Technol. 324 (2017), 353-360.

3.1 Abstract

Some of the current trends in cold spray include the production of metal-metal composite coatings; however, the deposition mechanisms of mixed powders are often vaguely understood. In this study, single component 316L stainless steel and Fe coatings, as well as composite 316L/Fe coatings, were deposited through cold spray and the deposition efficiencies (DE) were measured. The composite coatings featuring various feedstock fractions were produced using a dual powder feeder setup. Splat tests were then performed on the as-polished coatings to investigate the deposition behavior of each component powder on the previously deposited layers. Bond ratio (BR) was determined from the splat tests to correlate with DE. Results show that the 316L powder has a better DE than Fe; whereas the DE of 316L/Fe mixed powder increases with increasing the mixture feedstock Fe fraction. The BR was found to correlate well with the DE of both single component and mixed powders. For the individual deposition behavior of the component powder, the BR of 316L monotonically decreases on the composite coating with an increasing Fe fraction; while the BR of Fe plateaus at a relatively high value regardless of the composite coating composition, which results in the overall increase of mixture DE.

3.2 Introduction

Mixing powders in cold spray is a straightforward method to produce composite coatings and the use of mixed metal feedstock has been increasingly studied by researchers [3.1-3.6]. It has been found to offer benefits in improving cold sprayability of the component powder (e.g. increase deposition efficiency and decrease porosity), similar to those of ceramic additions to metal powders [3.7]. However, the mixed powder deposition in cold spray is a complicated process. For instance, it is not clear whether the critical velocity of the mixture is unique to any specific composition (i.e. combination of feedstock powders); or can be determined directly from a consideration of the critical velocities of individual components. This renders an issue in the selection of appropriate process parameters in cold spraying the mixed feedstock. A further concern is the compositional yield, i.e. how close the deposited composition is to the initial powder feedstock composition. Moreover, in a ceramic-metal system, the impinging ceramic powders cannot be deposited alone as they only contribute to tamping and roughening of the surface layers [3.8]. While in a metal-metal system, almost all metals can exhibit some cold sprayabilities and this generates an uncertainty of deposition behavior at the mixed interfaces. Often "unpredicted" situations in the cold sprayability of metal-metal mixtures can be observed; for instance, Aydin et al. [3.9] reported that an addition of 10 wt.% Ti into Ti6Al4V drastically lowers the coating porosity from 7.5% to 1.75%, but the 5 wt.% Ti would barely help. Sova et al. [3.10] for the first time developed a simple mathematical model to predict the DE and coating composition of 316L-Cu-Tribaloy mixtures on the basis of the adhesion probability between each component powder during deposition. But so far this model is only applicable for mixtures with similar size and still future improvements are required [3.10].

The cold spray coating deposition can be mainly divided into two distinct steps: first layer formation and coating build-up [3.11]. To understand the coating cold sprayability (e.g. DE), a few researchers investigated the deposition behavior of a single particle using experiments and/or FE simulations [3.12-3.17]. The splat test is an experimental approach to generate single particle impacts and it is commonly performed onto the as-polished substrates [3.12-3.16]. Thus, it only reveals the particle deposition behavior at the initial stage of coating deposition (particle-substrate adhesion), which is considered to contribute limitedly to the overall coating DE. Once the first layer has formed, the coating deposition then shifts to a case of particle-particle cohesion. Therefore, the DE of a feedstock might be mispredicted using the common approach of the splat test, especially when the deformability of the powder and substrate materials is remarkably dissimilar [3.16].

In this study, the DE of mixed 316L stainless steel and commercial purity Fe powders was investigated as part of an overall effort to produce metal-metal composites with controlled corrosion properties for biodegradable implants [3.18]. The splat tests were performed on as-polished coatings to reveal the particle deposition behavior during coating build-up. The increase of mixture DE with increasing feedstock Fe was discussed, and the scope of future efforts to fully explain the DE characteristics of 316L/Fe mixtures was narrowed.

Nomenclature

m_{316L}, m_{Fe}	Mass of a 316L or Fe particle
n_{316L}, n_{Fe}	Number of 316L or Fe particle impacting on coating surface
BR_{316L}, BR_{Fe}	Bond ratio of 316L or Fe impacts onto composite coatings (probability of a 316L or Fe particle to adhere on the coating surface)
$\mathbf{M}_{316L}, \mathbf{M}_{Fe}$	Total mass of 316L or Fe particles impacting on the coating surface
f_{Fe}	Feedstock Fe weight fraction
f_{cFe}	Coating Fe weight fraction
dM_{316L}, dM_{Fe}	Total mass of 316L or Fe particles in the coating

3.3 Materials and methods

3.3.1 Powders

Commercially available 316L stainless steel powder (Sandvik Osprey, Neath-Port Talbot, UK) and commercial purity Fe powder (Quebec Metal Powders, Sorel-Tracy, Canada) were used as the feedstock. The particle size distributions were examined using a Horiba LA-920 laser diffraction analyzer (Horiba, Tokyo, Japan). As shown in Fig. 3.1, the 316L powder is spherical, while the Fe is mainly spherical but with some irregular component. The particle size distributions of 316L and Fe feedstocks are also given in Fig. 3.1, exhibiting the mean sizes of 29.1 μm and 22.2 μm, respectively. The Vickers hardness of the feedstock was measured using a Clark CM-100AT Microhardness Tester (Sun-Tec, Novi, USA). The 316L powder has a higher average microhardness of 262.6 $HV_{0.01}$ compared with that of 141.3 $HV_{0.01}$ for the Fe.

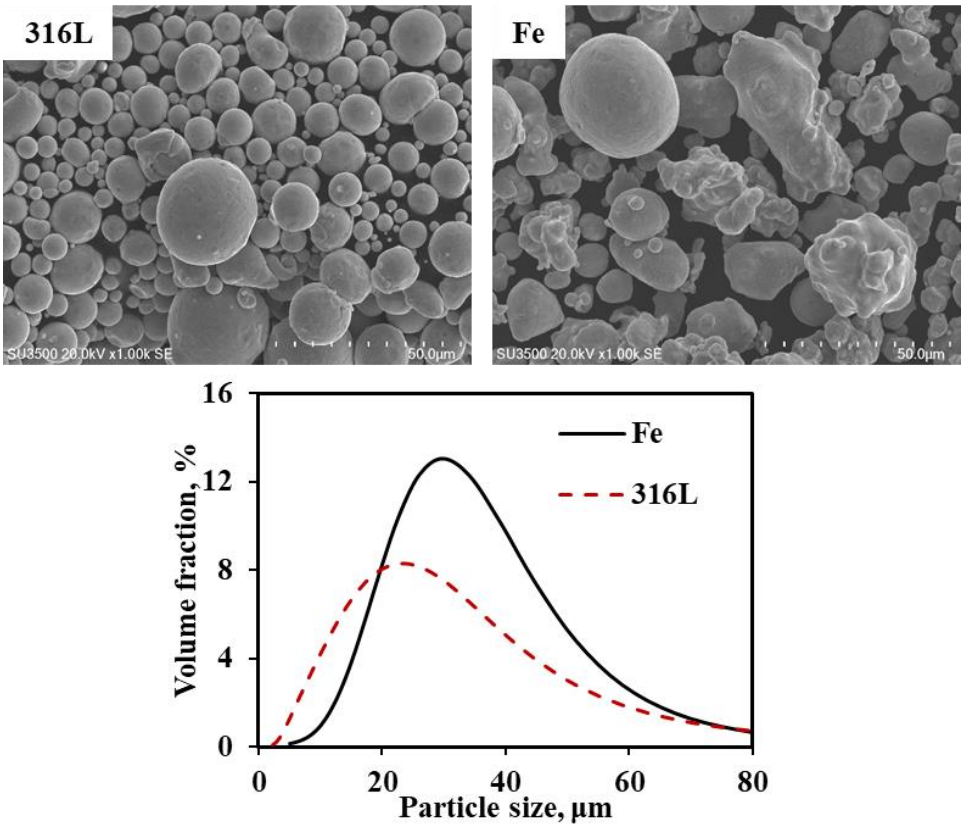

Fig. 3.1 Morphologies and size distributions of the feedstock powders.

3.3.2 Cold spray

Spraying was performed at the McGill-NRC cold spray facility, located at the National Research Council Canada, Boucherville, using a Plasma Giken PCS-800 cold spray system (Plasma Giken, Yoriimachi, Japan) with a PNFC2-010-30S tungsten carbide nozzle. Nitrogen was used as the propellant gas. The process parameters were set referring to [3.19] at a gas preheating temperature of 700 °C, a gas pressure of 4 MPa, and a stand-off distance of 80 mm. Two deposition modes were used as follows: high feed rate (18.7-24.8 g/min) with low gun traverse speed (300 mm/s) for coating deposition, and low feed rate (316L-8.5 g/min, Fe-11 g/min) with high gun traverse speed (1000 mm/s) for splat tests.

3.3.2.1 Composite coatings

Apart from the single component powders (316L and Fe), four different compositions of feedstock powders were deposited, namely (in terms of nominal compositions), 10 wt.% Fe (10Fe), 50 wt.% Fe (50Fe), 80 wt.% Fe (80Fe), 90 wt.% Fe (90Fe). The composite coatings were produced using a dual powder feeder setup due to its advantage in varying the feedstock fractions. As shown in Fig. 3.2, the 316L and Fe feedstock were fed separately, mixed before the cold spray gun to obtain desired compositions, and axially injected into high pressure region of the gun for codeposition. The feed rate was measured as the weight loss of the powder feeder per unit time, and the values for each feedstock powders are presented in Table 3.1.

The substrates used were 1018 carbon steel plates (McMaster-Carr, Aurora, OH) with dimensions of 76.2 mm × 76.2 mm × 6.4 mm. Prior to coating deposition, the substrates were blasted with 24 grit alumina to remove the scale and roughen the surface to promote adhesion. After spraying, DE was measured as the mass gain of the substrate divided by the total mass of spray material fed during the time that the gun was over the substrate. The coating cross-sections (transverse to the gun travel direction) were observed using a light optical microscope (LOM). The composite coating compositions were estimated by the relative surface areas of 316L and Fe phases using an image analysis method.

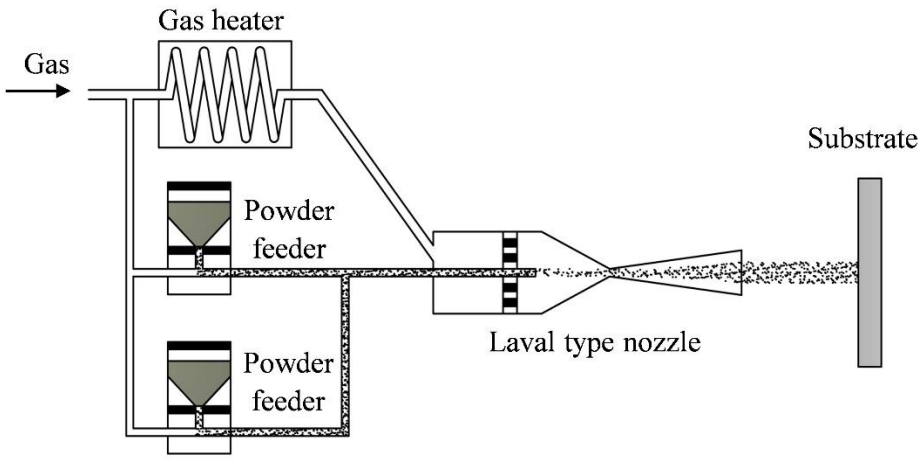

Fig. 3.2 Schematic of the cold spray process with dual powder feeder setup [3.20]. (Figure adapted with permissions)

Table 3.1 Feed rate settings for coating deposition.

Powder	Feed rate, g/min	
	316L	Fe
316L	23.8	-
10Fe	18.3	2.4
50Fe	7.8	10.9
80Fe	3.9	18.1
90Fe	3.1	21.7
Fe	-	21.7

3.3.2.2 Splat tests

Splat tests were performed by spraying 316Lor Fe powder onto both the single component and composite coatings produced as above. Before used as substrates for the splat tests, the as-sprayed coatings were polished to a mirror finish, in order to clearly reveal craters and deposits.

After impacts, the coating surfaces were characterized using a Hitachi SU3500 SEM (Hitachi, Tokyo, Japan). The bond ratio (BR) was determined as the fraction of the number of bonded particles (deposits) to the total incident particles (craters + deposits) by an image analysis method [3.14].

3.4 Results

3.4.1 Coating deposition

3.4.1.1 Deposition efficiency

The experimental DE values for each feedstock powder are shown in Fig. 3.3. For the single component powders, the 316L powder exhibits a slightly higher DE than Fe (50% vs 45%). However, for the mixed powders, it is found that the DE increases with increasing feedstock Fe. The result is consistent with a previous study [3.19] on the DE of 316L/ Fe mixed powders, despite the different particle sizes and hardnesses of feedstock powders used. These observations collectively reveal a fact that the addition of a poor DE component (Fe) instead facilitates the deposition of a good DE component (316L). Specifically, in this study, a small addition of 316L to Fe, i.e. 90Fe, is observed to "stimulate" the mixture DE to a higher value than pure 316L (55% vs 50%). On the other hand, a small addition of Fe to 316L (10Fe), gives the lowest DE, which is in fact much lower than the pure Fe DE (38% vs 45%). The experimental mixture DE are then compared with the predicted DE calculated by the rule of mixtures, $i.e. DE = DE_{316L} \times f_{316L} + DE_{Fe} \times f_{Fe}$; the comparison is also shown in Fig. 3.3. The predicted values show a decreasing trend with increasing feedstock Fe, which is totally opposite to the experimental DE. This result reveals the difficulty in predicting deposition characteristics of the 316L/Fe mixed powder, and

also indicates the behavior of the mixed powder should be considered as one entity instead of independent components during deposition.

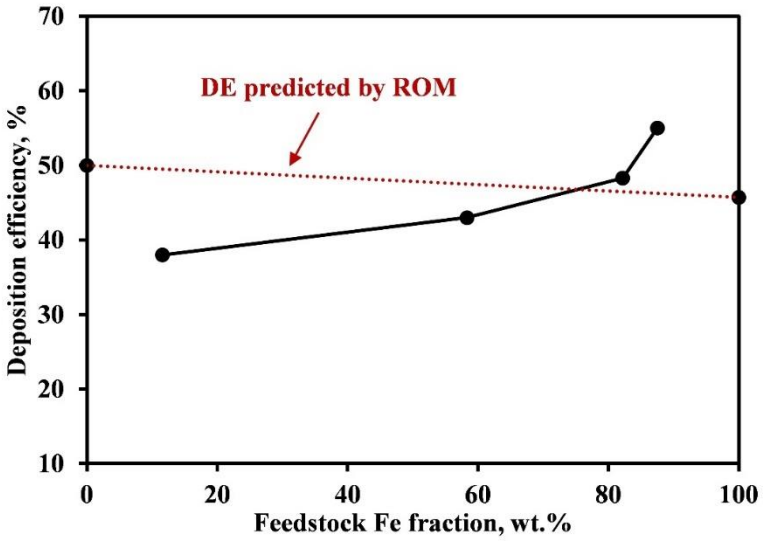

Fig. 3.3 Experimental DE of each feedstock powder (red dotted line: DE predicted by ROM).

3.4.1.2 Coating microstructure

The composite coating compositions are compared with the feedstock compositions, which can be determined from the feed rate settings (Table 3.1); the results are shown in Table 3.2. It can be seen that the coatings always exhibit a higher Fe fraction compared with the initial feedstock composition; and the largest deviation occurs at 50Fe, where an increment of 22.7% Fe fraction is observed in the coating. These composition deviations indicate a higher partial DE of the Fe component than 316L during mixed powder deposition.

Table 3.2 Fe content in the feedstock and coatings.

Coating	Feedstock Fe, wt.%	Coating Fe, %
316L	0	0
10Fe	11.6	16.1 ± 1.6
50Fe	58.3	81.0 ± 3.2
80Fe	82.2	92.3 ± 1.6
90Fe	87.5	96.4 ± 0.7
Fe	100	100

Examples of the coating cross-sectional microstructure are shown in Fig. 3.4. The impact direction is from top to bottom of the image. The dark regions in the images are Fe, the light regions are 316L and the black spots are pores. Figs. 3.4 (a) and (b) show the microstructures in the center part of the two DE extremes (10Fe and 90Fe coatings). It can be seen that both coatings are relatively dense and the Fe and 316L powders have sufficiently deformed after deposition. A closer look at 10Fe near top surface in Fig. 3.4 (c) reveals different characteristics. Compared to Fig. 3.4 (a), there seems to be more defects present which is due to the lack of sufficient tamping. In particular, a few crack-like defects are identified to be laterally distributed at the mixed 316L/Fe interfaces, transverse to the impact direction. These defects distributing along the impact interfaces are considered as indicators of a strong rebound of the impacted particles [3.16]. Also, it is noticed that these lateral defects mostly locate on the “top” of Fe and the “bottom” of 316L, as marked by red arrows. This finding implies a stronger rebound of 316L particles impacting on the previously deposited Fe compared with Fe on 316L.

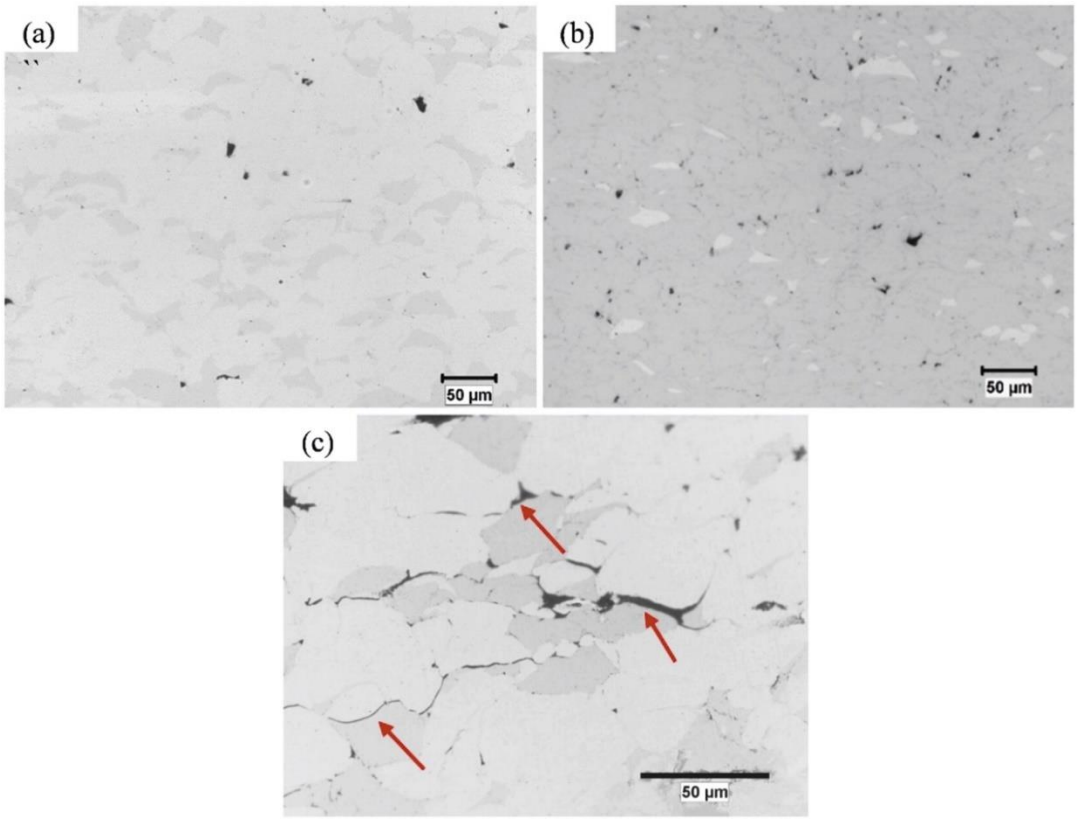

Fig. 3.4 Optical images of coating cross-sections: (a) 10Fe, (b) 90Fe, (c) magnified 10Fe (Red arrows: lateral defects at the mixed 316L/Fe interfaces).

3.4.2 Splat tests

To reveal the deposition behavior of the component powder, splat tests were performed onto the as-polished coatings. The SEM surface morphology of the single component coatings after impacts is shown in Fig. 3.5. The corresponding bond ratio (BR) and average deposit size were determined and tabulated in Table 3.3. Note that those ultrafine deposits ($d < 4$ μm) in Fig. 3.5 (a) were not included, since these particles having negligible masses barely contribute to the DE results. It is shown that the impact of 316L particle on 316L coating has a higher BR compared with Fe on Fe, which is consistent with the observation that 316L single component powder has higher DE than Fe. For the two types of impacts between 316L and Fe, it is observed that Fe on

316L has a much higher BR than 316L on Fe, and is the highest of all the combinations tested. Specifically, a closer look at deposits between impacts of 316L and Fe is shown in Fig. 3.6. The 316L deposits can be seen to lift off the Fe coating at the edges; whereas the Fe deposits show a close contact to the 316L coating. This result is consistent with the finding of preferred location of lateral defects at the mixed 316L/Fe interfaces, showing that the 316L impacts exhibit a stronger rebound on Fe layer than Fe on 316L. Similarly, the SEM surface morphology of the composite coatings after impacts is shown in Fig. 3.7 and the corresponding bond ratio (BR) and average deposit size are tabulated in Table 3.4. Interestingly, the BR values of 316L and Fe particles vary distinctly on different composite coatings. With increasing Fe fraction in the composite coatings, the BR of 316L monotonically decreases from 35.8% to 7.9%, while BR of Fe only undergoes little change, exhibiting a relatively high value of about 56%. This result indicates the different behavior of the component powder during the mixed powder deposition, and will be discussed in Section 3.5.2.

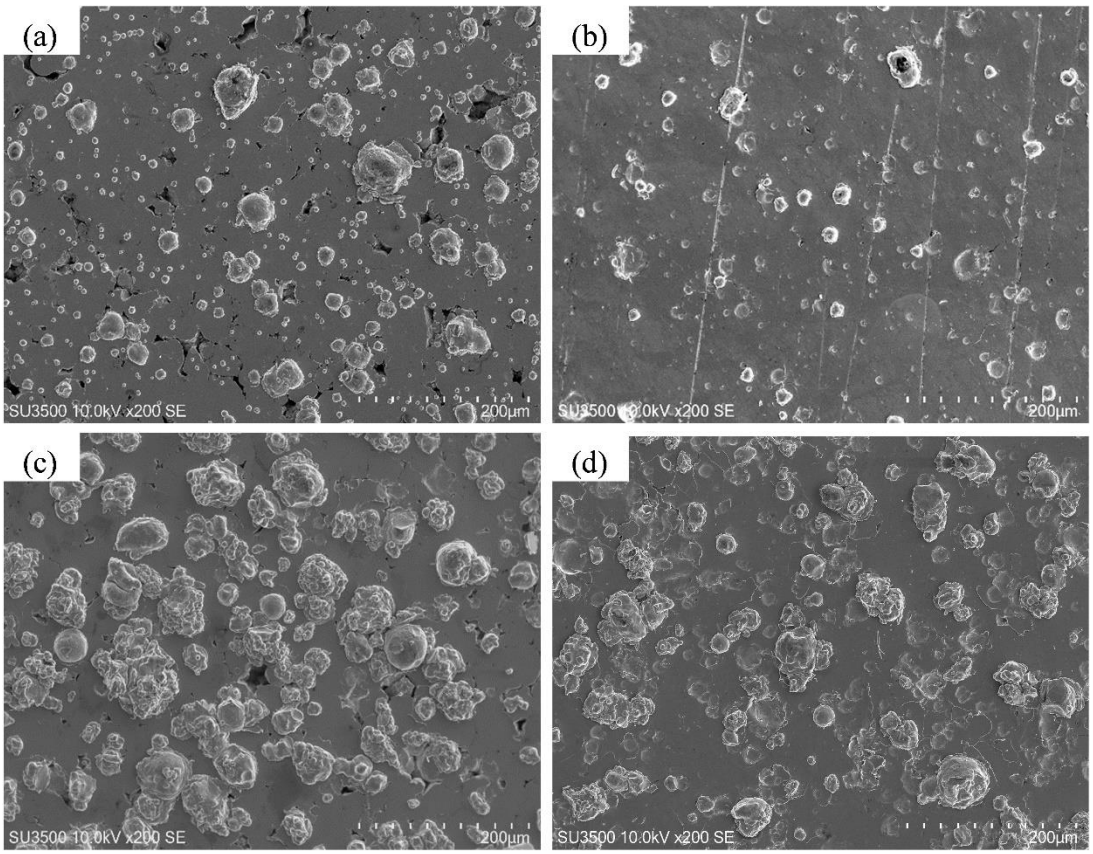

Fig. 3.5 SEM surface morphology after single particle impacts: (a) 316L on 316L, (b) 316L on Fe, (c) Fe on 316L, and (d) Fe on Fe.

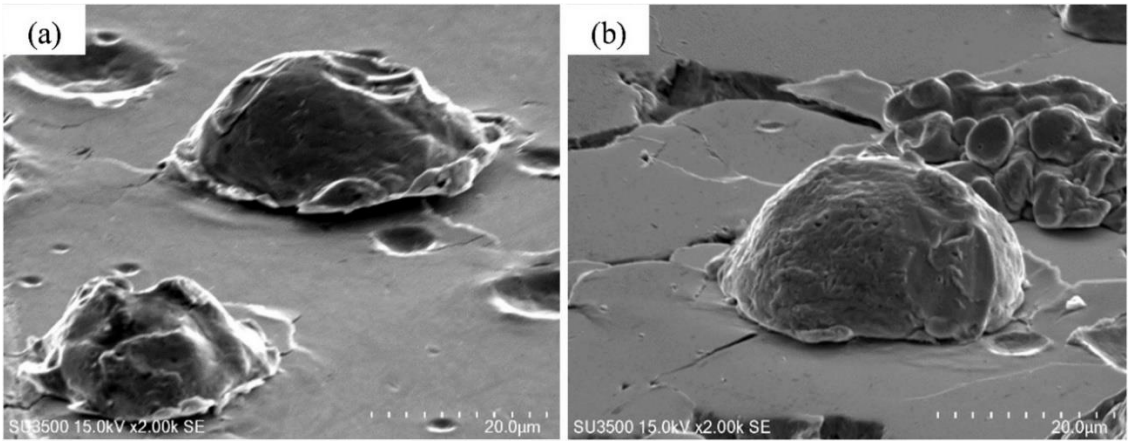

Fig. 3.6 SEM morphology of the deposits: (a) 316L on Fe, (b) Fe on 316L.

Table 3.3 Bond ratio (BR) and average deposit size of impacts onto single component coatings.

	316L BR, %	Average deposit size, μm	Fe BR, %	Average deposit size, μm
On 316L	45.8 ± 0.8	17.3 ± 0.8	87.3 ± 2.3	24.2 ± 1.0
On Fe	8.3 ± 1.1	12.1 ± 1.4	38.3 ± 1.5	21.2 ± 1.2

Similarly, the SEM surface morphology after impacts onto composite coatings are shown in Fig. 3.7 and the corresponding bond ratio (BR) and average deposit size are tabulated in Table 3.4. Interestingly, the BR values of 316L and Fe particles vary distinctly on different composite coatings. With increasing Fe fraction in the composite coatings, the BR of 316L monotonically decreases from 35.8% to 7.9%, while BR of Fe only undergoes little change, exhibiting a relatively high value of about 56%. This result indicates the different behaviors of the component powder during mixed powder deposition, and will be discussed in Section 3.5.2.

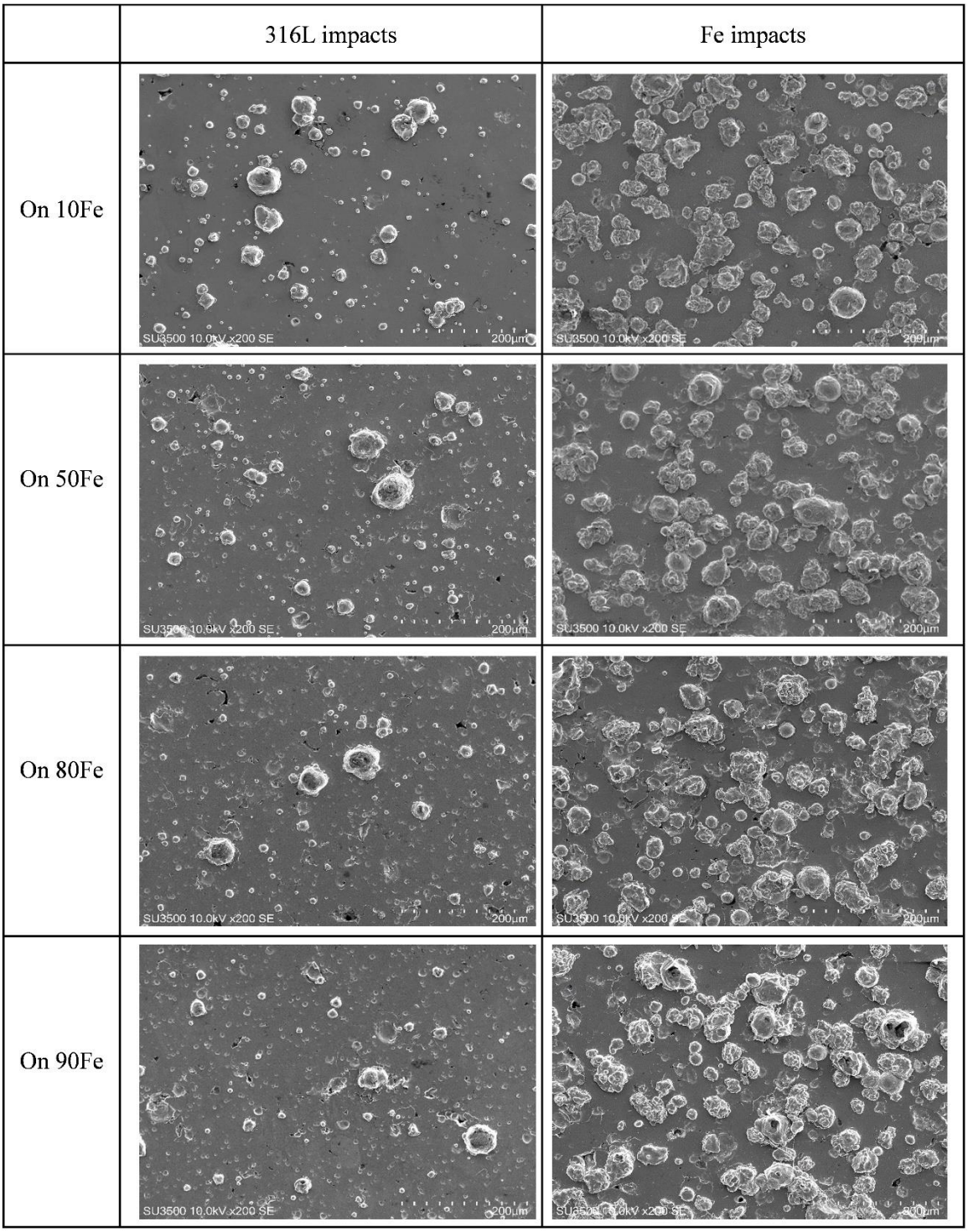

Fig. 3.7 SEM surface morphology after single particle impacts onto composite coatings.

Table 3.4 Bond ratio (BR) and average deposit size of single particle impacts onto composite coatings.

	316L BR, %	Average deposit size, μm	Fe BR, %	Average deposit size, μm
On 10Fe	35.8 ± 1.7	17.3 ± 1.5	59.5 ± 3.8	24.1 ± 1.2
On 50Fe	16.0 ± 1.1	15.8 ± 1.3	54.8 ± 1.9	21.8 ± 3.0
On 80Fe	12.3 ± 4.0	13.5 ± 0.2	54.3 ± 2.5	22.7 ± 1.1
On 90Fe	7.9 ± 0.4	13.1 ± 0.7	55.0 ± 2.0	22.2 ± 1.3

3.5 Discussion

3.5.1 Correlation between bond ratio and deposition efficiency

The idea of using BR results determined from splat tests to indicate coating DE is previously discussed in literature [3.12, 3.16]. Although in their experiments the single particles were sprayed onto the as-polished substrate, still some correlations between the splat BR and coating DE can be observed [3.12, 3.16]. This finding motivates us to perform splat tests onto the as-polished coatings to see if a more accurate correlation (e.g. in values) between BR and DE could occur. Also, the mild steel substrate used in this study is a commonly used material in cold spray on which particles can be easily deposited to form the first layer, thus the particle-particle cohesion during coating build-up should dominate the DE characteristics. Admittedly, there are a few other strategies to quantify the relative deposition behavior of a single particle, e.g. area fractions of deposits/(deposits + craters) or deposits/coating. However, these strategies were not discussed in this study due to the two main concerns: 1) the crater area might not reflect the actual area of the previously rebounded particle; 2) slight variations regarding the powder feed rate (e.g. total number of deposits + craters) were observed, even along the center of the spray trace.

It is understood that the bond ratio is a count-type measurement while the deposition efficiency is a weight fraction. Thus, there appears to be a consideration of particle size effect in order to relate together the two terms. As observed in Tables 3.3 and 3.4, the BR measurement has intrinsically included the particle size effect, since for both 316L and Fe powders, a higher BR almost always accompanies a larger average deposit size. Thus, assuming all the particles being fed have reached the coating surface, either deposited or deflected to leave craters; this BR metric could generate the probability of a particle to adhere during coating build-up.

Therefore, the BR results determined from splat tests were used to correlate with the experimental DE results. For single component powder deposition, the DE results of 316L and Fe were compared with the BR results of 316L on 316L and Fe on Fe, respectively. For the mixed powders, assuming that no interaction between the mixed powders has occurred prior to impact, then the masses of 316L and Fe particles deposited on per unit coating area are:

$$dM_{316L} = \mathrm{n}_{316L}\mathrm{m}_{316L}\mathrm{BR}_{316L} \tag{3.1}$$

$$dM_{Fe} = \mathrm{n}_{Fe}\mathrm{m}_{Fe}\mathrm{BR}_{Fe} \tag{3.2}$$

The total masses of 316L and Fe particles impacting on coating surface are:

$$\mathrm{M}_{316L} = n_{316L}m_{316L} \tag{3.3}$$

$$\mathrm{M}_{Fe} = n_{Fe}m_{Fe} \tag{3.4}$$

The relationship between total masses of 316L and Fe particles impacting on coating surface is:

$$f_{Fe} = \frac{M_{Fe}}{M_{316L}+M_{Fe}} \tag{3.5}$$

The overall deposition efficiency of the mixed powder is then expressed as:

$$DE = \frac{dM_{316L}+dM_{Fe}}{M_{316L}+M_{Fe}} \tag{3.6}$$

Substituting Eqs. (3.1)-(3.5) into Eq. (3.6), the calculated mixed powder DE is then given as:

$$DE = f_{Fe} \times BR_{Fe} + (1 - f_{Fe}) \times BR_{316L} \tag{3.7}$$

Taking the BR values from Tables 3 and 4, the calculated DE of the mixed powder was determined and plotted in Fig. 3.8. It can be seen although being slightly lower in values, in general, the calculated DE exhibits a good correlation with the experimental DE, for both single component and mixed powders. This demonstrates that the approach of performing splat tests onto as-polished coatings can well reflect the DE of feedstock materials. This small deviation might be due to the contributions of "substrate" temperature, surface roughness and successive tamping in actual coating deposition, which are excluded during performing splat tests. Moreover, the partial DE 316L and DE Fe determined in consideration of the feedstock composition, coating composition and mixture DE were also plotted in Fig. 3.8. In general, the DE Fe is higher and relatively stable than the DE 316L in the mixed composition region, which explains the composition deviations of the composite coatings from initial feedstocks (Table 3.2).

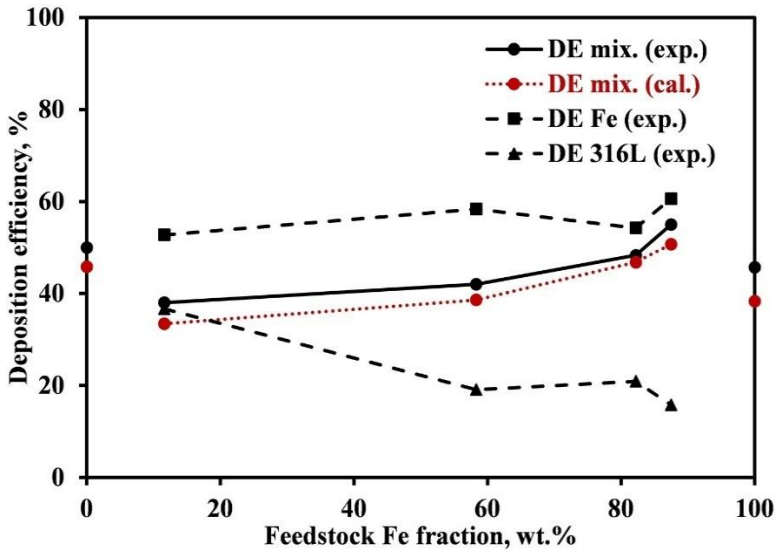

Fig. 3.8 Comparisons between the experimental and calculated DE results.

Furthermore, the BR results were used to determine the theoretical coating composition. The theoretical Fe content in the composite coatings is given as:

$$f_{cFe} = \frac{m_{Fe}}{m_{316L}+m_{Fe}} \tag{3.8}$$

Substituting Eqs. (3.1)-(3.5) into Eq. (3.8), the theoretical Fe content was determined and plotted with the measured results (Table 3.2) in Fig. 3.9. It shows that the calculated Fe fraction has a great coincidence with the measured Fe fraction. This indicates the BR results from splat tests can also be a valid metric of the partial DE of each component powder during mixed powder deposition.

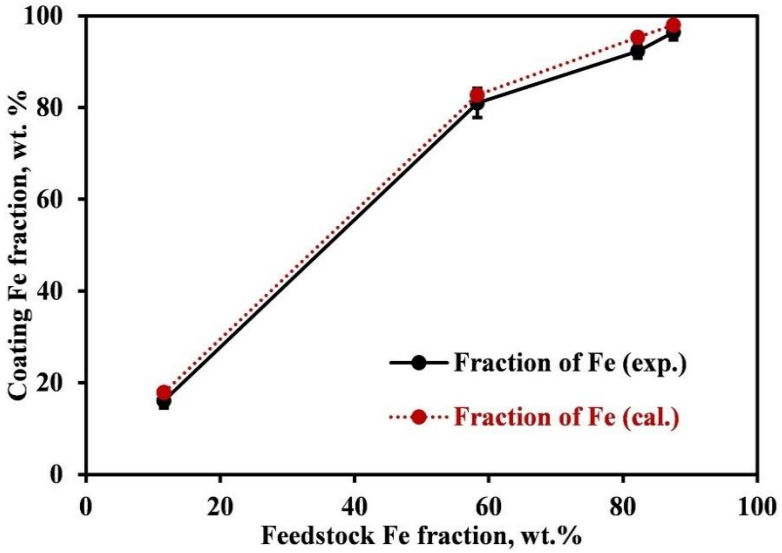

Fig. 3.9 Comparisons between the experimental and calculated Fe composition in the composite coatings.

3.5.2 Deposition behavior on the composite coatings

The expected splat BR on the composite coatings was made based on a hypothesis that the deposition behavior of an individual particle in cold spray is only related to the material at the impact interface, which has been validated by Sova et al. [3.10]. Following this theory, the expected BR is then calculated as an averaged contribution of splat impacts on single component coatings, weighted by the relative areas of the 316L and Fe components in the composite coatings (Table 3.2). Theoretically, both the 316L and Fe splats should exhibit a decreasing BR with an increasing feedstock Fe, since the Fe coating has exhibited a stronger rebound of impacting particles compared to 316L (Table 3.3). However, as shown in Fig. 3.10, only the 316L particles show a good correlation with the expected BR, whereas the Fe BR is independent of the composite composition. The high and insensitive value of Fe BR on the composite coatings can sufficiently explain the elevated DE at high Fe mixed regions; but the mechanisms behind the stable Fe

deposition behavior are still unclear. In particular, comparing the BR of 90Fe and Fe, only 3.6 wt.% 316L presence in Fe coating can "stimulate" an increase of the BR from 38.3% to 55%. It is speculated that there is a "substrate" effect for Fe impacts onto composite coatings, which involves not only the material at the impact interface, but also the surrounding and underlying previously deposited layers. Also, it appears that the results in this study contradict the previously mentioned hypothesis [3.10]. However, a careful examination of the cold spray process parameters reveals a new interpretation. In Sova's work [3.10], all the feedstocks were sprayed at a maximum particle acceleration and also the gun travel speed (10 mm/s) is low enough to generate sufficient substrate heating for deposition due to the high intensity particle impact. However, in this study, a significantly higher gun speed (300 mm/s) was used and the DE of 316L and Fe (50%-316L, 45%-Fe) is relatively low compared with their documented maximum DE (> 90%) [3.21]. Therefore, it is believed that the findings in this study could supplement the Sova's theory at a less optimal condition, e.g. low feedstock DE. But it is also understood that a complete interpretation of the splat deposition behavior should not be straightforward, since explanations might have to start from splat on the single component coatings and then to the composite coatings. Relevant studies are currently being carried out and will be presented in the future.

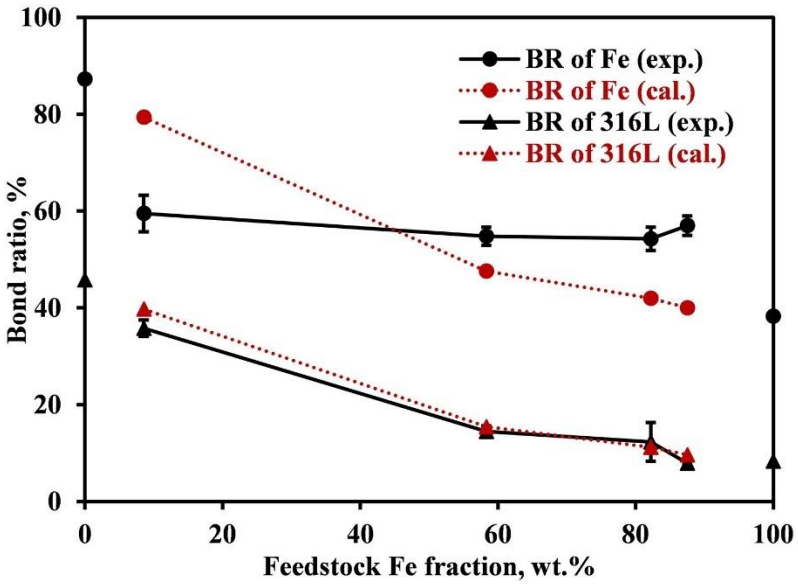

Fig. 3.10 Comparisons between the experimental and calculated BR of mixed powders.

3.6 Conclusion

In summary, single component 316L and Fe coatings, as well as composite 316L/Fe coatings were deposited through cold spray in this study. The DE of the mixed powder is found to increase with increasing feedstock Fe, although the single component Fe powder possesses an inferior DE to the 316L. Splat tests were performed onto the as-polished coatings to investigate the deposition behavior of the component powder during coating build-up. The BR results determined from splat tests have a good correlation with the DE of both single component powders and the mixed powders. The BR of 316L splats onto composite 316L/Fe coatings can be well predicted from the BR of 316L impacts onto each single component coating; whereas, the BR of Fe splats plateaus at a relatively high value regardless of composite coating composition, which results in the increase of overall mixture DE.

3.7 References

[3.1] S. Grigoriev, A. Okunkova, A. Sova, P. Bertrand, I. Smurov, Cold spraying: from process fundamentals towards advanced applications, Surf. Coat. Technol. 268 (2015) 77-84.

[3.2] K. Spencer, M.X. Zhang, Optimisation of stainless steel cold spray coatings using mixed particle size distributions, Surf. Coat. Technol. 205 (2011) 5135-5140.

[3.3] H.-T. Wang, C.-J. Li, G.-J. Yang, C.-X. Li, Cold spraying of Fe/Al powder mixture: coating characteristics and influence of heat treatment on the phase structure, Appl. Surf. Sci. 255 (2008) 2538-2544.

[3.4] X.-k. Wu, X.-l. Zhou, H. Cui, X. Zheng, J.-s. Zhang, Deposition behavior and characteristics of cold-sprayed Cu-Cr composite deposits, J. Therm. Spray Technol. 21 (2012) 792-799.

[3.5] B. Al-Mangour, R. Mongrain, E. Irissou, S. Yue, Improving the strength and corrosion resistance of 316L stainless steel for biomedical applications using cold spray, Surf. Coat. Technol. 216 (2013) 297-307.

[3.6] A. Sova, D. Pervushin, I. Smurov, Development of multimaterial coatings by cold spray and gas detonation spraying, Surf. Coat. Technol. 205 (2010) 1108-1114.

[3.7] S. Yue, W. Wong, H. Aydin, R. Mongrain, R. Barua, P. Vo, R. Dolbec, Improving cold sprayability: mixed metal powders, Proceedings of the International Thermal Spray Conference, USA, 2015, pp. 473-478.

[3.8] E. Irissou, J.-G. Legoux, B. Arsenault, C. Moreau, Investigation of Al-Al2O3 cold spray coating formation and properties, J. Therm. Spray Technol. 16 (2007) 661-668.

[3.9] H. Aydin, M. Alomair, W. Wong, P. Vo, S. Yue, Cold sprayability of mixed commercial purity Ti plus Ti6Al4V metal powders, J. Therm. Spray Technol. 26 (2017) 1-11.

[3.10] A. Sova, R. Maestracci, M. Jeandin, P. Bertrand, I. Smurov, Kinetics of composite coating formation process in cold spray: modelling and experimental validation, Surf. Coat. Technol. 318 (2017) 309-314.

[3.11] T. Van Steenkiste, J. Smith, R. Teets, Aluminum coatings via kinetic spray with relatively large powder particles, Surf. Coat. Technol. 154 (2002) 237-252.

[3.12] M. Fukumoto, M. Mashiko, M. Yamada, E. Yamaguchi, Deposition behavior of copper fine particles onto flat substrate surface in cold spraying, J. Therm. Spray Technol. 19 (2009) 89-94.

[3.13] S. Krebs, F. Gärtner, T. Klassen, Cold spraying of Cu-Al-bronze for cavitation protection in marine environments, J. Therm. Spray Technol. 45 (2014) 708-716.

[3.14] J. Wu, H. Fang, S. Yoon, H. Kim, C. Lee, The rebound phenomenon in kinetic spraying deposition, Scr. Mater. 54 (2006) 665-669.
[3.15] S. Yoon, J. Kim, G. Bae, B. Kim, C. Lee, Formation of coating and tribological behavior of kinetic sprayed Fe-based bulk metallic glass, J. Alloys Compd. 509 (2011) 347-353.
[3.16] Y. Xiong, G. Bae, X. Xiong, C. Lee, The effects of successive impacts and cold welds on the deposition onset of cold spray coatings, J. Therm. Spray Technol. 19 (2009) 575-585.
[3.17] F. Meng, S. Yue, J. Song, Quantitative prediction of critical velocity and deposition efficiency in cold-spray: a finite-element study, Scr. Mater. 107 (2015) 83-87.
[3.18] J. Frattolin, R. Barua, H. Aydin, S. Rajagopalan, L. Gottellini, R. Leask, S. Yue, D. Frost, O.F. Bertrand, R. Mongrain, Development of a novel biodegradable metallic stent based on microgalvanic effect, Ann. Biomed. Eng. 44 (2016) 404-418.
[3.19] R. Barua, Study of the Structural Properties and Control of Degradation Rate for Biodegradable Metallic Stents Using Cold Spray, PhD thesis, Department of Mechanical Engineering, McGill University, 2015.
[3.20] V.K. Champagne, D. Helfritch, P. Leyman, S. Grendahl, B. Klotz, Interface material mixing formed by the deposition of copper on aluminum by means of the cold spray process, J. Therm. Spray Technol. 14 (2005) 330-334.
[3.21] N. Espallargas, Future Development of Thermal Spray Coatings: Types, Designs, Manufacture and Applications, Elsevier, 2015.

Chapter 4

-

Investigation of the Feedstock Deposition Behavior in a Cold Sprayed 316L/Fe Composite Coating

In Chapter 3, single 316L or Fe particles (splats) were deposited onto as-polished coatings and different deposition behavior of each impact scenarios were observed. This chapter is an in-depth investigation towards the deposition behavior of four typical impact scenarios, i.e. 316L on 316L, 316L on Fe, Fe on 316L, Fe on Fe, which will occur during cold spray of mixed 316L/Fe powders.

This chapter has been published as:

- Xin Chu*, Rohan Chakrabarty, Hanqing Che, Lihong Shang, Phuong Vo, Jun Song, Stephen Yue, "*Investigation of the feedstock deposition behavior in a cold sprayed 316L/Fe composite coating*", Surf. Coat. Technol. 337 (2018), 53-62.

4.1 Abstract

Mixing powders in cold spray is a straightforward method to produce composite coatings, but a direct interpretation of the mixed powder deposition behavior from coating microstructure is often difficult. In this study, to investigate the feedstock deposition behavior in a cold sprayed 316L-10 wt.% Fe (10Fe) metal-metal composite coating, splats deposited onto the as-polished 316L and Fe coatings with four types of impact scenarios were studied: (i) 316L on 316L, (ii) 316L on Fe, (iii) Fe on 316L, and (iv) Fe on Fe. The splat flattening ratio and coating crater depth/diameter were measured using a light optical microscope (LOM) and an optical profilometer to evaluate the degrees of particle and coating deformation. Finite element (FE) simulations were performed to obtain the splat rebound behavior during impact. A modified ball bond shear test was performed to determine the adhesion strength/energy of the cold spray splats. Results reveal distinct interparticle bonding features in the 10Fe coating, especially at the mixed 316L/Fe interfaces where a preferential location of interlamellar cracks can be seen. Similar bonding features were also observed in the deposited splats, indicating the splat on coating tests to be indicative of the coating build-up process. Finally, the feedstock deposition behavior in the 10Fe coating was explained through splat characterizations and FE simulations from hardness, surface oxide layer and particle morphology.

4.2 Introduction

Cold spray can be an effective alternative to fabricate metal matrix composites (MMC) due to its low process temperature which minimizes the oxidation and chemical degradation of the feedstock. Some typical examples extensively studied by researchers are metal-ceramic composites, e.g. WC-based [4.1-4.6] and Al_2O_3-based [4.7-4.11]. Cold spray utilizes the plastic deformability of the metal thus the brittle ceramic can be deposited. Compared with metal-ceramic composites, however, relatively few studies of cold spraying metal-metal composites are reported, in particular, concerning the feedstock deposition behavior [4.12-4.14].

Among the various strategies to obtain composite coatings in cold spray, e.g. coating or mechanically milling the powders, mixing powders (pre-blending and dual feeding) is a straightforward approach [4.15, 4.16]. This method enables free interactions between the mixed components during flight and upon impact, which can lead to an improved cold sprayability of the component powder, e.g. reduced porosity and increased deposition efficiency (DE) [4.13, 4.17-4.21]. Whereas unlike metal-ceramic mixtures, where the impinging ceramic powders only contribute to tamping and roughening of the surface layers [4.20], almost all metal powders can exhibit certain degrees of cold sprayabilities and this generates uncertainties of the feedstock deposition behavior at mixed metal-metal interfaces. Thus, it is often difficult to prescribe the suitable process parameters for a specific metal-metal mixture in cold spray.

The coating formation process in cold spray incorporates, but is not limited to, the individual deposition behavior of a single particle [4.22]. Other factors such as characteristics of the previously deposited layers and the successive peening/erosion of the subsequent particles can all affect the individual particle deposition [4.22]. Individual particle impact tests (or splat tests) can be considered as a monolayer coating deposition and is often used to study the coating

deposition onset [4.23]. Due to the low investment in gas and feedstock material, the splat test is a suitable trial-and-error approach to explore the cold spray feasibility or to identify the optimal process parameters of specific particle/substrate combinations. As effects of successive tamping and surface roughness are avoided by performing splat tests, the individual behavior of a feedstock during deposition can be clearly observed, e.g. particle deformation, rebound, and jetting. Moreover, the splat behavior can often be indicative of several coating cold sprayability metrics (e.g. adhesion [4.24] and DE [4.25]) in the case of the similar particle and substrate material.

Splat tests are usually generated by low feed rate spraying of single particles onto an as-polished substrate. In a previous work [4.26], single component 316L, Fe, and composite 316L/Fe coatings were cold sprayed deposited and splat tests were performed onto the as-polished coatings. It was observed that the partial DE of the feedstock components in composite coatings can be indicated by the respective splat bond ratio in splat tests. This motivates us to study the single splats in order to investigate the feedstock deposition behavior in the composite coating, since a direct interpretation of it from coating microstructure is difficult. In this study, the feedstock deposition behavior in a 10Fe composite coating was mainly investigated. The interparticle bonding features in the cold sprayed coatings and deposited splats were discussed and compared. Experimental characterizations and finite element (FE) simulations of the splats were performed to explain the feedstock deposition behavior in the 10Fe coating.

4.3 Materials and methods

4.3.1 Experiments

Commercially available gas atomized 316L stainless steel powder (Sandvik Osprey, Neath-Port Talbot, UK) and water atomized commercial purity Fe powder (Quebec Metal Powders,

Sorel-Tracy, Canada) were used as the feedstock. SEM images of the feedstock are shown in Fig. 4.1 and characteristics of the feedstock are presented in Table 4.1. The average particle size was determined using a Horiba LA-920 laser diffraction analyzer (Horiba, Tokyo, Japan). The average Vickers hardness of the feedstock was measured using a Clark CM-100AT Microhardness Tester (Sun-Tec, Novi, USA) for a penetration time of 15 s under 10 g load. Spraying was performed at the McGill-NRC cold spray facility, located at the National Research Council Canada, Boucherville, using a Plasma Giken PCS-800 cold spray system (Plasma Giken, Yoriimachi, Japan) with a PNFC2-010-30S carbide nozzle. Nitrogen was used as the propellant gas and the process parameters were set at a gas preheating temperature of 700 °C, a gas pressure of 4 MPa, and a stand-off distance of 80 mm. Coatings with nominal compositions of 100 wt.% 316L (316L), 90 wt.% 316L-10 wt.% Fe (10Fe), and 100 wt.% Fe (Fe) were deposited (a dual feeder was used to deposit the composite coating) on mild steel substrates. The splat tests were performed by spraying 316L or Fe powder onto the single component 316L and Fe coatings. The coatings used as substrates for splat tests all have a thickness of about 1 mm in order to eliminate the effect of the mild steel substrate, and they were polished beforehand to a mirror surface. The process details regarding coating deposition and splat tests are shown in Table 4.2.

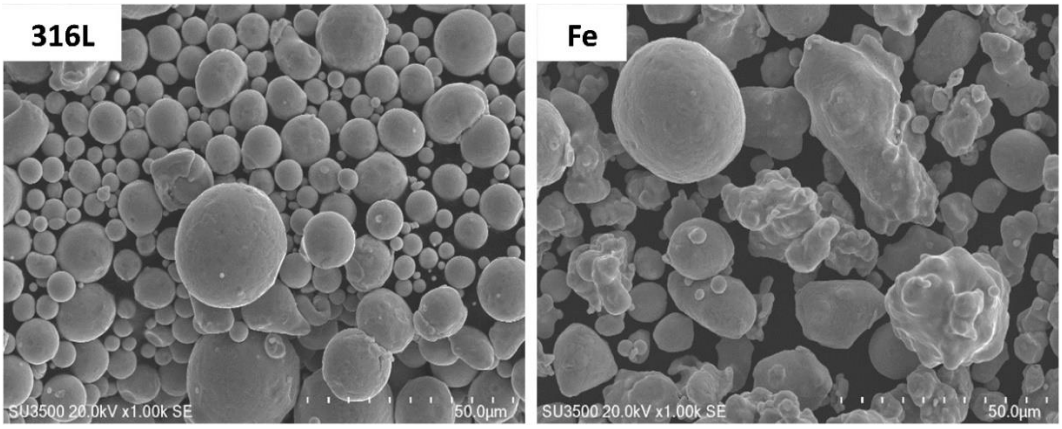

Fig. 4.1 SEM images of the feedstock powders.

Table 4.1 Characteristics of the feedstock powder.

Powder	Morphology	Size, μm	Microhardness, $HV_{0.01}$
316L	Spherical	22.2	262.6
Fe	Spherical, irregular	29.1	141.3

Table 4.2 Process details for coating deposition and splat tests.

Type	Feedstock	Substrate	Gun speed, mm/s	Feed rate, g/min	
				316L	Fe
Coating deposition	316L	Mild steel	300	23.8	-
	10Fe			18.3	2.4
	Fe			-	21.7
Splat test	316L	316L and Fe coatings	1000	8.5	-
	Fe			-	11

After coating deposition, DE was measured as the mass gain of the substrate divided by the total mass of spray material fed over the substrate. The coating cross-sections were characterized by a Hitachi SU3500 SEM (Hitachi, Tokyo, Japan). After splat tests, micrographs of coating surfaces and splats were observed by SEM. The splat deposition behavior was evaluated using bond ratio (BR). As previously discussed in [4.26], BR was determined as the average value of the fraction of the number of bonded particles (splats) to the total incident particles (splats + craters). The splats and craters from about 3-5 SEM images of the center of spray line with a field of 640 × 480 μm were counted for each impact scenario. The total numbers of splats + craters in a single image are about 240-300 for 316L impact and about 130-180 for Fe impact. The degree of

splat deformation was evaluated by the flattening ratio, which was calculated as the width over the height of a cross-sectioned splat. The degree of coating deformation was evaluated by a fraction of the depth of the crater over its diameter using a Zygo NewView 8000 optical profilometer (Zygo Corp., Middlefield, USA). Over 30 splats and craters were measured to calculate the respective flattening ratio and coating crater depth/diameter, and the average values were reported.

Splat adhesion tests were performed in reference to [4.24, 4.27] using a Micro-Combi Scratch Tester (CSM Instruments Inc., Needham, USA) equipped with a wedge-shaped stylus. Prior to testing, the average diameter of splat was measured by the integrated LOM to calculate the splat area (A). During tests, a constant normal force, F_N, of 100 or 300 mN was applied onto the stylus, which is 100 μm in the tip width. The substrate was moving at a 150 μm/min rate below the stylus to create a shearing behavior. When the stylus encountered the splat edge, the tangential force (F_T) gradually increased to a peak and then dropped sharply at splat failure (see Fig. 4.2). For each sample, between four to eight splats of 40 to 50 μm in diameter were shear tested. After testing, the adhesion strength was calculated using the peak tangential force (F_T(Peak)) subtracting the baseline tangential force (F_T(Baseline)). The adhesion energy (an energy required to debond the splat) was calculated by integrating the area under tangential force curve. This was normalized to the projected area of the splat (A). Similarly, the baseline friction force area was subtracted from the peak.

$$\text{Adhesion strength} = \frac{F_T(Peak) - F_T(Baseline)}{A} \tag{4.1}$$

$$\text{Adhesion energy} = \frac{\int_{Contact}^{Failure}(F_T(x) - F_T(Baseline))dx}{Projected\ Splat\ Area} \tag{4.2}$$

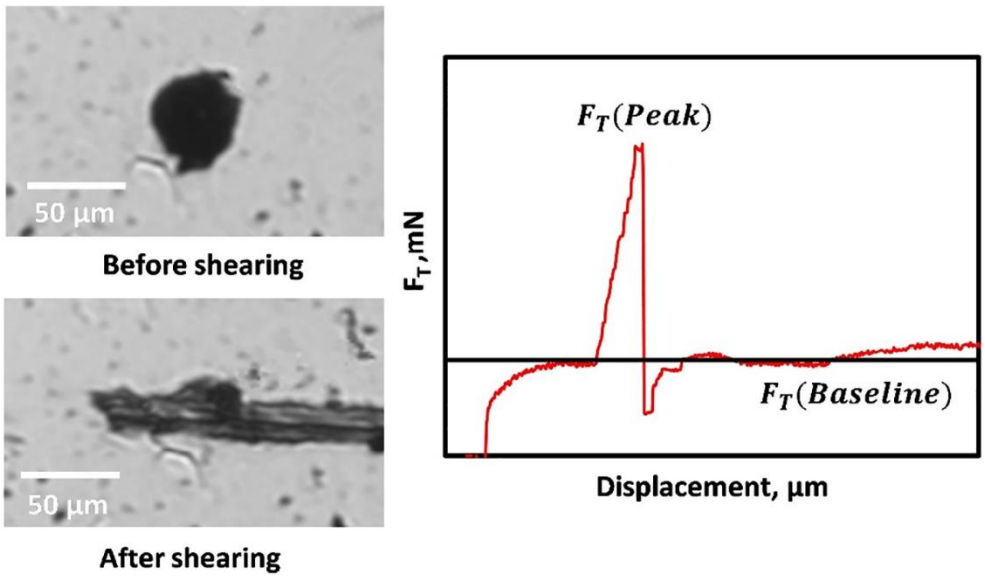

Fig. 4.2 Optical images of a splat before (top left) and after shearing (bottom left), and the respective load-displacement curve.

4.3.2 FE simulations

A 2D Lagrangian axisymmetric model was used to obtain the splat rebound behavior during impact using the FE analysis software ABAQUS/Explicit (version 6.11-1) [4.28]. The size of the feedstock was set to be the same as the one listed in Table 4.1. The velocities of the feedstocks were set at 585 m/s for 316L and 600 m/s for Fe, which were measured by a Coldspraymeter particle diagnostic system (Tecnar Automation, St. Bruno, CA) [4.20]. The dimensions of the substrate were set to be 10 times the particle radius to eliminate influence from boundary conditions. A 4-node bilinear plane strain quadrilateral mesh (CPE4R) was used for the simulation. A convergence study was carried out and a meshing resolution of 1/50 Dp (diameter of the particle) was considered for the particle and the substrate. This meshing resolution has been used in earlier studies [4.29, 4.30]. Distortion and hourglass controls were kept at default settings. Symmetry boundary conditions were imposed on the sides of the particle and substrate, while the

bottom of the substrate was fixed. The elastic response of the material was assumed isotropic while the plastic response of the material was described by the Johnson-Cook plasticity model [4.31].

$$\sigma = [A + B\varepsilon^n][1 + C \ln \dot{\varepsilon}^*][1 - T^{*m}] \tag{4.3}$$

$$T^{*m} = (T - T_{ref})/(T_m - T_{ref}) \tag{4.4}$$

where σ is the flow stress, ε is the equivalent plastic strain (PEEQ) defined as $\varepsilon = \int_0^t \sqrt{\frac{2}{3}\dot{\varepsilon}^{pl}:\dot{\varepsilon}^{pl}}dt$, with $\dot{\varepsilon}^{pl}$ being the plastic strain rate, $\dot{\varepsilon}^*$ is the equivalent plastic strain rate normalized by a reference strain rate, T_{ref} is reference transition temperature, and T_m is the melting temperature [25, 29, 30, 32]. In our simulations the deformation process is considered to be adiabatic due to the high rate of deformation, as previously explained by Assadi et al. [4.29]. The initial temperature of both the particle and substrate is kept at room temperatures (298 K). The material properties and parameters for the Johnson-Cook model are tabulated in Table 4.3 [4.26, 4.27].

To obtain the splat rebound behavior, the splat recoil coefficient e_r was determined. Recoil coefficient e_r defines the proportion of the particle kinetic energy to be rebounded upon impact due to elastic recovery and is given as [4.35]:

$$e_r = 11.47\left(\frac{\overline{\sigma}_Y^{\frac{5}{4}}}{E^*}\right)\rho_p^{-\frac{1}{4}}v_p^{-\frac{1}{2}} \tag{4.5}$$

where ρ_p, m_p, and v_p are respectively, the density, particle mass, and velocity of impacted particles, $\overline{\sigma}_Y$ is the particle effective yield stress during impact determined from FE simulations, and E^* is an elastic modulus that is experienced during particle impact.

Table 4.3 Material properties and parameters for Johnson-Cook model [4.33, 4.34].

Properties	Parameter	Unit	Value	
			316L	Fe
General	Density	kg/m^3	8000	7890
	Specific heat	$J/kg \cdot K$	500	452
	T_m	K	1668	1811
Elastic	Young's modulus	GPa	193	207
	Poisson's ratio	–	0.27	0.29
Plastic	A	MPa	514	175
	B	MPa	514	380
	n	–	0.508	0.32
	C	–	0.042	0.06
	m	–	0.533	0.55
	T_{ref}	K	293	293

4.4 Results

4.4.1 Characterization of coatings

The DE and BSE images of the single component 316L and Fe coatings are shown in Fig. 4.3. The 316L coating (Fig. 4.3 (a)) reveals small amounts of porosity (black regions) while the Fe (Fig. 4.3 (b)) has a dense structure. In cold sprayed coatings, the native oxide scales of the feedstock powder will be included and are presented between particles delineating as the interparticle boundaries (dark lines). By observing the interparticle boundaries of the 316L and Fe, a significant difference is revealed. The Fe/Fe particle interfaces in Fig. 4.3 (b) are seen to be wider and more clearly delineated compared to the 316L/316L interfaces in Fig. 4.3 (a), indicating a poorer interfacial bonding of the Fe coating than 316L. This feature can be attributed to the high

oxidation susceptibility of the Fe particles, and also appears to be consistent with a slightly inferior DE of the single component Fe to that of 316L (50% vs 55%). EDS scans were then performed on the 316L and Fe coatings at interparticle regions and also inner particle regions as a reference. As shown in Figs. 4.3 (c) and (d), the EDS spectra indicate the presence of oxygen at interparticle regions and the complete absence at inner particle regions. Thus, it is suggested that the dark lines in BSE images represent the oxide scale on the powder surface, and the Fe has a thicker oxide scale compared with 316L.

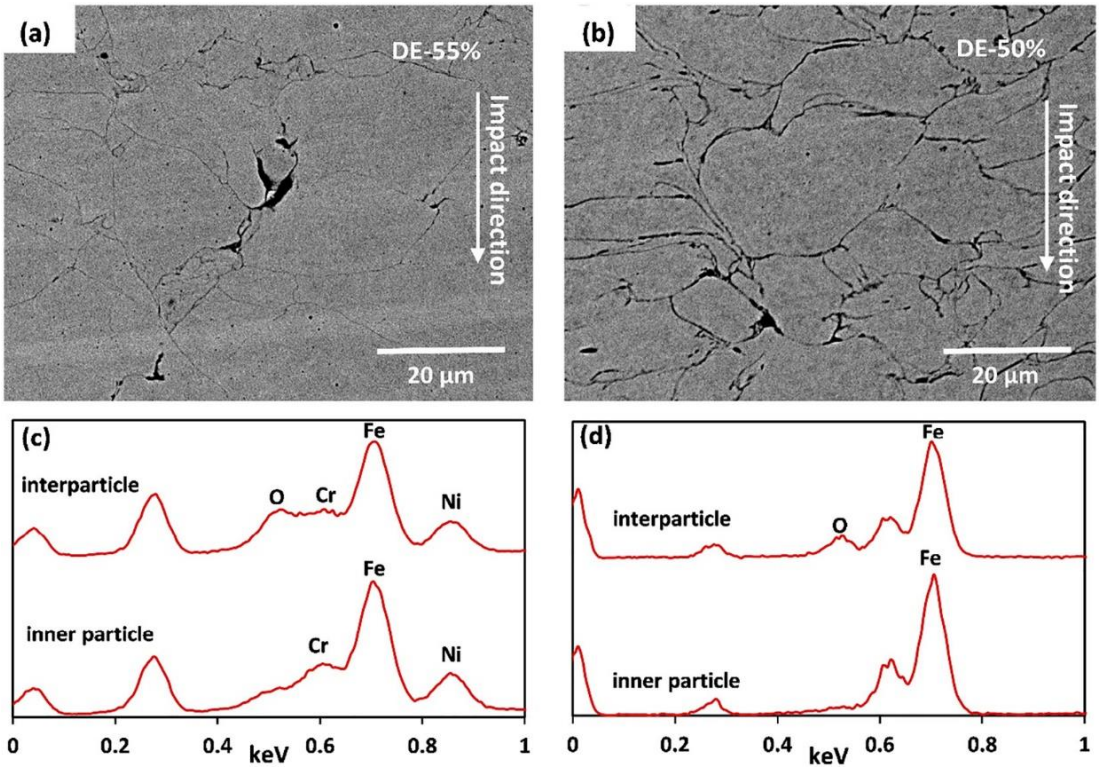

Fig. 4.3 SEM/EDS analyses on 316L (DE-55%) and Fe (DE-50%): (a) BSE image of 316L, (b) EDS spectrum of 316L, (c) BSE image of Fe, and (d) EDS spectrum of Fe.

The DE and BSE image of the 10Fe composite coating are shown in Fig. 4.4. The impact direction is indicated by the white arrow, and the dark regions are Fe, the light regions are 316L,

and the black spots are pores. For the 10Fe composite coating, the mixed 316L/Fe interfaces are generated. Firstly, comparing the non-mixed 316L/316L regions in 10Fe (Fig. 4.4) with those in single component 316L (Fig. 4.3 (a)), very similar optical characteristics, with few visible interparticle boundaries, are observed. This implies a blend of 10 wt.% Fe powder in the mixture has not affected the interfacial bonding of the matrix 316L powder in 10Fe. By looking at the mixed 316L/Fe interfaces in 10Fe, cracks are observed, as shown in Fig. 4.4, perpendicular to the impact direction. These inter-lamellar cracks can be considered as indicators of either poor interparticle bonding and/or a strong rebound of the impacted particles, which appears to explain the low DE of 10Fe (38%). It is also noticed that, the inter-lamellar cracks would mostly locate on the "top" of Fe and the "bottom" of 316L, as marked by red arrows. This observation implies a stronger rebound of 316L particles impacting on the previously deposited Fe compared with Fe on 316L.

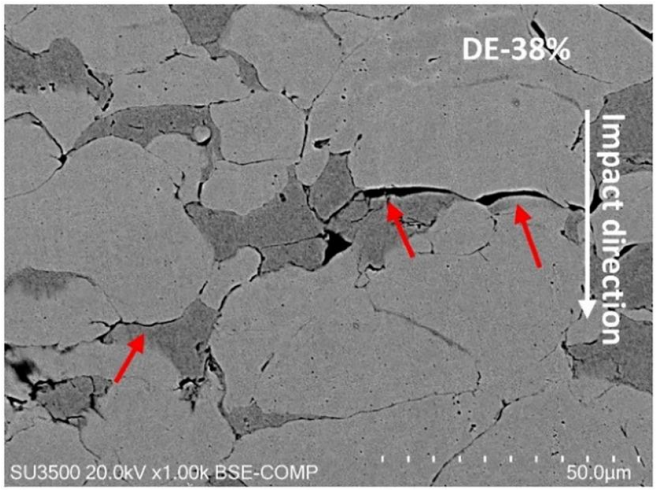

Fig. 4.4 BSE image of 10Fe (DE-38%). Red arrows: inter-lamellar cracks at the mixed 316L/Fe interfaces.

4.4.2 Characterization of splats

4.4.2.1 Splat morphology

The desire to explain the feedstock deposition behavior, especially at the mixed interfaces, leads to the effort of performing splat tests onto coatings. The coating SEM morphologies after splat tests are shown in Fig. 4.5. Four types of impact scenarios are generated, referred to as 316L on 316L, 316L on Fe, Fe on 316L and Fe on Fe below.

Results show that the different splat impact scenarios between the 316L and Fe give significantly different splat morphologies. For 316L on Fe (Fig. 4.5 (b)), some splats have shown an obvious lifting off at the edges (circled in red). However, the opposite case Fe on 316L (Fig. 4.5 (c)), reveals splats all being closely attached to the coating surface. This finding correlates with the previous observation of the preferential location of inter-lamellar cracks at the 316L/Fe mixed interfaces (Fig. 4.4). As for the impacts between same material, i.e. 316L on 316L and Fe on Fe, it appears the 316L splats exhibit a closer contact to 316L surface than Fe to Fe, as the latter case also exhibits some splats with lifted edges (circled in red in Fig. 4.5 (d)). This phenomenon is also consistent with the poorer interfacial bonding of Fe/Fe than 316L/316L, as previously observed in Figs. 4.4 (a) and (b). Therefore, it is considered that the splat on coating tests can be indicative of the coating build-up process.

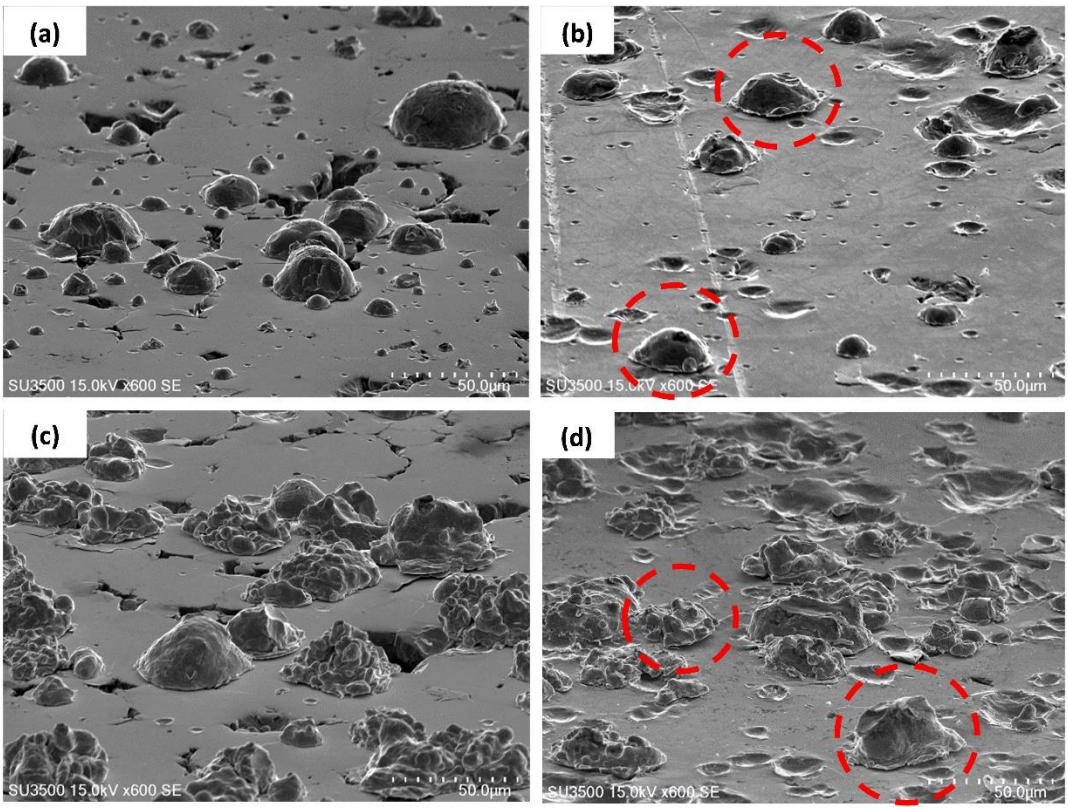

Fig. 4.5 SEM coating morphology after splat tests: (a) 316L on 316L, (b) 316L on Fe, (c) Fe on 316L, and (d) Fe on Fe.

4.4.2.2 Splat deposition and deformation behavior

To quantify the splat deposition behavior, the bond ratio (BR) for each impact scenario is plotted in Fig. 4.6 (a). The BR results explicitly show the distinct deposition behavior of impacts between dissimilar materials, i.e. 316L on Fe and Fe on 316L (8% vs 87%); whereas the deposition behavior of impacts between the same material is relatively similar (316L on 316L-45%, Fe on Fe-38%).

To explain the splat deposition behavior, the deformation levels of the splat and the coating were both quantified. The splat deformation behavior shown in Fig. 4.6 (b) was evaluated using

the common approach flattening ratio. The coating deformation shown in Fig. 4.6 (c) was evaluated by the average ratio of the depth of a crater over its diameter. It is believed this metric can normalize the effects of particle size and particle deforming on the coating deformation. Results show that the average FR values have a positive correlation with the BR results. The FR values can be explained by the relative particle/coating hardness, where a high FR is obtained from a soft particle impacting on the hard coating, e.g. Fe on 316L. Note that for the Fe splats with some irregular shape fractions, the splat FR might not reveal the actual particle deformation and is simply the splat aspect ratio. But it is believed that a high splat aspect ratio should similarly create a large particle/coating contact to facilitate deposition. As opposed to the splat deformation, in general, no correlations between the coating crater depth/diameter values and splat BR can be observed.

The rebound trend of a splat during impact was evaluated by the recoil coefficient e_r, which was determined from FE simulations (Section 4.3.2). The results for each impact scenario are plotted in Fig. 4.6 (d). In particular, a higher recoil coefficient is observed for the 316L on Fe (0.09) than Fe on 316L (0.05), which implies a higher proportion of the splat kinetic energy is transformed to initiate the splat rebound upon impact for the former case. This explains the preferential location of inter-lamellar cracks in the 10Fe coating (Fig. 4.4) and also the lower BR of 316L on Fe than Fe on 316L (Fig. 4.6 (a)). However, the recoil coefficient metric is observed to fail to explain the different BR of a splat onto 316L and Fe coatings (e.g. 316L on 316L and 316L on Fe have the same e_r but different BR). This finding implies that, apart from rebound, there might be other factors affecting the splat deposition to occur, e.g. adhesion, which will be discussed in Section 4.4.2.3.

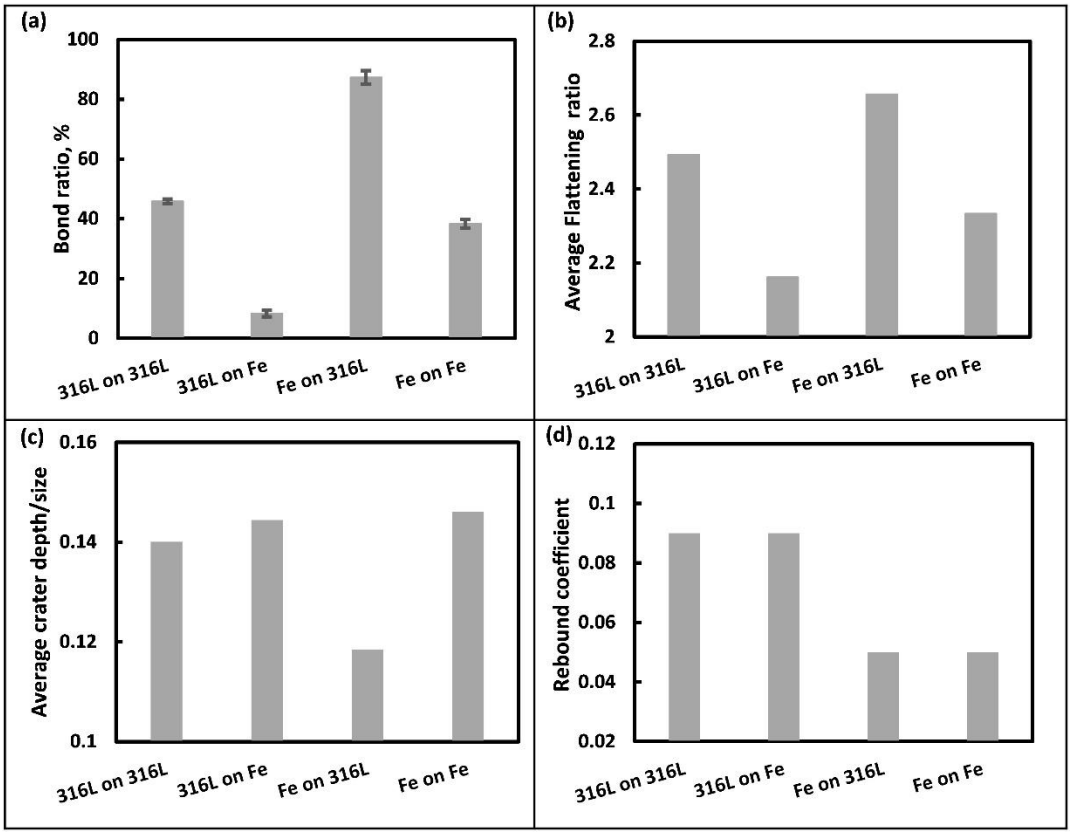

Fig. 4.6 (a) Bond ratio, (b) splat flattening ratio, (c) coating crater depth/size, and (d) recoil coefficient (from FE simulations) for each impact scenario.

4.4.2.3 Splat adhesion strength/energy

To quantify and compare the relative splat bond strength between different impact scenarios, the splat adhesion testing was performed. The experimental approach used in this study was similar to the previous investigators Goldbaum et al. [4.24, 4.27], but the splats being measured were deposited onto as-polished cold sprayed coatings instead of the bulk material substrate. The typical load-displacement curve for each impact scenario and the respective SEM morphology of the failure region are shown in Fig. 4.7. Results show three main types of splat shearing behavior of the different impact scenarios between 316L and Fe can be observed.

The first type, which is seen in 316L on Fe, shows only a small rise in the tangential force with tip displacement, indicating a poor splat adhesion strength. The failure region exhibits a presence of crater with an approximate size of the original splat (contour circled in red). No visible shear tracks are observed in the crater. This indicates the splat adhesion was mainly through a weak conformal bonding.

The second type, which is illustrated by Fe on Fe and 316L on 316L, shows the failure regions revealing a crater, but its size is smaller than the original splat (contour circled in red). The difference in radius between the crater and original splat is roughly the width of the tangential force peak. The peripheral regions where the shearing events mainly took place implies the formation of metallurgical bond in these regions. Examination of the respective load-displacement curves, however, reveals some different situations. For Fe on Fe, the tangential force peak appears to be higher and wider than the 316L on Fe (first type), but the difference is not significant. However, for 316L on 316L, there was a sharp rise in the tangential force and then followed by a rapid drop, and the peak tangential force has reached a high value of about 360 mN.

Finally, the third type is the Fe on 316L. It can be seen the sheared region gives a full outline of the splat and the width of the tangential peak is roughly the width of the original splat (contour circled in red). This type of phenomenon is considered to be comparable to the behavior of shearing a bulk material, and thus the splat is expected to have a high adhesion strength approaching the theoretical shear strength of the materials at the counterpart. Compared with the previous case 316L on 316L (second type), the peak value of the tangential force is lower, but there is a much smoother rise and drop. This feature could indicate either a higher proportion of the metallurgical bond formation or degree of particle deformation during the Fe impact.

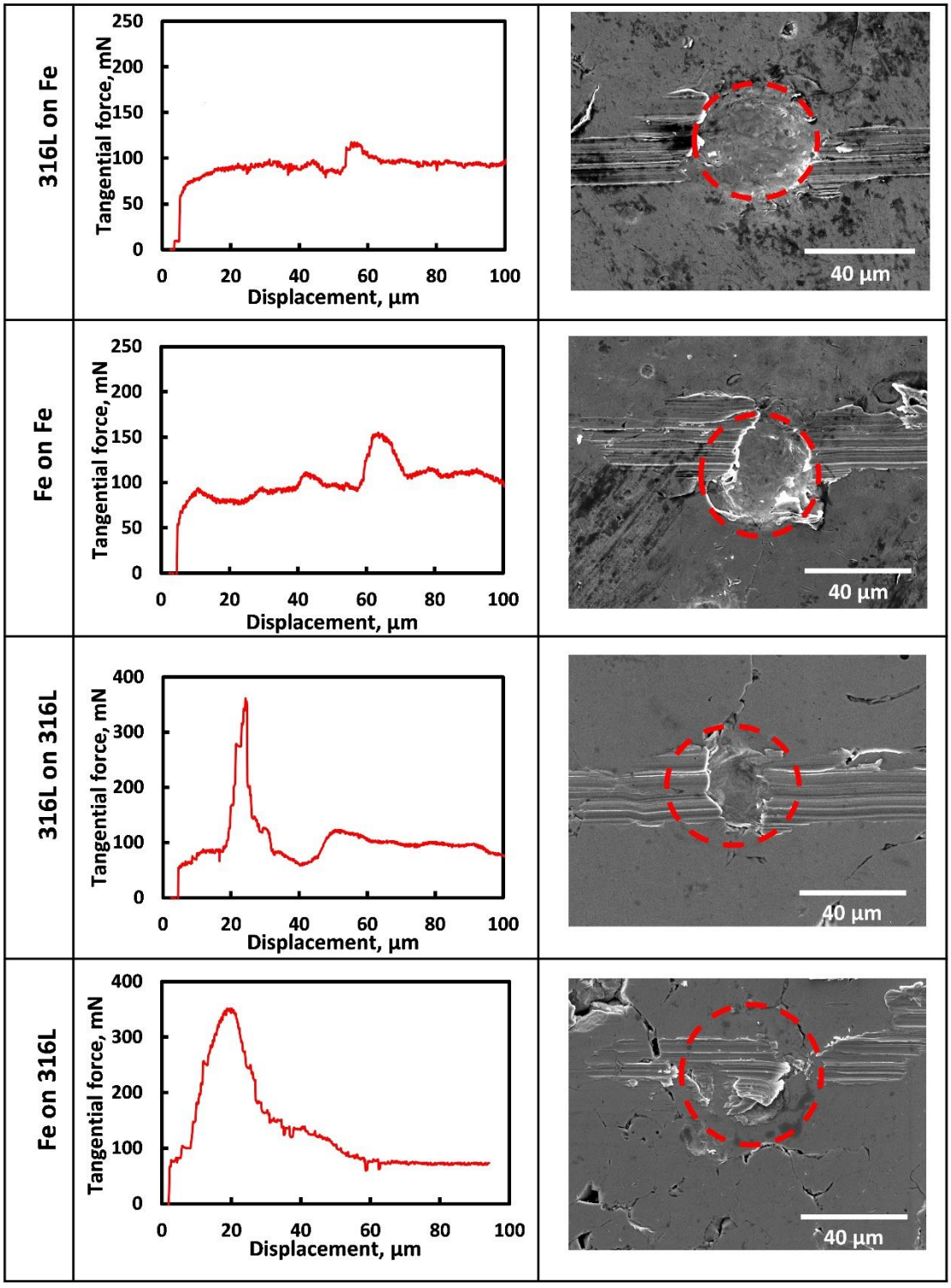

Fig. 4.7 Typical tangential force vs displacement curve with the respective SEM image of the failure region for each impact scenario (Red circles: contours of the original splats).

To further investigate the splat bonding features, the crater surfaces within the failure regions are shown in Fig. 4.8. For Fe on 316L (Fig. 4.8 (c)), a less well bonded splat (adhesion strength of 125 MPa) exhibiting the second type failure is presented instead. For 316L on 316L, some textures are observed at the crater surface. Considering that such features should not be resulted by the splat impact since the 316L powder has a smooth surface (Fig. 4.1), it is believed that they indicate the metallic bond formation at the crater region. For Fe on 316L and 316L on Fe, similarly, textures can also be observed in the crater surfaces, but appear to be finer than those in 316L on 316L. For Fe on Fe, however, the crater surface appears to be relatively smooth, which implies the adhesion in the crater was simply the weak conformal bonding.

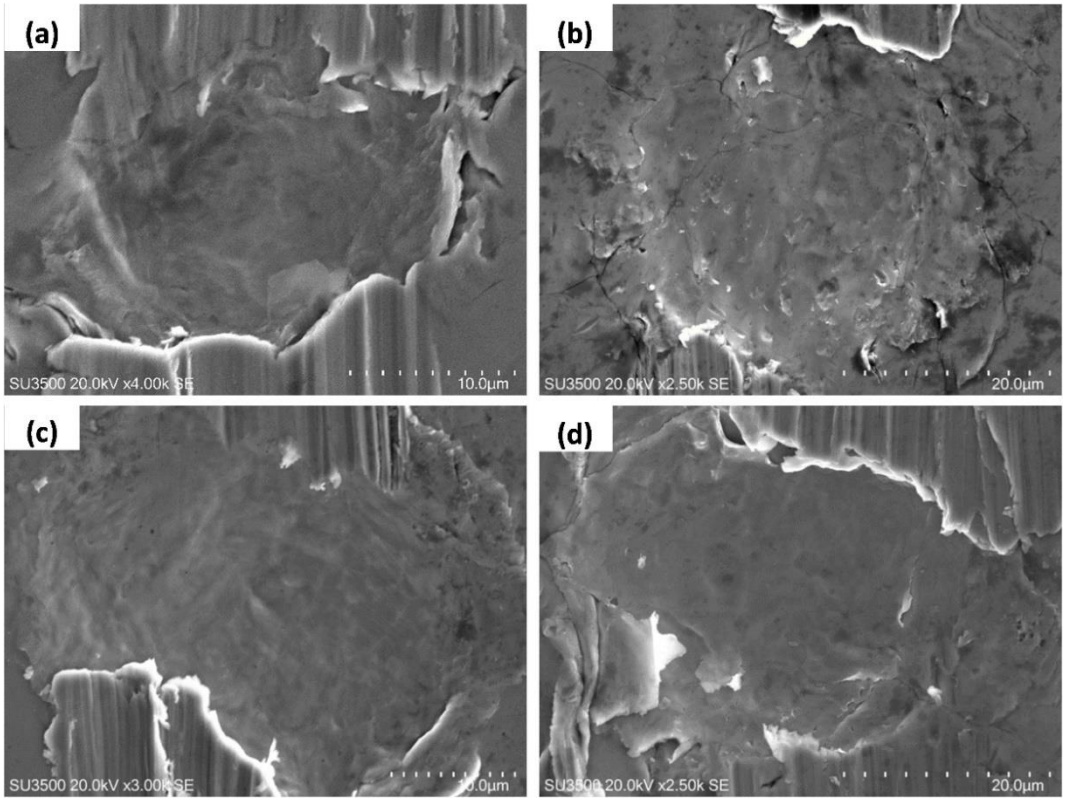

Fig. 4.8 High magnification SEM morphology of the crater failure surface: (a) 316L on 316L, (b) 316L on Fe, (c) Fe on 316L, and (d) Fe on Fe.

The adhesion strength and adhesion energy of each impact scenario were calculated from the respective load-displacement curve and are plotted in Fig. 4.9. As for the adhesion strength, the 316L on 316L (215 MPa) and Fe on 316L (167 MPa) are the two highest types, while the Fe on Fe and 316L on Fe types are the two lowest ones (< 50 MPa). Regarding the adhesion energy, the Fe on 316L with a smooth shear curve (Fig. 4.7) exhibits the highest adhesion energy, even higher than 316L on 316L (3 vs 1.6 kJ/m^2) despite its adhesion strength is lower (167 vs 215 MPa). Whereas the 316L on Fe and Fe on Fe types still exhibit a similar relative magnitude and remain the two lowest ones in adhesion energy. Moreover, it is noticed that the adhesion energy plots exhibit a positive correlation with the bond ratio results (Fig. 4.6 (a)). This result, combined with the rebound coefficient plots (Fig. 4.6 (d)), demonstrate the dominant contribution of adhesion energy in determining the splat BR.

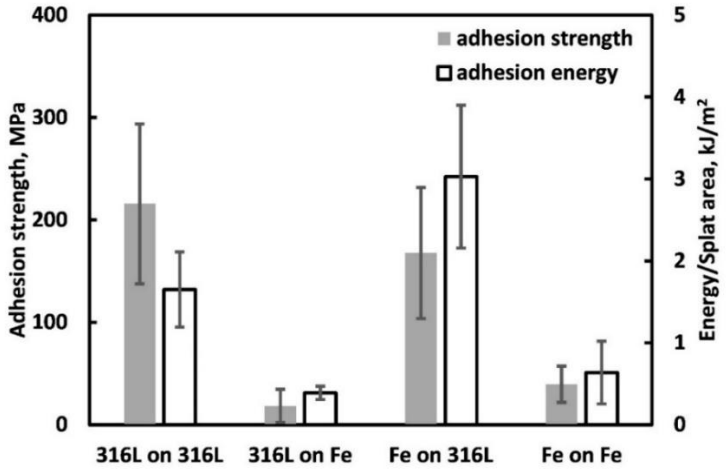

Fig. 4.9 Splat adhesion strength and adhesion energy for each impact scenario.

4.5 Discussion

Previous results (Fig. 4.6 (a)) have shown the distinct splat deposition behavior between the four impact scenarios, especially for impacts between the dissimilar materials (316L on Fe and

Fe on 316L), which corresponds to the mixed interface inter-lamellar cracks in the 10Fe coating (Fig. 4.4). To explain the splat deposition behavior, the powder characteristics (Table 4.1) and material properties (e.g. Table 4.3) of the feedstock were investigated. A few disparities between the 316L and Fe feedstocks are identified to be the contributing factors, i.e. hardness, surface oxide layer, and particle morphology, which are discussed individually as follows.

Hardness indicates the ability of a material to resist the plastic deformation. Generally, in cold spray, the soft particle can exhibit a high degree of deformation (e.g. flattening) during impact, which enlarges the particle/substrate interface contact to facilitate the mechanical anchorage effect [4.24, 4.36]. The high level of deformation at the interfaces can also help to disrupt the surface oxide layer and provide a direct metal-metal contact favoring the metallic bond formation [4.36, 4.37]. In this study, the 316L powder has almost double the microhardness of the Fe (262.6 $HV_{0.01}$ vs 141.3 $HV_{0.01}$). As the coatings on which splats deposit are the work hardened particle layers, most of the splat impact scenarios are categorized as the soft on hard case [4.30]. Thus, during cold spray, deformation at the impact interfaces tends to be mostly localized at the particle side rather than the coating. Comparing the impacts between dissimilar materials, the Fe on 316L type with a higher BR than 316L on Fe (87% vs 8%), corresponds to a higher particle FR (2.7 vs 2.2) and a shallower coating penetration (0.118 vs 0.144). Thus, it is considered for the soft on hard case, as the substrate is reluctant to deform during impact, the particle deformation can be more effective than the substrate deformation in facilitating particle deposition.

The splat deposition is considered as a competition between adhesion and rebound [4.35]. The hardness and the hardening behavior of the feedstock material also affect the rebound behavior of a splat during impact. According to Eq. (4.5), a higher recoil coefficient (stronger rebound) is associated with a higher dynamic yield strength of a particle, which is determined by its static yield

strength and the increment from effects of strain hardening, strain rate hardening and thermal softening during the kinetic impact process (Eq. (4.3)). As opposed to Fe, the 316L with a higher particle hardness implies a higher static yield strength, and its larger strain hardening parameter B and n (Table 4.2) also indicate a more rapid strain hardening behavior of the 316L during impact. Thus, this explains the stronger rebound of the 316L on Fe (preferentially located inter-lamellar cracks at the 316L/Fe interfaces) and the lower BR (8% vs 87%), as compared with the Fe on 316L case.

During cold spray, the formation of adiabatic shear instabilities (e.g. metal jetting) at impact interfaces is an effective material behavior to remove the interfacial oxide layer, and the accompanying heat can induce a locally molten region to form strong metallurgical bond [4.36]. However, the jetting phenomenon of the deposited splats is not clearly observed in any of the four cases (Fig. 4.5). This observation implies that, under these cold spray conditions, there will be a significant interfacial oxide layer effect. The chromium content in 316L can form a thin but tenacious chromium surface oxide layer to protect the inner material from further oxidation [4.38, 4.39]; while the iron oxide is reported to be unstable/porous in nature [4.40] thus the oxide film tends to be thicker in Fe. The difference in the oxide film thickness between 316L and Fe can be indicated by the different interparticle boundary conditions shown in Fig. 4.3. Evidence of the effect of oxide layer interference was found at the crater surfaces within the sheared regions (Fig. 4.8), where the Fe/Fe crater surfaces are smoother than any interfaces involving the 316L. This implies that metallurgical bonding is inhibited in the Fe/Fe case, which could be due to the thicker oxide layer being harder to disrupt during impact. The difference in surface oxide film thickness between the 316L and Fe feedstocks can contribute to the ease of particle deposition (higher BR) on the 316L coating as opposed to the Fe coating (Fig. 4.6 (a)).

In the adhesion strength/energy plots (Fig. 4.9), comparing the Fe on 316L with 316L on 316L, it is noticed that the former case has a lower adhesion strength (167 vs 215 MPa) but its adhesion energy is almost double that of the latter (3 vs 1.6 kJ/m^2). The high adhesion energy in Fe on 316L is attributed to its bulk-like shearing behavior during testing (Fig. 4.7), which implies the occurrence of either a higher proportion of metallurgical bond formation or degree of particle deformation during deposition. However, as discussed above, due to the thicker oxide film presence in the Fe feedstock, theoretically the metallurgical bond formation in the Fe on 316L case should be less favored than in 316L on 316L. Also, the difference in splat deformation (splat FR: Fe on 316L-2.66 vs 316L on 316L-2.50) appears not significant enough to result in such different shearing behavior. Thus, it is believed there is a significant effect of the irregular splat morphology on the splat adhesion. As reported in literature, the large surface area provided by the irregular powder could increase the particle/substrate contact during deposition, thus the mechanical interlocking effect is enhanced (compared with spherical ones) [4.41]. Also, the irregular morphology increases the stress concentration at the particle surface during impact, which is expected to facilitate the localized shear deformation and disruption of the surface oxide layer to help the metallurgical bond formation [4.41]. However, the contribution of the irregular morphology on the splat adhesion has not yet been quantitatively determined.

Overall, this study presents an approach of performing splats tests onto as-polished coatings to investigate the mixed powder deposition behavior, which is often difficult to interpret from coating microstructure. Theoretically, this approach can be extended to investigate powder mixtures of any number of components. However, it is understood that there might be issues of using this approach. Firstly, the splat on coating tests have avoided the effects of roughness and tamping which will occur during the actual coating deposition. This simplification was justified in

this case as the 316L and Fe feedstocks are similar in the particle size, velocity and density (Section 4.3). However, for other mixtures, e.g. hard/soft and large/small, where the tamping or retention effect of the component powder tends to be significant, the splat deposition behavior might not be indicative of the coating build-up process. Secondly, in order to investigate the 10Fe composite coating build-up process, the most straightforward approach is to directly spray single particles onto the as-polished 10Fe coatings. However, in this study an indirect approach was used as all splat tests were performed onto single component coatings for the ease of producing the specific impact scenarios. This thus generates a concern of the effect of different substrates on the splat deposition.

4.6 Conclusions

In this study, single component 316L, Fe, and a composite 10Fe coatings were cold spray deposited. A preferential location of inter-lamellar cracks was observed at the mixed 316L/Fe interfaces in the 10Fe coating. Splat tests were performed onto the as-polished single component 316L and Fe coatings and four types of impact scenarios (316L on 316L, 316L on Fe, Fe on 316L and Fe on Fe) were studied. Similar bonding features were observed in the deposited splats and cold spayed coatings, showing the splat on coating tests to be indicative of the coating build-up process. To investigate the feedstock deposition behavior in the 10Fe coating, experimental characterizations (deformation, adhesion) and FE simulations (rebound behavior) of the splats were performed. Finally, the feedstock deposition behavior in the 10Fe coating was explained from hardness, surface oxide layer, and particle morphology.

4.7 References

[4.1] C.-J. Li, G.-J. Yang, P.-H. Gao, J. Ma, Y.-Y. Wang, C.-X. Li, Characterization of nanostructured WC-Co deposited by cold spraying, J. Therm. Spray Technol. 16 (2007) 1011-1020.

[4.2] H.-J. Kim, C.-H. Lee, S.-Y. Hwang, Fabrication of WC-Co coatings by cold spray deposition, Surf. Coat. Technol. 191 (2005) 335-340.

[4.3] N. Melendez, A. McDonald, Development of WC-based metal matrix composite coatings using low-pressure cold gas dynamic spraying, Surf. Coat. Technol. 214 (2013) 101-109.

[4.4] P.-H. Gao, C.-J. Li, G.-J. Yang, Y.-G. Li, C.-X. Li, Influence of substrate hardness transition on built-up of nanostructured WC-12Co by cold spraying, Appl. Surf. Sci. 256 (2010) 2263-2268.

[4.5] P.-H. Gao, Y.-G. Li, C.-J. Li, G.-J. Yang, C.-X. Li, Influence of powder porous structure on the deposition behavior of cold-sprayed WC-12Co coatings, J. Therm. Spray Technol. 17 (2008) 742-749.

[4.6] R. Lima, J. Karthikeyan, C. Kay, J. Lindemann, C. Berndt, Microstructural characteristics of cold-sprayed nanostructured WC-Co coatings, Thin Solid Films 416 (2002) 129-135.

[4.7] K.J. Hodder, J.A. Nychka, A.G. McDonald, Comparison of 10 μm and 20 nm Al-Al2O3 metal matrix composite coatings fabricated by low-pressure cold gas dynamic spraying, J. Therm. Spray Technol. 23 (2014) 839-848.

[4.8] H. Koivuluoto, P. Vuoristo, Effect of powder type and composition on structure and mechanical properties of Cu + Al2O3 coatings prepared by using low-pressure cold spray process, J. Therm. Spray Technol. 19 (2010) 1081-1092.

[4.9] K. Spencer, D.M. Fabijanic, M.X. Zhang, The influence of Al2O3 reinforcement on the properties of stainless steel cold spray coatings, Surf. Coat. Technol. 206 (2012) 3275-3282.

[4.10] H.Y. Lee, S.H. Jung, S.Y. Lee, Y.H. You, K.H. Ko, Correlation between Al2O3 particles and interface of Al-Al2O3 coatings by cold spray, Appl. Surf. Sci. 252 (2005) 1891-1898.

[4.11] Y. Tao, T. Xiong, C. Sun, H. Jin, H. Du, T. Li, Effect of α-Al2O3 on the properties of cold sprayed Al/α-Al2O3 composite coatings on AZ91D magnesium alloy, Appl. Surf. Sci. 256 (2009) 261-266.

[4.12] X.-k. Wu, X.-l. Zhou, H. Cui, X. Zheng, J.-s. Zhang, Deposition behavior and characteristics of cold-sprayed Cu-Cr composite deposits, J. Therm. Spray Technol. 21 (2012) 792-799.

[4.13] H. Che, X. Chu, P. Vo, S. Yue, Cold spray of mixed metal powders on carbon fibre reinforced polymers, Surf. Coat. Technol. 329 (2017) 232-243.
[4.14] A. Sova, R. Maestracci, M. Jeandin, P. Bertrand, I. Smurov, Kinetics of composite coating formation process in cold spray: modelling and experimental validation, Surf. Coat. Technol. 318 (2017) 309-314.
[4.15] A. Moridi, S.M. Hassani-Gangaraj, M. Guagliano, M. Dao, Cold spray coating: review of material systems and future perspectives, Surf. Eng. 30 (2014) 369-395.
[4.16] S. Grigoriev, A. Okunkova, A. Sova, P. Bertrand, I. Smurov, Cold spraying: from process fundamentals towards advanced applications, Surf. Coat. Technol. 268 (2015) 77-84.
[4.17] X.-T. Luo, Y.-K. Wei, Y. Wang, C.-J. Li, Microstructure and mechanical property of Ti and Ti6Al4V prepared by an in-situ shot peening assisted cold spraying, Mater. Des. 85 (2015) 527-533.
[4.18] R.G. Maev, V. Leshchynsky, Air gas dynamic spraying of powder mixtures: theory and application, J. Therm. Spray Technol. 15 (2006) 198-205.
[4.19] H. Koivuluoto, P. Vuoristo, Effect of ceramic particles on properties of cold-sprayed Ni-20Cr + Al2O3 coatings, J. Therm. Spray Technol. 18 (2009) 555-562.
[4.20] E. Irissou, J.-G. Legoux, B. Arsenault, C. Moreau, Investigation of Al-Al2O3 cold spray coating formation and properties, J. Therm. Spray Technol. 16 (2007) 661-668.
[4.21] H. Aydin, M. Alomair, W. Wong, P. Vo, S. Yue, Cold sprayability of mixed commercial purity Ti plus Ti6Al4V metal powders, J. Therm. Spray Technol. 26 (2017) 1-11.
[4.22] T. Van Steenkiste, J. Smith, R. Teets, Aluminum coatings via kinetic spray with relatively large powder particles, Surf. Coat. Technol. 154 (2002) 237-252.
[4.23] Y. Xiong, G. Bae, X. Xiong, C. Lee, The effects of successive impacts and cold welds on the deposition onset of cold spray coatings, J. Therm. Spray Technol. 19 (2009) 575-585.
[4.24] D. Goldbaum, J.M. Shockley, R.R. Chromik, A. Rezaeian, S. Yue, J.-G. Legoux, E. Irissou, The effect of deposition conditions on adhesion strength of Ti and Ti6Al4V cold spray splats, J. Therm. Spray Technol. 21 (2011) 288-303.
[4.25] F. Meng, S. Yue, J. Song, Quantitative prediction of critical velocity and deposition efficiency in cold-spray: a finite-element study, Scr. Mater. 107 (2015) 83-87.

[4.26] X. Chu, H. Che, P. Vo, R. Chakrabarty, B. Sun, J. Song, S. Yue, Understanding the cold spray deposition efficiencies of 316L/Fe mixed powders by performing splat tests onto as-polished coatings, Surf. Coat. Technol. 324 (2017) 353-360.

[4.27] R.R. Chromik, D. Goldbaum, J.M. Shockley, S. Yue, E. Irissou, J.-G. Legoux, N.X. Randall, Modified ball bond shear test for determination of adhesion strength of cold spray splats, Surf. Coat. Technol. 205 (2010) 1409-1414.

[4.28] D. Simulia, Abaqus 6.11 analysis user's manual, Abaqus 6.11 Documentation, 22 2011, p. 22.

[4.29] H. Assadi, F. Gärtner, T. Stoltenhoff, H. Kreye, Bonding mechanism in cold gas spraying, Acta Mater. 51 (2003) 4379-4394.

[4.30] G. Bae, Y. Xiong, S. Kumar, K. Kang, C. Lee, General aspects of interface bonding in kinetic sprayed coatings, Acta Mater. 56 (2008) 4858-4868.

[4.31] G.R. Johnson, W.H. Cook, A constitutive model and data for metals subjected to large strains, high strain rates and high temperatures, Proceedings of the 7th International Symposium on Ballistics, The Netherlands, 1983, pp. 541-547.

[4.32] M. Grujicic, C.L. Zhao, W.S. DeRosset, D. Helfritch, Adiabatic shear instability based mechanism for particles/substrate bonding in the cold-gas dynamic-spray process, Mater. Des. 25 (2004) 681-688.

[4.33] The influence of johnson-cook parameters on SPH modeling of orthogonal cutting of AISI 316L, 10th European LS-DYNA Conference, 2015 Würzburg, Germany.

[4.34] O. Bielousova, J. Kocimski, R.G. Maev, I. Smurov, W. Scharff, V. Leshchynsky, Localisation of deformation in cold gas dynamic spraying, Surf. Eng. 32 (2016) 655-662.

[4.35] J. Wu, H. Fang, S. Yoon, H. Kim, C. Lee, The rebound phenomenon in kinetic spraying deposition, Scr. Mater. 54 (2006) 665-669.

[4.36] T. Hussain, D.G. McCartney, P.H. Shipway, D. Zhang, Bonding mechanisms in cold spraying: the contributions of metallurgical and mechanical components, J. Therm. Spray Technol. 18 (2009) 364-379.

[4.37] T. Samson, D. MacDonald, R. Fernández, B. Jodoin, Effect of pulsed waterjet surface preparation on the adhesion strength of cold gas dynamic sprayed aluminum coatings, J. Therm. Spray Technol. 24 (2015) 984-993.

[4.38] P.S. Korinko, S.H. Malene, Considerations for the weldability of types 304L and 316L stainless steel, Pract. Fail. Anal. 1 (2001) 61-68.
[4.39] S. Tardio, M.-L. Abel, R.H. Carr, J.E. Castle, J.F. Watts, Comparative study of the native oxide on 316L stainless steel by XPS and ToF-SIMS, J. Vac. Sci. Technol. A 33 (2015) 05E122.
[4.40] C. Leygraf, I.O. Wallinder, J. Tidblad, T. Graedel, Atmospheric Corrosion, John Wiley & Sons, New York, 2016.
[4.41] L. Ajdelsztajn, B. Jodoin, J.M. Schoenung, Synthesis and mechanical properties of nanocrystalline Ni coatings produced by cold gas dynamic spraying, Surf. Coat. Technol. 201 (2006) 1166-1172.

Chapter 5

-

A Multiple Particle Arrangement Model to Understand Cold Spray Characteristics of Bimodal Size 316L/Fe Powder Mixtures

In Chapters 3 and 4, the distinct particle deposition behavior at mixed 316L/Fe impact interfaces (i.e. 316L on Fe, Fe on 316L) was observed and in-depth knowledge was obtained. In this Chapter, the coating microstructure and cold sprayability (deposition efficiency (DE), porosity, bond strength) of cold sprayed bimodal size 316L/Fe powder mixtures were studied, and results show strong effects of mixing powders. To explain the observed effects, several associated deposition mechanisms of bimodal size 316L/Fe powder mixtures were discussed, and a multiple particle arrangement model was proposed.

This chapter has been accepted by Surf. Coat. Technol.:

- Xin Chu, Hanqing Che*, Chaoyi Teng, Phuong Vo, Stephen Yue, "*A multiple particle arrangement model to understand cold spray characteristics of bimodal size 316L/Fe powder mixtures*", 2019.

5.1 Abstract

Cold spray of mixed metal powders is of significant research interest as it often generates unpredictable effects on deposition efficiency (DE) and porosity. Thus, analyzing the cold spray characteristics of two metal powders can lead to a better understanding of mechanisms of cold spray deposition and consolidation. In this study, average 43 μm 316L stainless steel and 22 μm commercial purity Fe powders were used as feedstock. The following coatings were deposited through cold spray: single component 316L and Fe, and their binary composites with different feedstock mixing compositions of 316L-20 wt.% Fe (20Fe), 316L-50 wt.% Fe (50Fe), and 316L-80 wt.% Fe (80Fe). Results show that the composite coating microstructure and cold sprayability (DE, porosity, coating bond strength) exhibit strong effects of mixing powders. Several particle and coating metrics (particle in-flight velocity, coating flattening ratio, coating microhardness) were also measured to further exhibit the effects of mixing. To explain these observations, a multiple particle arrangement model based on the calculated particle number fraction of the mixture is proposed. Using this model, mechanisms associated with the deposition of bimodal size 316L/Fe powder mixtures are discussed, and the effects of mixing powders on the cold spray characteristics are explained accordingly.

5.2 Introduction

Cold spray of mixed metal powders has attracted considerable attention in the past few years [5.1-5.3]. Foremost, it is a straightforward (does not require complicated feedstock pre-processing) approach to fabricate novel metal-metal composites and intermetallics (via post spray heat treatment). Due to the low process temperature (solid state deposition) and protective process gas atmosphere in cold spray, severe feedstock oxidation or other chemical degradation can be minimized [5.4-5.6]. Some examples of previous explorations include: Al/(Ti [5.4], Ni [5.5], Fe [5.6], Zn [5.7]), 316L/Co-Cr [5.8], Cu/(W [5.9], Cr [5.10]). Alternatively, the mixing approach can also be applied to powders of the same alloy but different characteristics (e.g. sizes and hardnesses). For instance, mixing the readily available fine and coarse powders can be a practical approach, when powders of the desired size are commercially unavailable or there is only a limited supply. Spencer et al. [5.11] also found that 316L coatings fabricated using mixed particle size distributions can exhibit similar coating properties to those from fine particles alone, but without any processing issues of fine particles such as inconsistent feeding or nozzle fouling. Moreover, cold spraying mixed metal powders is of significant research interest as it has been observed to generate interesting (i.e. unpredictable) effects on the feedstock cold sprayability, e.g. deposition efficiency (DE) [5.12, 5.13] and porosity [5.14]. Thus, fundamentally, analyzing the cold spray characteristics of two metal powders with different characteristics (e.g. materials, sizes, and morphologies) can lead to a better understanding of the mechanisms of cold spray deposition and consolidation [5.15]. However, most cold spray studies of mixed metal powders are centered on producing materials with novel properties, and the mechanisms behind the cold spray characteristics are often vaguely understood. Challenges remain in understanding the mixed powders deposition, e.g. i) how to expect the cold sprayability of a certain mixture by knowing

that of the individual component; ii) what is the compositional yield, i.e. deposited composition vs initial feedstock. These issues have been found to partly arise from the uncertainties of feedstock deposition behaviors at mixed metal-metal interfaces [5.16, 5.17].

In this study, mixtures of average 43 μm 316L stainless steel and 22 μm commercial purity Fe powders were investigated as part of an overall effort to produce metal-metal composites with controlled galvanic corrosion properties for bio-degradable implants [5.18]. There are also other reasons that justify studying this particular mixture: (i) the two powders can be conveniently separated by metallography, thus it is possible to individually investigate the component behavior after deposition; (ii) the mixed impact interface effects are known, i.e. 316L on Fe: strong rebound, Fe on 316L: well adhered [5.16, 5.17]; (iii) the two powders are both Fe-based alloys and of similar characteristics e.g. melting point and density [5.19, 5.20], thus, the insights gained might be generic to other same species bimodal size mixtures. Coatings of the single component 316L, Fe, and the binary composites with three nominal compositions (20Fe, 50Fe, 80Fe) were made by cold spray. The coating microstructure was characterized, cold sprayability metrics (DE, porosity, coating bond strength strength) were measured, and particle and coating metrics (particle in-flight velocity, coating flattening ratio, coating microhardness) were analyzed. Based on the results, several mechanisms associated with the deposition of bimodal size 316L/Fe mixtures are proposed. Finally, the effects of mixing powders on the cold spray characteristics are discussed.

5.3 Materials and methods

Commercially available gas atomized 316L stainless steel and commercial purity Fe powders provided by Sandvik Osprey Limited (Neath Port Talbot, UK) were used as feedstock. SEM images of the feedstock are shown in Fig. 5.1 and characteristics of the feedstock are

presented in Table 5.1. The volume weighted particle size distribution (PSD) was determined using a Horiba LA-920 laser diffraction analyzer (Horiba, Tokyo, Japan). The average Vickers hardness was measured using a Clark CM-100AT Microhardness Tester (Sun-Tec, Novi, USA) for a penetration time of 15 s under 10 g load. Both the feedstock powders are spherical, and the 316L is about twice the average size of the Fe whereas the Fe is slightly harder than the 316L.

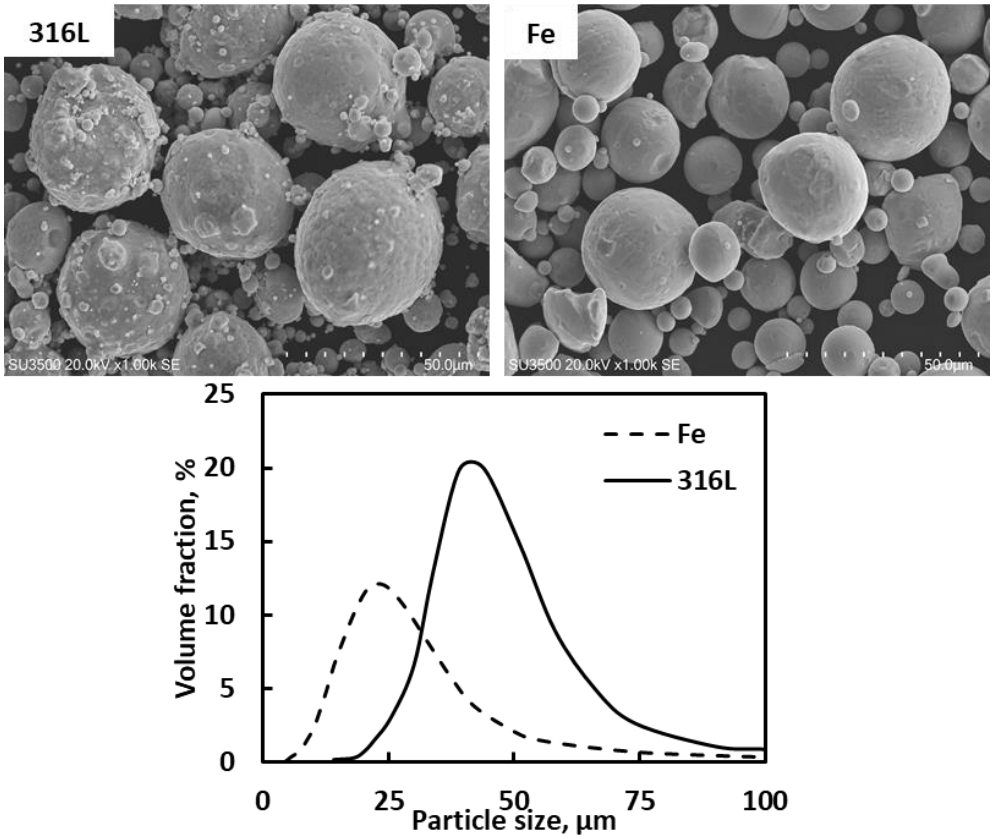

Fig. 5.1 SEM images and volume weighted PSDs of the feedstock powders.

Table 5.1 Characteristics of the feedstock powders.

Powder	Morphology	$HV_{0.01}$	Mean size, µm
316L	Spherical	239	43
Fe		292	22

Spraying was performed at the McGill-NRC cold spray facility, located at the National Research Council of Canada, Boucherville, using a KINETIKS® 4000 cold spray system (Oerlikon Metco, Westbury, USA) with a MOC24 tungsten carbide nozzle. Nitrogen was used as the propellant gas and the process parameters were set at a gas preheating temperature of 700 °C, a gas pressure of 4 MPa, and a stand-off distance of 80 mm, a gun traverse speed of 300 mm/s, and a step size of 1 mm. Coatings with feedstock mixing compositions of 100 wt.% 316L (316L), 316L-20 wt.% Fe (20Fe), 316L-50 wt.% Fe (50Fe), 316L-80 wt.% Fe (80Fe) and 100 wt.% Fe (Fe) were deposited. Prior to spraying, the mixed feedstock was admixed in a rolling mixer (without media) for 1 hour. The substrates used were 100 mm×100 mm×3 mm Al 6061 plates, which were blasted with 24 grit alumina to remove scale and roughen the surface to promote adhesion. The feedstock was sprayed at a feed rate of 19.5 to 24.1 g/min using 4-6 spray passes and roughly 2 mm thick coatings were produced per sample.

After spraying, coating cross-sections were observed under an optical microscope (OM). The weight fractions of the 316L and Fe particles in composite coatings and the coating porosity were measured by image analyses using a minimum of 10 random optical images captured at 100× or 200× magnification. The weight fractions of 316L and Fe particles in composite coatings were measured by image analyses using 5 random EDS maps captured at 200× magnification. The average values of the coating composition and porosity as well as their standard deviations were reported. The DE was determined as the mass gain of the substrate divided by the total mass of spray material fed over the substrate. The coating bond strength was measured using tensile pull-off tests at a constant strain rate of 1 mm/min following the ASTM C633-01 standard [5.21]. The HTK Ultrabond 100 (HTK Hamburg GmbH, Hamburg-Sasel, Germany) epoxy adhesive was used

to join the sample with couplings and was cured in air at 190 °C for 35 mins under a load of 100 N to ensure proper adhesion.

To further exhibit the effects of mixing powders, several particle and coating metrics were also determined. The particle in-flight velocity was measured in a free jet by an optical time-of-flight ColdSprayMeter particle diagnostic system (Tecnar Automation, St. Bruno, Canada) [5.22] under the same process parameters as coating deposition. Velocities of 5000 particles were measured and the average value and standard deviation were calculated for each powder. Particle velocities of single component Fe and 316L/Fe mixtures with compositions of 90 wt.% Fe, 80 wt.% Fe, 65 wt.% Fe, and 40 wt.% Fe were measured. The coating flattening ratio was calculated as the width to height ratio of a deformed particle from etched optical images of coating cross-sections captured at 200× magnification and the average value was reported about 50 particles per component per sample. The standard error of four average flattening ratio values was also calculated. The coating microhardness was obtained through Vickers indentations at center regions of the deposited 316L and Fe particles using about 15 measurements per sample for a penetration time of 15 s under 50 g load.

5.4 Results

5.4.1 Coating microstructure

The as-polished optical cross-sectional microstructure of the single component 316L and Fe coatings are shown in Fig. 5.2. A few pores (black spots) are observed in both coatings, but a higher quantity is presented in the Fe. As for the interparticle bonding, the Fe/Fe interparticle

boundaries are more clearly delineated, as compared with the 316L/316L boundaries which are not visible.

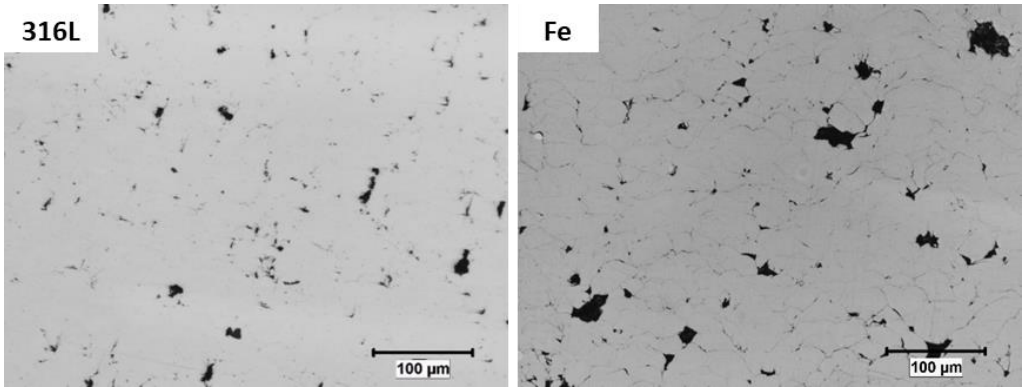

Fig. 5.2 Optical cross-sectional microstructure of the single component 316L and Fe coatings.

The as-polished optical cross-sectional microstructure of the composite 316L/Fe coatings is shown in Fig. 5.3. The light regions are 316L, dark regions are Fe, and black spots are pores. In general, very different characteristics can be seen in different composition coatings. For 20Fe, certain amounts of pores and interparticle defects are observed and are mainly located at the mixed 316L/Fe interfaces, which implies the 316L/Fe mixed interfaces are the "sources" of defects during deposition. Also, the preferentially located defects (on "top" of Fe and "bottom" of 316L) are present (arrowed in red), which has been previously discussed in [5.16, 5.17] and is attributed to the poor deposition/adhesion of 316L on Fe impacts due to the strong rebound trend of 316L particles and thick oxide layer of the Fe "substrate". For 50Fe, the coating is very dense and the interparticle boundaries (mixed and non-mixed) all exhibit very few defects, implying excellent bonding conditions. For 80Fe, pores are present but fewer than in 20Fe. As for the interparticle boundaries, different characteristics are seen, where the mixed interfaces have good bonding conditions while the non-mixed Fe/Fe bonding is relatively poor. To sum, in terms of the quantity of defects (i.e. pores and interparticle defects), the 20Fe is most inferior and the 50Fe is most

superior. Moreover, by looking at the 316L on Fe interfaces in each coating, the preferentially located defects are found to be present in 20Fe and almost absent in 50Fe and 80Fe.

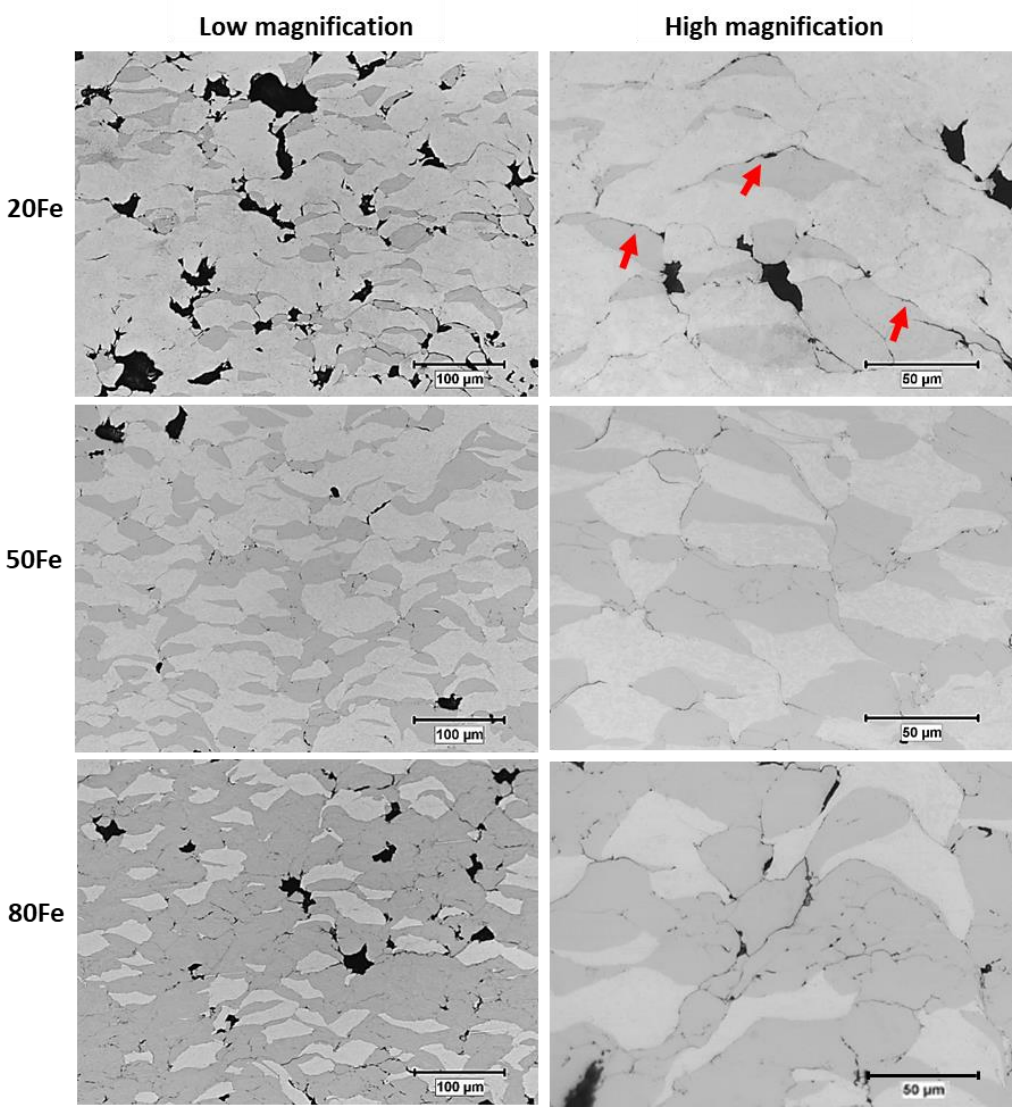

Fig. 5.3 Optical cross-sectional microstructure of the composite 316L/Fe coatings (light-316L; dark-Fe).

The weight fractions of the 316L and Fe in composite coatings measured from image analyses of EDS maps are presented in Table 5.2. Interestingly, the composite coating

compositions are very close to their initial as-mixed ratios, i.e. there seems to be no effect of mixing on the compositional yield, which is somewhat unexpected.

Table 5.2 The weight fractions of the 316L and Fe in composite coatings.

Powder	Feedstock Fe wt.%	Coating Fe wt.%
20Fe	20	19.5 ± 1.7
50Fe	50	50.0 ± 2.3
80Fe	80	79.6 ± 2.2

5.4.2 Cold sprayability and other metrics

To quantify the effects of mixing powders, the cold sprayability metrics, i.e. DE (also partial DEs for mixed powders), porosity, and coating bond strength (maximum value), were measured and are presented in Fig. 5.4. Note that in Fig. 5.4 (c), the failure of 316L coatings after pull-off tests is in the epoxy; this implies the coating cohesion strength is higher than 53 MPa (epoxy strength).

In Fig. 5.4, the characteristics of the single component coatings are revealed at 0 and 100 wt.% Fe; the 316L has "superior" coating characteristics than the Fe, exhibiting a higher DE (72% vs 32%) and coating cohesion strength (> 53 MPa vs 37.8 MPa), as well as a lower porosity (2.2% vs 2.8%). For the composite coatings, one would normally expect that there will be a continuing deterioration of the above cold sprayability metrics with increasing the Fe fraction. But in fact, the measured results are different to these expectations. In terms of DE and porosity, the 20Fe coating with the closest composition to the single component 316L, is a "poor" coating having the second lowest DE (42%) and the highest porosity (4.5%). With increasing Fe fraction, the 50Fe coating

exhibits a medium DE (48%) and the lowest porosity (1.5%). For 80Fe, the coating is in fact a "good" one although it has the closest composition to the single component Fe, showing the second highest DE (66%) and the second lowest porosity (2.0%). Regarding the coating cohesion strength, unlike DE and porosity, the values do not differ strongly at the composite regions and plateau at 46. 7 to 52.5 MPa. However, it is still surprising to see that the 80Fe coating would exhibit a cohesion strength (52.5 MPa) comparable to the 20Fe (52.4 MPa) and much higher than the single component Fe (37.8 MPa). To sum, the cold sprayability metrics of the composite coatings are very different to the common expectations, and the results imply strong effects of mixing powders to occur during deposition.

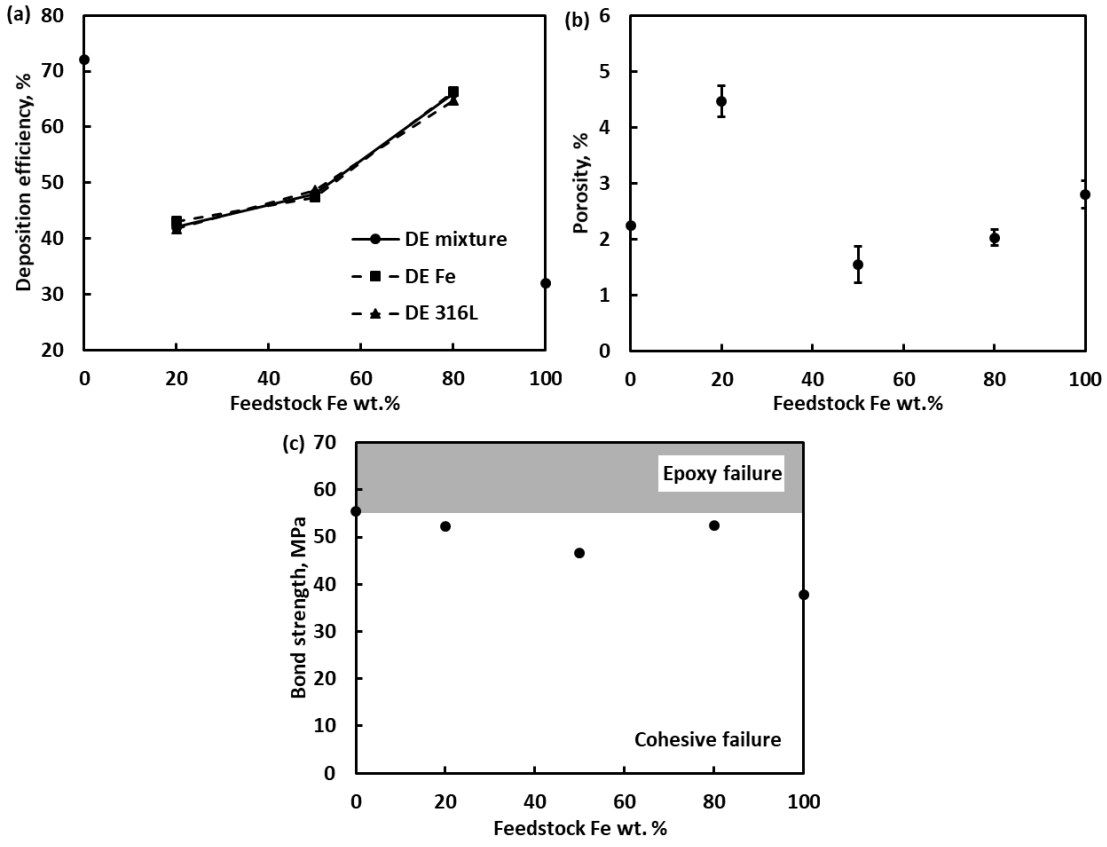

Fig. 5.4 The cold sprayability metrics. (a) DE, (b) porosity, (c) bond strength.

To further exhibit the effects of mixing powders, several particle and coating metrics, i.e. particle in-flight velocity, coating microhardness, and coating flattening ratio, were measured and are shown in Fig. 5.5.

As shown in Fig. 5.5 (a), the velocity of the mixed powder gradually increases with increasing the Fe fraction; this would appear to correlate with the fact that the Fe is finer than the 316L. The average velocity for single component Fe is about 700 m/s. A fitting line was drawn through the data points, and it shows a linear effect of mixing composition on the particle velocity. Note that the large scattering of the velocity is due to the distribution of the particle size (Fig. 5.1). However, the change in velocity is so small and this is not expected to affect the cold sprayability metrics significantly. Also, extrapolating the line to 0 wt.% Fe suggests that the large 316L powder has an average velocity lower than the Fe of about 633 m/s. Note that the critical velocities of Fe and 316L powders in literature with the similar sizes as the ones used in this study are about 650 m/s and 561 m/s, respectively [5.23]. It can be seen that the measured particle velocities of both powders are higher than their respective critical velocities, which to some extent validates the velocity measurements.

The coating flattening ratio (FR) is a measure of the bulk deformation of a particle during deposition. As shown in Fig. 5.5 (b), in the single component coatings, the deposited 316L particles exhibit a higher average FR as compared with the Fe (3 vs 2.4). Whereas, in the composite coatings, with increasing Fe fraction, the 316L FR only experiences slight fluctuations and the Fe FR shows a monotonic decrease (20Fe: 3.3; 50Fe: 2.9; 80Fe: 2.4). In the literature concerning the cold spray of single component Ti powder [5.24, 5.25], the coating FR and DE were both observed to increase with increasing the particle velocity, which generally suggests that the particle plastic deformation is beneficial for particle deposition. But it appears that this correlation from single component

powder deposition cannot be applied to the mixed powder deposition in this case, e.g. the 80Fe with the highest DE (Fig. 5.4 (a)) in fact has the lowest FR of both components. This indicates there could be other deposition mechanisms at play, e.g. retention (the rebounding 316L particle gets retained by the incoming Fe particles), as will be discussed in Section 5.5. It is also noted that, in terms of the relative deformation behavior between the 316L and Fe powders in each composite coating (difference in component FR), the largest difference is in 20Fe, the second is in 80Fe, and in 50Fe the component FR is similar.

The coating microhardness measurements are shown in Fig. 5.5 (c). In each coating, the deposited 316L is always harder than the Fe, even though in the feedstock the 316L powder is in fact softer (226 HV vs 287 HV). This result is indicative of the higher strain hardening rate and strain rate sensitivities of 316L compared to Fe during impact deformation [5.19, 5.20]. Moreover, except for the higher hardness of Fe in 80Fe, there is no obvious microhardness difference of each component in different coatings. The high hardness of Fe in 80Fe appears to correlate with its highest DE, and further discussion will be presented in Section 5.5.

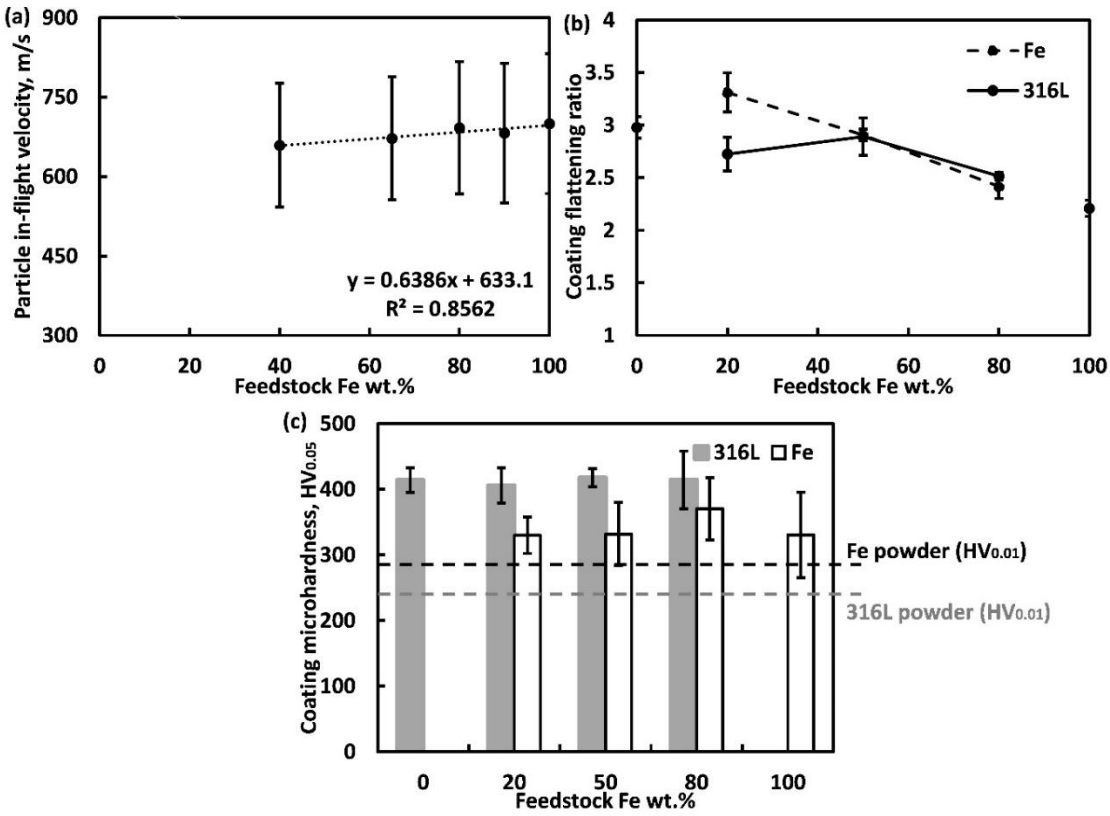

Fig. 5.5 (a) Particle in-flight velocity [5.26], (b) coating flattening ratio, and (c) coating microhardness.

5.5 Discussion

Results in Figs. 5.3 and 5.4 have shown that the cold spray of bimodal size 316L/Fe powder mixtures generates an unpredictable coating microstructure and cold sprayability, which indicates strong effects of mixing powders. In cold spray, the effects of mixing can be considered to occur mainly during two stages: particle in-flight and upon impact deposition. In Fig. 5.5 (a), the small linear variation of particle in-flight velocity as a function of feedstock Fe wt.% is not expected to affect the cold sprayability metrics significantly. In this paper, investigations towards explaining the mixed powder deposition characteristics are mainly focused on the deposition end.

In cold spray, the weight (or volume) fraction metric is commonly used to define the composition of the feedstock powder mixture. Thus, normal expectations of the mixed powder cold spray behavior are often based on the Rule of Mixtures method. For instance, the DE of the mixed powders can be expected to be the weighted average of the DE of the individual components. However, using this approach is totally unsuccessful in this case. There are several possible explanations for this. In this study, both the feedstock powders are spherical, and the 316L is about twice the average size of the Fe. Firstly, in the 316L/Fe binary mixture, knowledge of the DE of the individual components means that the impacts of "316L on 316L" and "Fe on Fe" are known, but impacts between the dissimilar components e.g. "316L on Fe" and "Fe on 316L" are not considered. It has been previously discussed in [5.16, 5.17] that the impact of 316L on Fe will generate poor bonding/strong rebound, indicating a significant mixed impact interface effect. Secondly, since the coating is built up by particle impacts, the DE of a powder should be directly correlated to its particle size distribution, e.g. the weight of a single particle and number of successful impacts per unit time. For instance, in the 50/50 wt.% 316L/Fe mixture, the small Fe particles will outnumber the large 316L per unit weight/volume of feedstock and thus there will be more impacts associated with Fe during deposition. It is reasonable to believe that its coating formation process (e.g. particle-particle interaction) would be different from a similar size 50/50 wt.% powder mixture. However, such a difference cannot be reflected by expectations based on quantifying the feedstock mixing composition only in terms of weight. Thirdly, the inclusion of hard/heavy particles (316L) in mixtures with larger kinetic energies could exert effects such as tamping to affect the cold sprayability metrics (e.g. porosity and DE) [5.12], and the contributions of such effects in different composition 316L/Fe mixtures are different. To sum, during the deposition of bimodal size 316L/Fe mixtures, there will be various mechanisms at play, e.g. mixed

impact interfaces, feedstock size difference, and tamping. This mainly explains the difficulties in quantitative predictions (e.g. rule of mixtures method) of the mixture cold spray characteristics as shown in Figs. 5.3 and 5.4.

To incorporate the various mechanisms of multi-particle interactions, it is believed that the mixed powder should be considered as an entity instead of separate components for deposition. Maev et al. [5.12] considered that, during the large/small mixture deposition, the powder ensemble structure (i.e. multiple particle arrangement) prior to impact could affect the deposition. A few literature also considered that such multi-particle interactions would occur in cold spray [5.27-5.29]. As shown in Fig. 5.3, since each composite coating exhibits a homogenous microstructure, it is reasonable to believe that the large/small component feedstock forms a random spatial arrangement upon impact. Using the particle size distribution (Fig. 5.1) and density values, the composition of each mixture sample was converted from weight fraction to the ratio of the numbers of component particles in a mixture, namely, the particle number fraction, as shown in Table 5.3. Note that a cut-off particle size was set at 10 μm to discount the fine particles since according to literature [5.30] these particles can be easily decelerated and deflected away from the substrate by the bow shock wave. The number weighted average particle size was also calculated as: 316L-35 μm and Fe-17 μm. Based on the results, a 2D schematic diagram of the random multiple particle arrangement of bimodal size 316L/Fe mixtures upon impact is shown in Fig. 5.6. The speculated deposition mechanisms are also presented and are qualitatively discussed in detail.

Table 5.3 The feedstock Fe weight fraction and the respective number fraction.

Powder	Fe weight fraction, wt.%	Fe number fraction, %
20Fe	20	66.7
50Fe	50	88.9
80Fe	80	97.0

For the weight fraction 20Fe (316L:Fe=80:20 wt.%), the relative particle number fraction is 316L:Fe=1:2, thus, Fe particles with twice the number of 316L particles would be present in this mixture. Because the mixed feedstock forms a random spatial arrangement, as schematically shown in Fig. 5.6, the small Fe particles tend to be dispersed at the interstices between the large 316L particles. During deposition, these Fe particles absorb the impact energies of 316L and were highly deformed (high FR of Fe in 20Fe in Fig. 5.5 (b)) to create significant barriers inhibiting the 316L/316L contact. As previously discussed [5.16, 5.17], the 316L on Fe impacts will generate the poor bonding behavior/strong rebound (the preferentially located defects at mixed 316L/Fe interfaces in Fig. 5.3). Thus, the widely dispersed small Fe particles in 316L then adversely affect the entire mixture during deposition, as can be seen in Fig. 5.3 as defects (i.e. pores and interparticle cracks) that mainly originate from the mixed 316L/Fe interfaces. This finally leads to a “poor” coating of 20Fe having a low DE (42%) and the highest porosity (4.5%).

For the weight fraction 50Fe, the particle number fraction is 316L:Fe=1:8. More small Fe particles are present in the mixture, and each 316L particle appears to be entirely surrounded by a single layer of Fe particles (Figs. 5.3 and 5.6). Therefore, in this mixture, each 316L particle is generally expected to experience the 316L on Fe impacts, which would generate poor very deposition/bonding behavior. However, in 50Fe, more small Fe particles are replacing the large

316L particles compared with 20Fe, which increases the total particle number density and thus the possibility of multi-particle interactions upon impact. Considering the excellent interparticle bonding condition in 50Fe (Fig. 5.3), it is thus believed that the multiple subsequent high velocity small Fe particles on top of the 316L during deposition will stop the 316L from escaping by rebounding and force it to retain in the coating. Moreover, in the 50/50% large/small 316L/Fe mixture, the multiple small Fe particles would surround the large 316L to create more contact points, which could maximize the interaction between the large/small components. The evidence can be found in Fig. 5.5 (b) that the 316L and Fe components exhibit a similar coating FR in 50Fe, although in feedstock they are materials with different deformabilities (e.g. different crystal structures). It is believed that the enhanced contact between the feedstock could benefit the interparticle bonding and also lead to a better DE. Last but not least, it has been reported in powder metallurgy that in a 50/50 wt.% large/small mixture, an optimum packing density can often be obtained [5.11]. The lowest coating porosity in 50Fe (1.5%) is thus speculated to indicate some correlations between the powder packing and coating porosity in cold spray.

For the weight fraction 80Fe, the particle number fraction is 316L:Fe=1:32, the large 316L is expected to be surrounded by a "sea" of small Fe particles prior to impact and direct 316L/316L contact is difficult (Fig. 5.3). In this mixture, the large 316L particles are less deformed (low 316L FR in 80Fe in Fig. 5.5 (b)). Thus, a more effective tamping can be achieved as a larger proportion of their high kinetic energies can be absorbed by the poorly bonded Fe matrix to facilitate the conversion of plastic work into heat and stored energy (leading to adhesion [5.31]) [5.14]. Evidence can be found in the higher hardness of the Fe in 80Fe (Fig. 5.5 (c)), the lower porosity of 80Fe than Fe (Fig. 5.4 (b)), and also the higher cohesion strength of 80Fe compared to the single component Fe (Fig. 5.4 (c)). Meanwhile, similar to 50Fe, the small Fe particles on "top" of the

316L with a high velocity and quantity would deposit like a “blanket” to interact and inhibit the large 316L particles from rebound and generate defects. This explains the observation that mixed 316L/Fe interfaces in 80Fe all exhibiting good bonding conditions (Fig. 5.3). Since a higher Fe number density is present in 80Fe than 50Fe, a better retention of 316L is realized, and a higher partial DE of 316L can be observed in this mixture (Fig. 5.4 (a)). Therefore, through this mutual effect of tamping and retention exerted by both the large and small components, the high DE of 80Fe can be explained. Note that modeling the “sweet point” mixing composition leading to the optimal cold sprayability metrics (e.g. DE) requires the quantitative knowledge of the contribution of each effect, i.e. mixed impact interfaces, retention, tamping, which has to be determined separately from experiments and is thus considered as the future work.

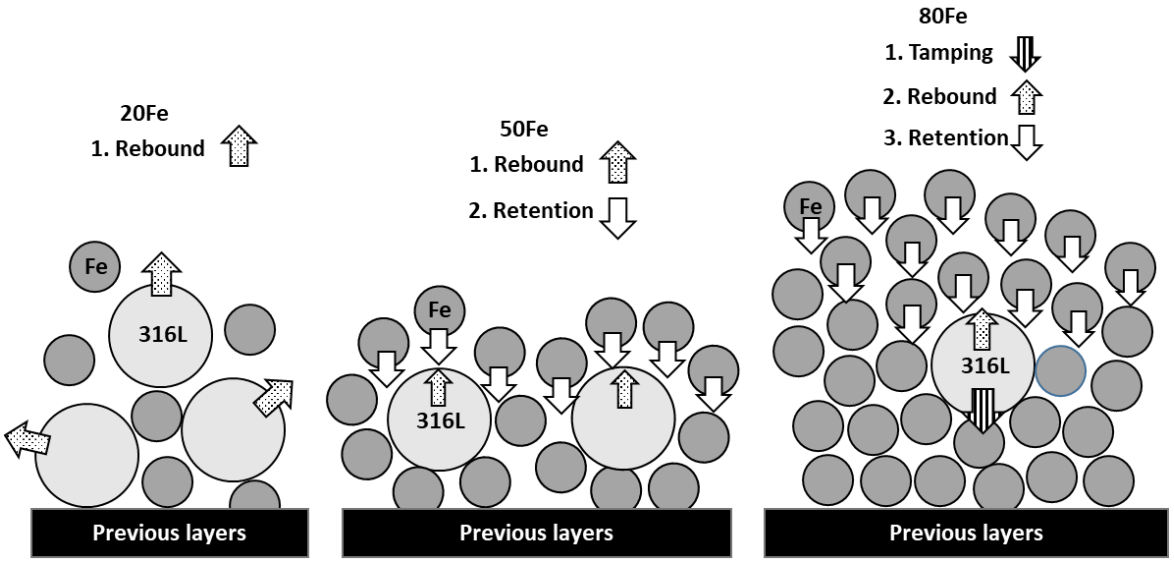

Fig. 5.6 A 2D schematic diagram of the random multiple particle arrangement of bimodal size 316L/Fe mixtures and the associated deposition mechanisms upon impact.

5.6 Conclusion

In this study, average 43 μm 316L stainless steel and 22 μm commercial purity Fe powders were used as feedstock. Coatings of the single component 316L and Fe, and binary composites of 20Fe, 50Fe, and 80Fe were cold spray deposited. Results show the single component 316L has a "superior" cold sprayability to the Fe. However, the composite 316L/Fe coatings generate an unpredictable coating microstructure and cold sprayability, implying strong effects of mixing powders. During cold spray of bimodal size 316L/Fe mixtures, there will be various mechanisms at play, e.g. mixed impact interfaces, feedstock size difference, and tamping. To explain the cold spray characteristics, it is believed that the mixed metal powder should be considered as an entity instead of separate components for deposition. Describing the mixture composition on the basis of particle number fraction as opposed to weight or volume fraction furnishes a viable explanation for the observed results. The mixture multiple particle arrangement upon impact is proposed based on the coating microstructure and the calculated particle number fraction, and the speculated deposition mechanisms are qualitatively discussed. In particular, the 20Fe has the low DE and highest porosity due to the dispersion of small Fe particles and the poor deposition/bonding behavior of 316L on Fe impacts; the 50Fe exhibits the excellent interparticle bonding conditions, which can be attributed to the retention of the subsequent incoming Fe particles and also the sufficient interaction between the large/small feedstock; the 80Fe features the high DE due to the mutual effect of tamping and retention.

5.7 References

[5.1] A. Moridi, S.M. Hassani-Gangaraj, M. Guagliano, M. Dao, Cold spray coating: review of material systems and future perspectives, Surf. Eng. 30 (2014) 369-395.

[5.2] A. Sova, D. Pervushin, I. Smurov, Development of multimaterial coatings by cold spray and gas detonation spraying, Surf. Coat. Technol. 205 (2010) 1108-1114.

[5.3] S. Grigoriev, A. Okunkova, A. Sova, P. Bertrand, I. Smurov, Cold spraying: from process fundamentals towards advanced applications, Surf. Coat. Technol. 268 (2015) 77-84.

[5.4] T. Novoselova, P. Fox, R. Morgan, W. O'Neill, Experimental study of titanium/aluminium deposits produced by cold gas dynamic spray, Surf. Coat. Technol. 200 (2006) 2775-2783.

[5.5] H.Y. Lee, S.H. Jung, S.Y. Lee, K.H. Ko, Alloying of cold-sprayed Al-Ni composite coatings by post-annealing, Appl. Surf. Sci. 253 (2007) 3496-3502.

[5.6] H.-T. Wang, C.-J. Li, G.-J. Yang, C.-X. Li, Cold spraying of Fe/Al powder mixture: coating characteristics and influence of heat treatment on the phase structure, Appl. Surf. Sci. 255 (2008) 2538-2544.

[5.7] Z.B. Zhao, B. Gillispie, J. Smith, Coating deposition by the kinetic spray process, Surf. Coat. Technol. 200 (2006) 4746-4754.

[5.8] B. Al-Mangour, R. Mongrain, E. Irissou, S. Yue, Improving the strength and corrosion resistance of 316L stainless steel for biomedical applications using cold spray, Surf. Coat. Technol. 216 (2013) 297-307.

[5.9] H.-K. Kang, S.B. Kang, Tungsten/copper composite deposits produced by a cold spray, Scr. Mater. 49 (2003) 1169-1174.

[5.10] X.-k. Wu, X.-l. Zhou, H. Cui, X. Zheng, J.-s. Zhang, Deposition behavior and characteristics of cold-sprayed Cu-Cr composite deposits, J. Therm. Spray Technol. 21 (2012) 792-799.

[5.11] K. Spencer, M.X. Zhang, Optimisation of stainless steel cold spray coatings using mixed particle size distributions, Surf. Coat. Technol. 205 (2011) 5135-5140.

[5.12] R.G. Maev, V. Leshchynsky, Air gas dynamic spraying of powder mixtures: theory and application, J. Therm. Spray Technol. 15 (2006) 198-205.

[5.13] H. Che, X. Chu, P. Vo, S. Yue, Cold spray of mixed metal powders on carbon fibre reinforced polymers, Surf. Coat. Technol. 329 (2017) 232-243.

[5.14] H. Aydin, M. Alomair, W. Wong, P. Vo, S. Yue, Cold sprayability of mixed commercial purity Ti plus Ti6Al4V metal powders, J. Therm. Spray Technol. 26 (2017) 1-11.

[5.15] S. Yue, W. Wong, H. Aydin, R. Mongrain, R. Barua, P. Vo, R. Dolbec, Improving cold sprayability: mixed metal powders, Proceedings of the International Thermal Spray Conference, USA, 2015, pp. 473-478.
[5.16] X. Chu, R. Chakrabarty, H. Che, L. Shang, P. Vo, J. Song, S. Yue, Investigation of the feedstock deposition behavior in a cold sprayed 316L/Fe composite coating, Surf. Coat. Technol. 337 (2018) 53-62.
[5.17] X. Chu, H. Che, P. Vo, R. Chakrabarty, B. Sun, J. Song, S. Yue, Understanding the cold spray deposition efficiencies of 316L/Fe mixed powders by performing splat tests onto as-polished coatings, Surf. Coat. Technol. 324 (2017) 353-360.
[5.18] J. Frattolin, R. Barua, H. Aydin, S. Rajagopalan, L. Gottellini, R. Leask, S. Yue, D. Frost, O.F. Bertrand, R. Mongrain, Development of a novel biodegradable metallic stent based on microgalvanic effect, Ann. Biomed. Eng. 44 (2016) 404-418.
[5.19] A.A. Olleak, M.N. Nasr, H.A. El-Hofy, The influence of johnson-cook parameters on SPH modeling of orthogonal cutting of AISI 316L (2015).
[5.20] O. Bielousova, J. Kocimski, R.G. Maev, I. Smurov, W. Scharff, V. Leshchynsky, Localisation of deformation in cold gas dynamic spraying, Surf. Eng. 32 (2016) 655-662.
[5.21] Standard test method for adhesion or cohesion strength of thermal spray coatings, ASTM Standard C633-01, ASTM international, West Conshohocken, PA, 2001.
[5.22] E. Irissou, J.-G. Legoux, B. Arsenault, C. Moreau, Investigation of Al-Al2O3 cold spray coating formation and properties, J. Therm. Spray Technol. 16 (2007) 661-668.
[5.23] T. Schmidt, F. Gärtner, H. Assadi, H. Kreye, Development of a generalized parameter window for cold spray deposition, Acta Mater. 54 (2006) 729-742.
[5.24] W. Wong, P. Vo, E. Irissou, A.N. Ryabinin, J.G. Legoux, S. Yue, Effect of particle morphology and size distribution on cold-sprayed pure titanium coatings, J. Therm. Spray Technol. 22 (2013) 1140-1153.
[5.25] D. Goldbaum, R.R. Chromik, S. Yue, E. Irissou, J.-G. Legoux, Mechanical property mapping of cold sprayed Ti splats and coatings, J. Therm. Spray Technol. 20 (2010) 486-496.
[5.26] R. Barua, Study of the Structural Properties and Control of Degradation Rate for Biodegradable Metallic Stents using Cold Spray, PhD thesis, Department of Mechanical Engineering, McGill University, 2015.

[5.27] S. Ahmad Alidokht, P. Vo, S. Yue, R.R. Chromik, Erosive wear behavior of cold-sprayed Ni-WC composite coating, Wear 376-377 (2017) 566-577.
[5.28] P.C. King, S.H. Zahiri, M.Z. Jahedi, Rare earth/metal composite formation by cold spray, J. Therm. Spray Technol. 17 (2007) 221-227.
[5.29] J. Perry, P. Richer, B. Jodoin, E. Matte, Pin fin array heat sinks by cold spray additive manufacturing: economics of powder recycling, J. Therm. Spray Technol. 28 (2019) 144-160.
[5.30] J. Pattison, S. Celotto, A. Khan, W. O'Neill, Standoff distance and bow shock phenomena in the cold spray process, Surf. Coat. Technol. 202 (2008) 1443-1454.
[5.31] G. Bae, Y. Xiong, S. Kumar, K. Kang, C. Lee, General aspects of interface bonding in kinetic sprayed coatings, Acta Mater. 56 (2008) 4858-4868.

Chapter 6

-

Understanding Particle-Particle Interactions from Deposition Efficiencies in Cold Spray of Mixed Fe/316L Powders with Different Particle Size Combinations

In Chapter 5, a multiple particle arrangement model was proposed to explain the cold spray characteristics of bimodal size 316L/Fe powder mixtures. This model is based on the speculation that particle-particle interactions would occur during cold spray. In this Chapter, we further validated this speculation by looking into the deposition efficiencies (DEs) of different sizes of mixed Fe/316L powders.

This chapter has been accepted by J. Therm. Spray Technol.:

- Xin Chu, Hanqing Che*, Chaoyi Teng, Phuong Vo, Stephen Yue, "*Understanding particle-particle interactions from deposition efficiencies in cold spray of mixed Fe/316L powders with different particle size combinations*", 2019.

6.1 Abstract

In this study, Fe and 316L powders with two different particle sizes were used as the feedstock. They were also premixed using different mixing ratios and combinations: (i) either 316L or Fe powder with large particles blended with small ones, (ii) a blend of 316L and Fe powder using three particle size combinations. Both single component and mixed powders were deposited by cold spray and the deposition efficiencies (DE) were calculated and discussed. The results show that the DE of a mixture of large and small particles of the same powder follows the Rule of Mixtures. Whereas, the variation of the DE of the 316L and Fe mixture depends on the particle size combinations; specifically, mixtures with smaller size particles show better DEs than the respective Fe powder. The difference in the DEs of different Fe/316L mixtures can be explained by the particle-particle interactions (i.e. tamping and retention) upon impact. In addition, a relationship between the average particle size and density is proposed to determine the occurrence of particle-particle interactions in cold spray of mixed generic powders. The industrial significance of the knowledge of particle-particle interactions is finally explained in the context of the fabrications of metal matrix composites.

6.2 Introduction

Cold spray is a relatively new coating technique in which micron-sized (e.g. 10-50 μm) particles are accelerated to supersonic velocities by a high-pressure gas stream in a de-Laval nozzle and are impacted onto substrates in the solid state [6.1]. Due to its advantages, such as the low process temperature, cold spray has become an effective alternative to fabricate coatings from metals that are highly sensitive to temperature or oxidation [6.2-6.4]. During cold spray, not all particles impacting onto substrates necessarily deposit; the term "cold sprayability" is introduced to evaluate the ease with which a powder can be deposited [6.5]. Deposition efficiency (DE) is one important metric of cold sprayability and is usually defined as the ratio of powder mass deposited on the substrate to the total powder mass sprayed over the substrate [6.5]. The DE of a powder depends on its material (e.g. hardness, oxide layer thickness) and characteristics (e.g. size, morphology), and can be improved by increasing the "intensity" of cold spray process parameters (i.e. gas pressure and temperature) [6.6]. In cold spray literature, it has also been reported that adding a second component (SC) powder (ceramic or metal) into a metal can improve its DE [6.7-6.9]. This finding is of industrial significance since it may help to: i) enhance the feedstock deposition and adhesion in low-pressure cold spray repair practices (e.g. add Al_2O_3 to various metals [6.7]); ii) improve the DE of low DE metals (e.g. add Cu or Zn to Sn [6.8]) or expensive metals (e.g. add softer or irregular Ta to harder Ta [6.9]). However, fundamental mechanisms behind such DE improvements in cold spray are often not clear.

To fully understand the DE-improving effects, knowledge of interaction behaviors between mixed powder particles during deposition is required. Regarding the effect that SC applies to the matrix powders (SC on matrix), tamping (or hammering, peening) is the one most accepted since SC powders are often large/dense/hard metals or ceramics [6.8, 6.10, 6.11]. Tamping could lead

to forced deformation thus further densification of previously deposited layers [6.11], but its effect on DE is still not clear. For instance, Fernandez et al. [6.12] proposed that tamping could benefit particle deposition if a subsequent hard particle interacts with a soft particle which is depositing at the substrate surface and enhances its interfacial strain/temperature in real time (scenario I in Fig. 6.1); however, there are still debates over the occurrence of such interactions in cold spray [6.12-6.14]. Besides tamping, other common effects of SC on matrix are surface roughening and/or surface activation (removal of surface oxides) which often associate with the addition of irregular powders (metals [6.8, 6.9] or ceramics [6.11]). Regarding the effect that a matrix applies to SC (matrix on SC), soft/rough surface deposits could provide a mechanical anchorage effect (e.g. embedding [6.15] or trapping [6.8]) to facilitate the SC deposition. This explains the partial retention of SC particles (e.g. ceramics) in metal/ceramic mixed coatings which cannot reach any deposition alone. Moreover, a few researchers [6.16, 6.17] proposed that SC retention can also be contributed by particle-particle interactions: subsequent particles collide with and retain rebounded SC particles (scenario II in Fig. 6.1). But it is also argued that interactions of excessive/large rebounding particles could otherwise decelerate/deflect subsequent particles to result in reduced DE and defective coatings [6.10, 6.18].

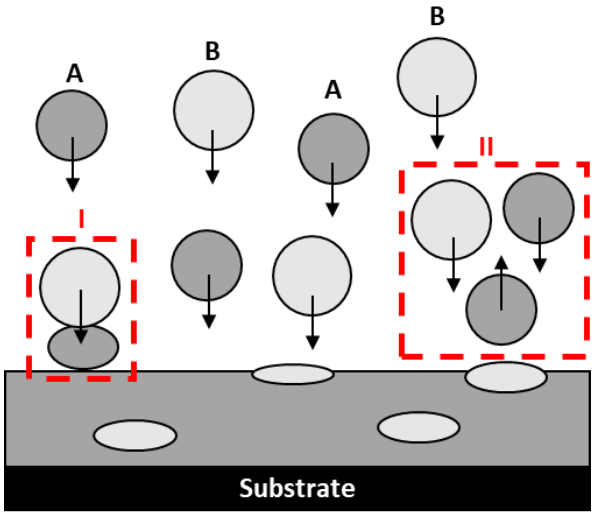

Fig. 6.1 Schematic diagram of particle-particle interactions (i.e. collisions between moving particles) during mixed powders deposition (summarized from [6.12, 6.16]).

In our previous studies, an increase in DE was observed when 316L stainless steel powder was premixed with commercial purity Fe to cold spray fabricate bio-degradable composite stents [6.19]. To better understand the mechanism of such an improvement, more detailed research towards DE was performed. In this study, DE characteristics of the particle size mixtures of single component 316L and Fe powders, as well as the binary Fe/316L mixtures with different particle size combinations were measured and discussed, and the DE-improving mechanisms of mixed Fe/316L powders are elucidated. It is proposed that this research finding generates additional insights into documented mechanisms of particle-particle interactions and provides industrial guidances in cold spray of generic hard/soft mixtures.

6.3 Materials and methods

Commercially available gas atomized 316L stainless steel powder (Sandvik Osprey, Neath-Port Talbot, UK) and water atomized commercial purity Fe powder (Goodfellow, Cambridge, UK) are used as the feedstock. Sieving was performed on some powders using 400-mesh (38 μm) sieves to obtain desired particle size distributions and four powders were prepared, namely, Fe large, Fe small, 316L large, and 316L small. SEM images and characteristics of the feedstock are presented in Fig. 6.2 and Table 6.1, respectively. The Vickers hardness of the feedstock was measured using a Clark CM-100AT Microhardness Tester (Sun-Tec, Novi, USA) using a load of 10 g and a dwell time of 15 s. The feedstock particle size was determined using a Horiba LA-920 laser diffraction analyzer (Tokyo, Japan). Results show no significant hardness difference in hardness between large and small powders of the same species, and 316L has roughly triple hardness than Fe.

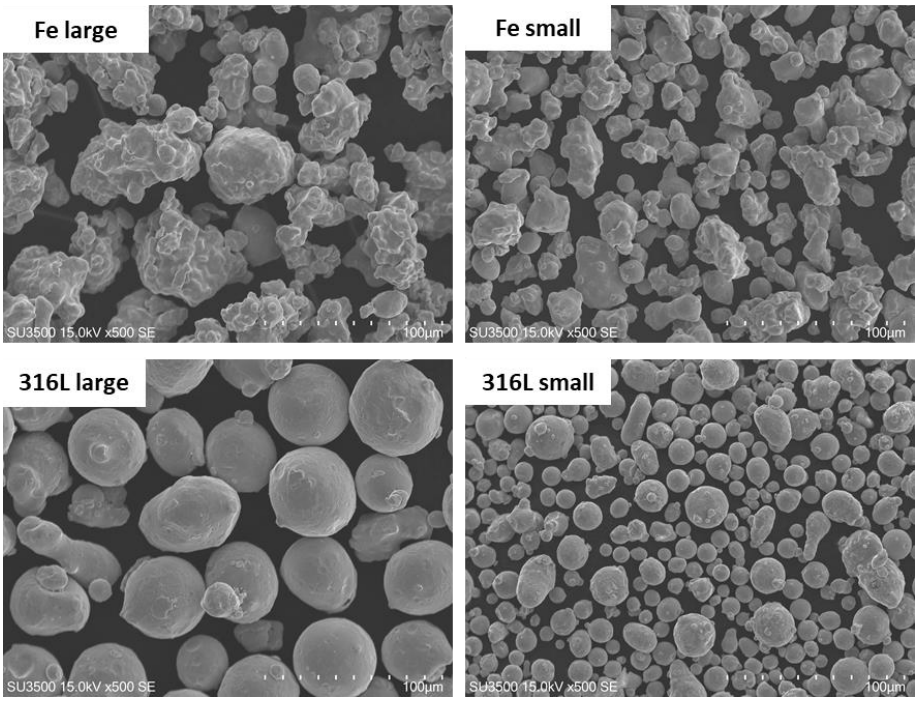

Fig. 6.2 SEM images of the feedstock powders.

Table 6.1 Characteristics of the feedstock powders.

Feedstock	Microhardness, $HV_{0.01}$	d10, μm	d50, μm	d90, μm
Fe large	127 ± 19	29.5	46.7	67.8
Fe small	118 ± 15	17.6	27.8	43.2
316L large	353 ± 11	36.7	46.1	57.7
316L small	347 ± 13	11.7	17.7	25.5

All cold spray campaigns were carried out at the McGill-NRC cold spray facility, located at National Research Council of Canada, Boucherville, using a CGT KINETIKS® 4000 cold spray system (Sulzer Metco, Westbury, USA) with a MOC 24 carbide nozzle. Al 6061 plates with dimensions of 3 × 3 inch (75 × 75 mm) were used as substrates and were blasted with 60 grit alumina to remove scale and promote adhesion. Nitrogen was used as the propellant gas. To investigate the effects of mixing powders on DE, aforementioned single component powders were premixed in a rolling mixer (without medium) for 1 hour using the following recipes: (i) 10, 20, 50 wt.% of large powder in small powder for 316L and Fe, and (ii) 10, 20, 50 wt.% of 316L into Fe (10SS, 20SS, 50SS) using three size combinations (Fe small/316L large, Fe large/316L large, Fe small/316L small). The cold spray process parameters were all set at a gas temperature of 600 °C, a gas pressure of 3 MPa, a stand-off distance of 80 mm, a gun travel speed of 300 mm/s, and a feed rate of 20-60 g/min.

After cold spray, coating cross-sections were characterized using a Hitachi SU3500 SEM (Tokyo, Japan). The compositions of the composite coatings (area fractions of Fe and 316L particles) were estimated by image analyses using a minimum of 30 random images at 200 × magnification. The coating flattening ratio (FR) was calculated as the width to height ratio of a

deformed particle from etched cross-sections at 200 × magnification and the average value of about 50 particles per component per sample was reported along with the standard error. The particle in-flight velocity was measured in a free jet by an optical time-of-flight particle diagnostic system DPV-2000 (Tecnar Automation, St. Bruno, Canada) under the same process parameters as coating deposition. Velocities of 5000 particles were measured and the average value and standard deviation were calculated for each powder. The DE was measured according to Eq. (6.1) as the mass gain of the substrate divided by the total mass of the spray material fed over the substrate. Two to three measurements were performed for each powder composition (relative DE difference < 5% was obtained) and the average value was reported. In addition to the overall mixture DE, partial DEs (i.e. DEs of the 316L and Fe components in composite coatings) of mixed Fe/316L powders were also calculated based on the mixture DE and compositional yield (powder composition vs coating composition) [6.11, 6.12].

$$DE = \frac{\Delta m_s \cdot t \cdot v}{\Delta m_f \cdot d} \tag{6.1}$$

Where, Δm_s is the mass change of the substrate after deposition, t is the total spray time, v is the gun travel speed, Δm_f is the mass change of the powder in the hopper after deposition, d is the total distance traveled by the nozzle over substrate. The feed rate was calculated as $FR = \frac{\Delta m_f}{t}$.

6.4 Results

6.4.1 Mixed particle sizes

The measured in-flight velocities of four single component powders are shown in Table 6.2. Small powders of both 316L and Fe have slightly higher average velocities compared with

respective large ones. The large standard deviation of particle velocity is due to the size distribution of each powder.

Table 6.2 The measured in-flight velocities of single component powders.

Coating	Particle velocity, m/s
Fe small	612 ± 107
Fe large	584 ± 67
316L small	583 ± 112
316L large	552 ± 70

The DEs of four single component 316L and Fe powders as well as their large/small mixtures are presented in Fig. 6.3. In each figure, 0 wt.% composition corresponds to only small powder and 100 wt.% composition corresponds to only large powder. Results show that 316L small has doubled DE compared with 316L large (60% vs 30%) which is consistent with its slightly higher particle velocity. On the other hand, Fe small has similar or even slightly lower DE than Fe large (57% vs 65%) despite its higher particle velocity. Moreover, larger powders were added into respective smaller ones and the measured DEs of the mixtures are plotted in Fig. 6.3. The predicted mixture DEs calculated by Rule of Mixtures ($DE_{Mix} = DE_{316L} \times f_{316L} + DE_{Fe} \times f_{Fe}$) from non-mixed large and small powders are also plotted as dashed lines. Results show that the measured mixture DEs are consistent with the predictions, and this indicates inducing large/small particle impacts in cold spray cannot stimulate DE.

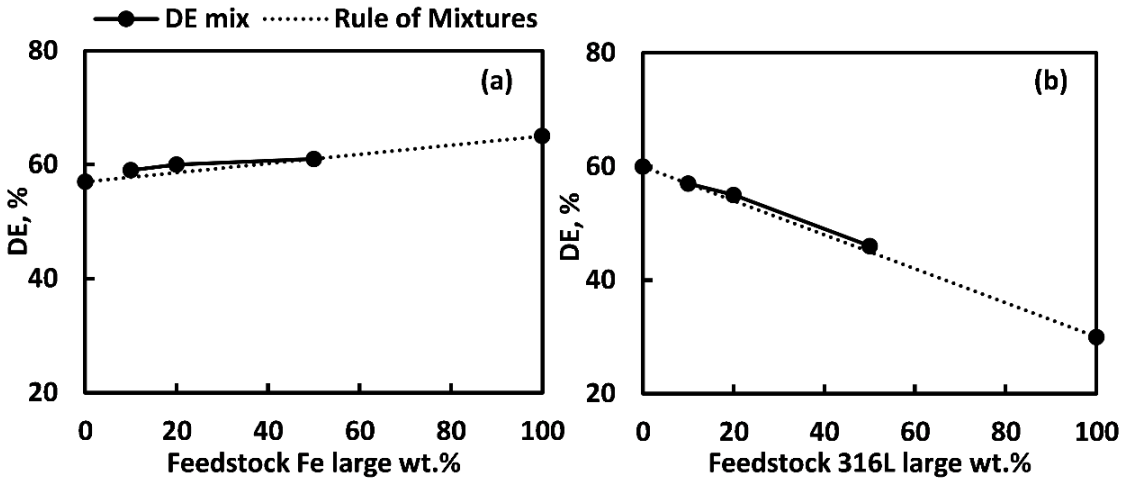

Fig. 6.3 The DEs of large/small mixtures. (a) Fe small/Fe large and (b) 316L small/316L large. Dashed lines indicate the Rule of Mixtures predictions.

6.4.2 Mixed Fe/316L powders

The 50SS cross-sectional microstructure of different sizes of Fe/316L composite coatings is shown in Fig. 6.4. In these images, light regions are 316L, dark regions are Fe, and black spots are pores. In general, all composite coatings are dense, and both Fe and 316L particles in each coating have deformed and are homogenously distributed. It is also noted that the 316L particles in the deposited coatings are mostly separated by Fe and there are a limited number of 316L-316L contacts. The composite coating compositions measured by image analyses are presented in Table 6.3. In general, the 316L contents in all binary Fe/316L composite coatings are similar and are always much lower than their initial as-mixed ratios.

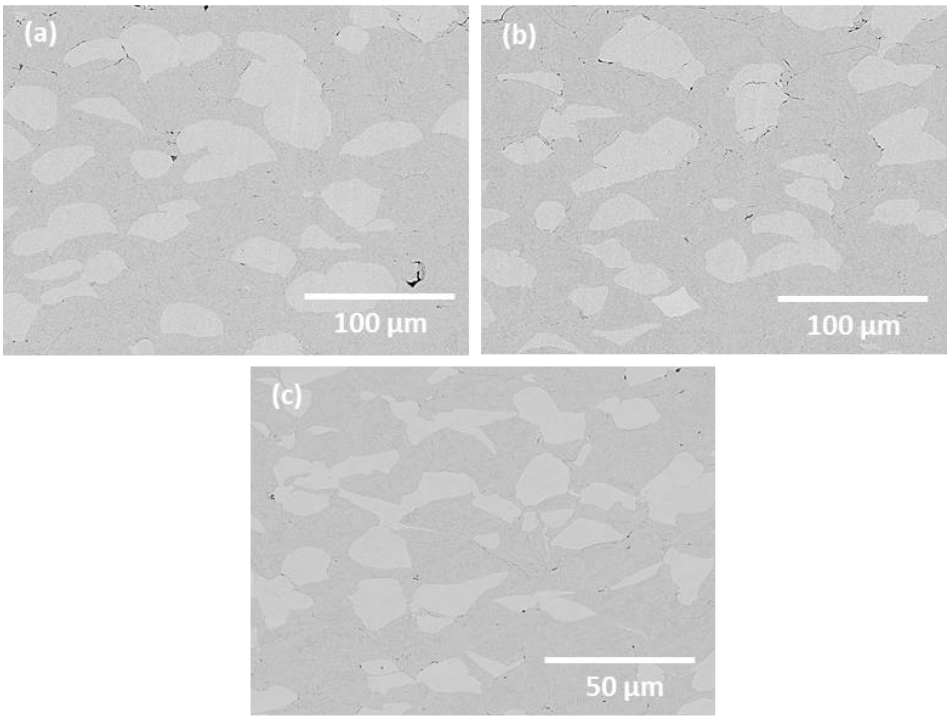

Fig. 6.4 The BSE images of 50SS Fe/316L composite coating cross-sections. (a) Fe small/316L large, (b) Fe large/316L large, and (c) Fe small/316L small.

Table 6.3 The average 316L weight fractions in Fe/316L composite coatings.

Coating	Fe small/316L large	Fe large/316L large	Fe small/316L small
10SS	5.8 ± 0.2	4.8 ± 0.6	4.9 ± 0.5
20SS	11.5 ± 0.4	11.2 ± 0.5	11.3 ± 0.5
50SS	32.9 ± 1.3	30.2 ± 0.7	30.7 ± 0.7

The Fe flattening ratios (FR) in single component coatings and different 50SS coatings were calculated and are presented in Table 6.4. Note that average FR is commonly used as an

indication of the bulk deformation of a spherical particle during deposition [6.5, 6.11], thus the value might not be representative of the actual degree of Fe particle deformation due to its irregularity. Attention is mainly focused on the relative difference in Fe FR between coatings. Results show that the Fe in the Fe/SS mixed coatings always exhibits higher flattening ratios compared with respective single component Fe, indicating that a tamping effect of 316L is realized in all mixed coatings. Specifically, the Fe small/316L large combination is observed to be most effective in further deforming Fe compared to Fe small/316L small and Fe large/316L large as it exhibits the largest increment of Fe flattening ratio relative to single component Fe (5.3 vs 3.2).

Table 6.4 The Fe flattening ratios in single component and 50SS Fe/316L composite coatings.

Coating	Fe flattening ratio
Fe small	3.2 ± 0.1
Fe large	3.4 ± 0.2
Fe small/316L large	5.3 ± 0.2
Fe large/316L large	3.7 ± 0.1
Fe small/316L small	3.6 ± 0.3

The DE results of single component Fe and 316L powders, as well as Fe/316L mixtures of different particle size combinations are shown in Fig. 6.5. Regarding the mixture DEs (solid lines), results from different Fe/316L mixtures generally exhibit in common a decreasing trend with increasing feedstock SS wt.%. This observation is consistent with our previous works [6.20, 6.21] and it is mainly explained by the increasing number of poorly deposited 316L on Fe impacts with increasing SS content. Moreover, comparing the low SS mixtures (10SS and 20SS) with single component Fe in each figure, it is found that the additions of 316L in Fe did not necessarily lead

to an increase in DE. The DE improvements are observed to be dependent on the particle size of the mixtures, and are only found in the Fe small/316L large and Fe small/316L small mixtures; in particular, a more long-lasting effect (slower rate of DE decrease) is found in the latter.

The partial DEs of Fe and 316L components in different particle size combinations of Fe/316L mixtures were calculated and the results are also plotted in Fig. 6.5 (dashed lines). In general, variations of partial DEs of Fe and 316L in each binary Fe/316L mixture are complicated and they do not necessarily follow the same trend as its respective overall mixture DE. The partial DEs from representative mixtures were compared to investigate the effects of the particle size.

Regarding the partial DEs of Fe (dashed lines with squares), mixtures of Fe large/316L large (Fig. 6.5 (b)) and Fe small/316L small (Fig. 6.5 (c)) were compared. With increasing SS wt.%, the partial DE Fe in Fe large/316L large (line ④) remains relatively unchanged and is the same as the single component Fe DE (i.e. 0 wt.% SS); while in Fe small/316L small the partial Fe DE (line ⑤) exhibits a monotonic increasing trend and is always higher than its relative single component Fe DE.

Regarding the partial DEs of 316L (dashed lines with triangles), mixtures of Fe small/316L large (Fig. 6.5 (a)) and Fe large/316L large (Fig. 6.5 (b)) were compared. In 10 wt.% SS, the partial DE of 316L in Fe small/316L large (line ①) is about 8 % higher than that in Fe large/316L large (line ③). With further increases in the feedstock SS wt.%, the former (line ①) experiences a sudden drop and becomes the same as that in the latter (line ③), which remains unchanged throughout from 10 to 50 wt.% SS. It is also noticed that there is a similar drop of the partial DE of Fe (line ②) along with the partial DE of 316L (line ①) from 10 to 20 wt.% SS in Fe small/316L large in Fig. 6.5 (a). In sum, the above results show that there are significant effects of the particle

size on both mixture DEs and partial DEs of mixed Fe/316L powders, which will be discussed in Section 6.5.

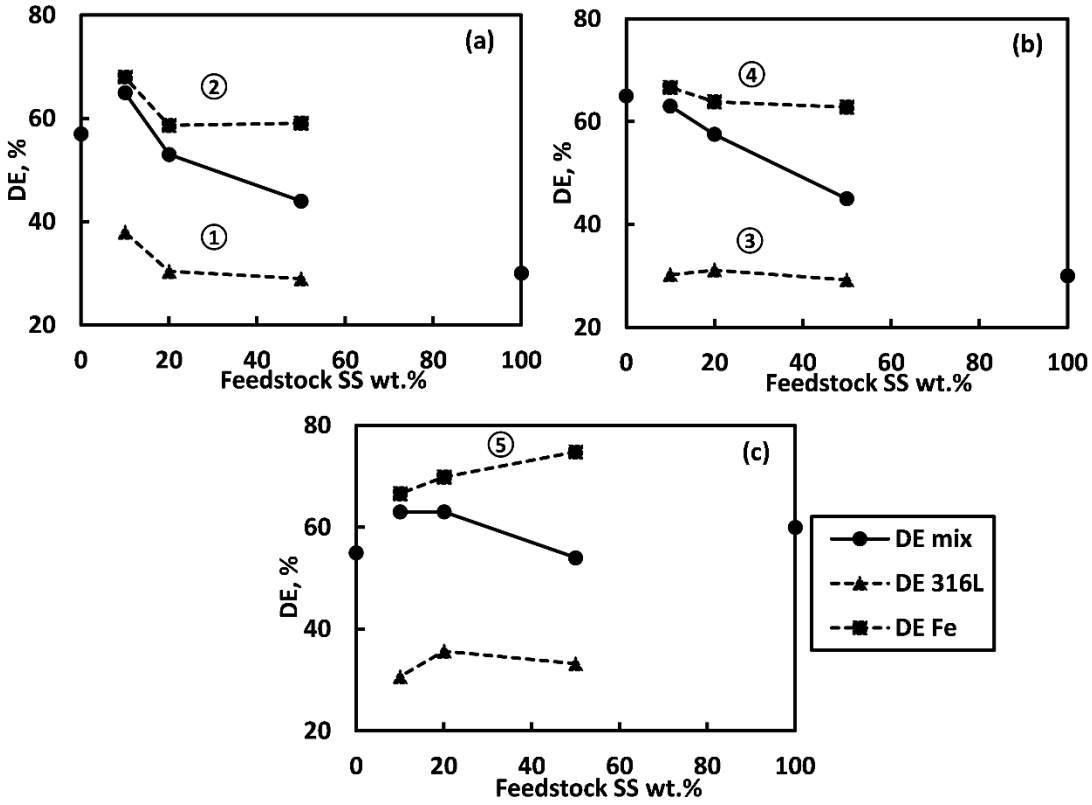

Fig. 6.5 The DE and partial DE results of different particle size combinations of Fe/316L mixtures. (a) Fe small/316L large, (b) Fe large/316L large, and (c) Fe small/316L small.

6.5 Discussion

In the cold spray literature, the effectiveness of tamping is often associated with impact energy and hardness of second component powders [6.22]. Larger particles can provide more intensive tamping effects than smaller ones due to the higher mass and thus higher impact energy of an individual particle [6.23]. In this study, 10, 20, 50 wt.% of larger powders were mixed into respective smaller ones and the mixture DEs were measured to be following the Rule of Mixtures

($DE_{Mix} = DE_{316L} \times f_{316L} + DE_{Fe} \times f_{Fe}$) (Fig. 6.3). This observation shows that simply inducing tamping provided by larger powders of the same species (i.e. large/small impacts) cannot stimulate DE in cold spray. It appears that the additions of harder powders are required to improve DE, as observed in Fig. 6.5 that illustrates adding 316L into Fe. To understand the mechanisms of the DE-improving effects, one possible explanation is associated with the fragmentations of surface oxides on Fe due to the impact of hard 316L additions, and this will benefit subsequent Fe particle deposition [6.12, 6.24]. Following this hypothesis, increasing hard 316L fractions in the initial feedstocks would increase tamping intensity; thus more Fe deposition (i.e. higher partial DE Fe) should be expected. Also, since surface oxide fragmentations are often due to deformation/flattening of particles [6.24], Fe small/316L large which exhibits largest increment in Fe flattening ratio (Table 6.4) should exhibit the most significant DE-improving effects compared with the other two combinations. However, the measured results in Fig. 6.5 show that improved DEs are particle-size-dependent and Fe small/316L small instead exhibits the most significant DE-improving effects. Therefore, it is considered that oxide fragmentations induced by the impact of hard 316L are unlikely to be the main mechanism to explain the DE characteristics of Fe/316L mixed powders with different particle size combinations.

As mentioned in Section 6.2, one effective scenario to improve the matrix powder deposition through additions of hard powders is that hard particles interact with soft particles which are depositing at the substrate surface and increase their interfacial deformation/temperature in real time [6.12]. In other words, if particle deposition is realized, then the tamping effect of subsequent particles would no longer benefit its deposition (although still increases its deformation) and might otherwise erode it to reduce DE. From this viewpoint, a close inter-particle distance during flight or a short time interval between successive particle impacts is important. Compared

with large size feedstocks, using small size feedstocks in cold spray could significantly increase the particle number density (ND) (ND ~ particle size $(D)^{-3}$) upon impact and potentially establish more SS/Fe interactions. This could explain the observations in Fig. 6.5 that the DE-improving effects only occurred in the smaller particle size mixtures, i.e. 10 wt.% SS of Fe small/316L large (line ②) and Fe small/316L small (line ⑤).

Similarly, differences in partial DE of 316L between each binary Fe/316L mixture can also be explained from the viewpoint of particle-particle interactions. In 50SS mixtures, which have the highest feedstock 316L fractions, 316L particles in the deposited coatings are mostly separated by Fe and there are a limited number of direct 316L-316L contacts (Fig. 6.4). Therefore, in all mixing compositions used in this work (10SS, 20SS, 50SS), deposition of a single 316L particle should be only associated with 316L on Fe (impacts) and possible Fe on 316L (interactions). Comparing the partial DEs of 316L in Fe small/316L large (line ①) and in Fe large/316L large (line ③) in Fig. 6.5, similar and unchanged partial DE of 316L is observed from 20 to 50 wt.% SS, which indicates that the 316L particles in both mixtures experienced the same scenario during deposition. However, in 10 wt.% SS, the partial DE of 316L in Fe small/316L large (line ①) is ~8% higher than in Fe large/316L large (line ③); this difference appears to be only explained from the perspective of Fe on 316L, i.e. particle-particle interactions. According to [6.16], in order to retain a rebounded 316L, its rebound momentum should be overcome by the subsequent incoming Fe particles, as shown in Eq. (6.2).

$$n_{Fe} m_{Fe} v_{Fe} \geq m_r v_r \tag{6.2}$$

Where, n_{Fe}, m_{Fe}, v_{Fe} are the number, mass, and velocity of a subsequent incoming Fe particle, respectively. m_r and v_r are the mass and velocity of a rebounded 316L particle. On the

right side of Eq. (6.2), the rebound velocity (v_r) of a 316L particle is normally much lower than its impact velocity [6.20] due to the plastic deformation and adhesive interactions upon impact, so retention of a rebounded 316L particle is reasonable. On the left side of Eq. (6.2), for a given powder feed rate and feedstock mixing fraction, $n_{Fe}m_{Fe}$ is constant. Compared with larger Fe powder, a mixture containing smaller Fe not only acquires a higher impact velocity (v_{Fe}) but also a much higher particle number density upon impact, which significantly enhances the probability of a particle hitting another at the substrate surface. This could explain ~8% higher DE 316L in Fe small/316L large compared with Fe large/316L large for 10 wt.% SS (Fig. 6.5). Moreover, in Fig. 6.5 (a), a similar decrease of the partial DE of Fe (line ②) is observed along with 316L (line ①) from 10 to 20 wt.% SS; this indicates that the effects of tamping and retention occur simultaneously upon impact.

From above discussion, it can be concluded that the feedstock particle size affects the occurrence of particle-particle interactions, and the improved DE of Fe/316L powders is a result of the SS/Fe interactions, i.e. tamping and retention which occur simultaneously during deposition. The simplified schematics of particle-particle interactions in different particle size combinations of low SS mixed Fe/316L powders are presented in Fig. 6.6. Note that the total volumes of particles that impact on the substrate in all three figures are kept the same. However, due to the smaller particle size in Fe small/316L large and Fe small/316L small, a much higher particle number density is realized, leading to more SS/Fe particle interactions (i.e. tamping and retention) and improved DEs relative to single component Fe. In particular, Fe small/316L small exhibits the most SS/Fe interactions, therefore, the most significant DE-improving effects are obtained (Fig. 6.5 (c)). In Fe small/316L large with higher feedstock SS contents, the large 316L particles replace small Fe and this decreases the overall particle number density. This could explain the plateaus of

partial DEs of 316L and Fe, which are observed from 20 to 50 wt.% SS in Fig. 6.5 (a), indicating no SS/Fe interactions have occurred. In Fe large/316L large, due to the low particle number density, it is considered that all particles deposit as an isolated scenario without particle-particle interactions. With increases in the feedstock SS wt.%, more poorly deposited 316L on Fe impacts [6.20, 6.21] present and its overall mixture DE monotonically reduces (Fig. 6.5 (b)).

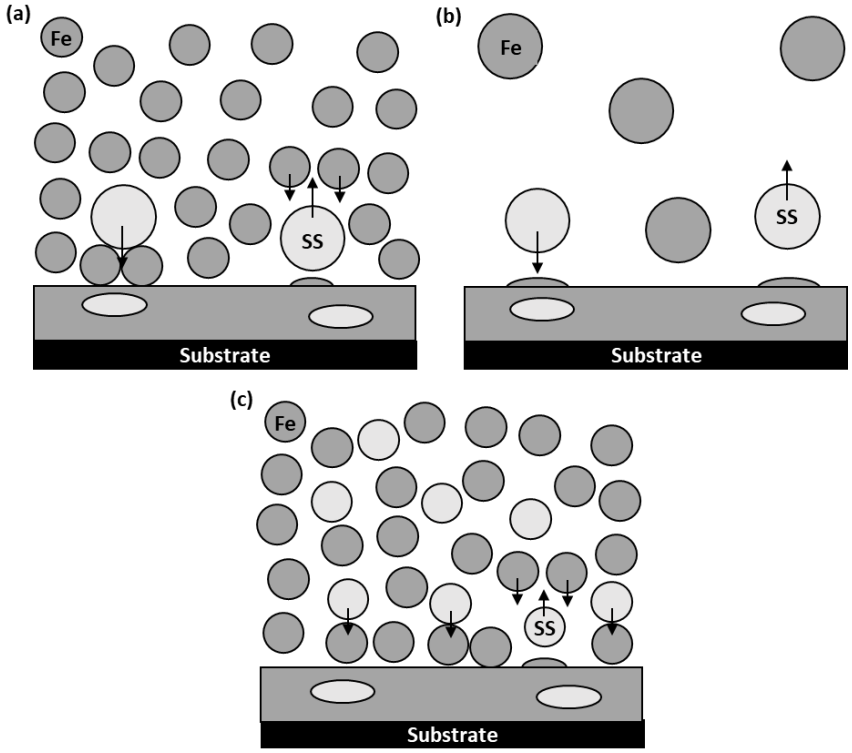

Fig. 6.6 Simplified schematics of particle-particle interactions in different particle size combinations of low SS mixed Fe/316L powders. (a) Fe small/316L large, (b) Fe large/316L large, and (c) Fe small/316L small.

Besides the particle size, there are also some considerations of the effects of process parameters on particle-particle interactions. A few process parameters were adjusted in this work based on the speculation that particle-particle interactions may be enhanced by increasing particle

number density above the substrate (by increasing feed rate and reducing gun travel speed) or reducing inter-particle in-flight separations (by reducing gas temperature/pressure). These results were shown in the supplementary file and no obvious effects on the numbers of particle-particle interactions can be identified. Thus, the feedstock particle size remains the most crucial factor to affect the particle number density upon impact and the particle-particle interactions at the substrate surface in cold spray. Based on above findings, the correlations of particle number density (ND) upon impact with regards to powder characteristics and process details can be roughly denoted as:

$$ND \sim \frac{1}{\rho \cdot D^3 \cdot L^2} \tag{6.3}$$

where ρ is the density of a powder material, D is the diameter (size) of a powder, and L is the nozzle exit diameter of a specific gun. Using Eq. (6.3) and the critical particle size for particle-particle interactions in SS/Fe mixtures in this study (ρ: 8 g/cm^3, d50: 30 μm), a relationship between the average particle size and density can be plotted to determine the occurrence of particle-particle interactions in cold spray of generic powders, as shown in Fig. 6.7. The powder characteristics from literature [6.13, 6.14, 6.16, 6.18] are also plotted for validation, and the occurrences of particle-particle interactions determined by this curve are all consistent with the respective researchers' opinions. Note that to the best of our knowledge, the nozzle exit diameters of cold spray guns used in above literature are very close to the one used in this study. This figure thus explains why in literature researchers have different opinions towards the occurrence of particle-particle interactions in cold spray.

These findings of particle-particle interactions could be industrially significant. One example is that during the fabrication of metal matrix composites (MMCs), ductile metal powders are premixed with SC powders (e.g. ceramics or hard metals) for subsequent cold spray. From the

considerations of particle-particle interactions, if only a small SC amount is needed, interactions (tamping) can be beneficial and can be realized using hard SC and smaller size mixtures. Conversely, when a high SC amount is needed to exhibit certain functionalities (e.g. ceramics for wear resistance), excessive rebounding of the SC powders during deposition might be detrimental by decelerating/deflecting subsequent particles; such interactions could be avoided by using relatively large size feedstock mixtures.

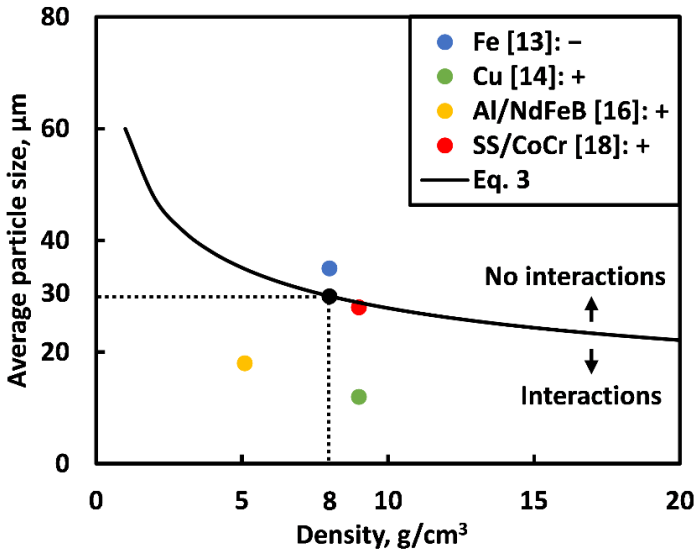

Fig. 6.7 Divisions of particle interactions using Eq. (6.3) and critical size of SS/Fe mixtures and powder characteristics plots from literature (+: interactions; -: no interactions).

These findings of particle-particle interactions could be industrially significant. One example is that during the fabrication of metal matrix composites (MMCs), ductile metal powders are premixed with SC powders (e.g. ceramics or hard metals) for subsequent cold spray. From the considerations of particle-particle interactions, if only a small SC amount is needed, interactions (tamping) can be beneficial and can be realized using hard SC and smaller size mixtures. Conversely, when a high SC amount is needed to exhibit certain functionalities (e.g. ceramics for

wear resistance), excessive rebounding of the SC powders during deposition might be detrimental by decelerating/deflecting subsequent particles; such interactions could be avoided by using relatively large size feedstock mixtures.

6.6 Conclusions

In this study, Fe and 316L powders with two different particle sizes were used as the cold spray feedstock. These powders were also premixed into different mixtures using different mixing ratios and combinations: (i) either 316L or Fe powder with large particles blended with small ones, (ii) a blend of 316L and Fe powders using three sizes combinations. Both single component and mixed powders were cold spray deposited and the deposition efficiencies (DE) are mainly studied. The main conclusions can be drawn as follows:

- Adding large powders into respective small ones for either 316L or Fe cannot further simulate DE; whereas adding hard 316L powders into soft Fe can improve DE due to SS/Fe particle interactions (i.e. tamping and retention).
- The occurrence of particle-particle interactions upon impact on the substrate is mainly affected by the feedstock particle size. Small SS/Fe mixtures (< 30 μm in this study) can exhibit particle-particle interactions due to the high particle number density upon impact.

6.7 References

[6.1] A. Moridi, S.M. Hassani-Gangaraj, M. Guagliano, M. Dao, Cold spray coating: review of material systems and future perspectives, Surf. Eng. 30 (2014) 369-395.

[6.2] T. Novoselova, P. Fox, R. Morgan, W. O'Neill, Experimental study of titanium/aluminium deposits produced by cold gas dynamic spray, Surf. Coat. Technol. 200 (2006) 2775-2783.

[6.3] H.Y. Lee, S.H. Jung, S.Y. Lee, K.H. Ko, Alloying of cold-sprayed Al-Ni composite coatings by post-annealing, Appl. Surf. Sci. 253 (2007) 3496-3502.

[6.4] H.-T. Wang, C.-J. Li, G.-J. Yang, C.-X. Li, Cold spraying of Fe/Al powder mixture: coating characteristics and influence of heat treatment on the phase structure, Appl. Surf. Sci. 255 (2008) 2538-2544.

[6.5] W. Wong, P. Vo, E. Irissou, A.N. Ryabinin, J.G. Legoux, S. Yue, Effect of particle morphology and size distribution on cold-sprayed pure titanium coatings, J. Therm. Spray Technol. 22 (2013) 1140-1153.

[6.6] H. Aydin, M. Alomair, W. Wong, P. Vo, S. Yue, Cold sprayability of mixed commercial purity Ti plus Ti6Al4V metal powders, J. Therm. Spray Technol. 26 (2017) 1-11.

[6.7] T. Piwowarczyk, M. Winnicki, A. Małachowska, A. Ambroziak, Casting defects filling by low pressure cold spraying method, Arch. Foundry Eng. 14 (2014) 109-114.

[6.8] H. Che, X. Chu, P. Vo, S. Yue, Cold spray of mixed metal powders on carbon fibre reinforced polymers, Surf. Coat. Technol. 329 (2017) 232-243.

[6.9] S. Yue, W. Wong, H. Aydin, R. Mongrain, R. Barua, P. Vo, R. Dolbec, Improving cold sprayability: mixed metal powders, Proceedings of the International Thermal Spray Conference, USA, 2015, pp. 473-478.

[6.10] R.G. Maev, V. Leshchynsky, Air gas dynamic spraying of powder mixtures: theory and application, J. Therm. Spray Technol. 15 (2006) 198-205.

[6.11] E. Irissou, J.-G. Legoux, B. Arsenault, C. Moreau, Investigation of Al-Al2O3 cold spray coating formation and properties, J. Therm. Spray Technol. 16 (2007) 661-668.

[6.12] R. Fernandez, B. Jodoin, Cold spray aluminum-alumina cermet coatings: effect of alumina content, J. Therm. Spray Technol. 27 (2018) 603-623.

[6.13] K. Ito, Y. Ichikawa, Microstructure control of cold-sprayed pure iron coatings formed using mechanically milled powder, Surf. Coat. Technol. 357 (2019) 129-139.

[6.14] J. Perry, P. Richer, B. Jodoin, E. Matte, Pin fin array heat sinks by cold spray additive manufacturing: economics of powder recycling, J. Therm. Spray Technol. (2018) 144-160.
[6.15] X.-T. Luo, Y.-K. Wei, Y. Wang, C.-J. Li, Microstructure and mechanical property of Ti and Ti6Al4V prepared by an in-situ shot peening assisted cold spraying, Mater. Des. 85 (2015) 527-533.
[6.16] P.C. King, S.H. Zahiri, M.Z. Jahedi, Rare earth/metal composite formation by cold spray, J. Therm. Spray Technol. 17 (2007) 221-227.
[6.17] S. Ahmad Alidokht, P. Vo, S. Yue, R.R. Chromik, Erosive wear behavior of cold-sprayed Ni-WC composite coating, Wear 376-377 (2017) 566-577.
[6.18] S.M. Hassani-Gangaraj, A. Moridi, M. Guagliano, Critical review of corrosion protection by cold spray coatings, Surf. Eng. 31 (2015) 803-815.
[6.19] R. Barua, Study of the Structural Properties and Control of Degradation Rate for Biodegradable Metallic Stents Using Cold Spray, PhD thesis, Department of Mechanical Engineering, McGill University, 2015.
[6.20] X. Chu, R. Chakrabarty, H. Che, L. Shang, P. Vo, J. Song, S. Yue, Investigation of the feedstock deposition behavior in a cold sprayed 316L/Fe composite coating, Surf. Coat. Technol. 337 (2018) 53-62.
[6.21] X. Chu, H. Che, P. Vo, R. Chakrabarty, B. Sun, J. Song, S. Yue, Understanding the cold spray deposition efficiencies of 316L/Fe mixed powders by performing splat tests onto as-polished coatings, Surf. Coat. Technol. 324 (2017) 353-360.
[6.22] W.Y. Li, C. Zhang, H.T. Wang, X.P. Guo, H.L. Liao, C.J. Li, C. Coddet, Significant influences of metal reactivity and oxide films at particle surfaces on coating microstructure in cold spraying, Appl. Surf. Sci. 253 (2007) 3557-3562.
[6.23] Y.-K. Wei, X.-T. Luo, C.-X. Li, C.-J. Li, Optimization of in-situ shot-peening-assisted cold spraying parameters for full corrosion protection of Mg alloy by fully dense Al-based alloy coating, J. Therm. Spray Technol. 26 (2016) 173-183.
[6.24] X.-T. Luo, M.-L. Yao, N. Ma, M. Takahashi, C.-J. Li, Deposition behavior, microstructure and mechanical properties of an in-situ micro-forging assisted cold spray enabled additively manufactured Inconel 718 alloy, Mater. Des. 155 (2018) 384-395.

Chapter 7

-

Conclusions and Future Work

7.1 Conclusions

The main objective of this work is to develop a better understanding of the cold spray characteristics of mixed 316L/Fe powders. This was conducted in the following stages: the single particle deposition behavior onto as-polished coatings and its correlation with coating deposition efficiency (DE) (**Chapter 3**); the deposition behavior and governing factors of different splat impact scenarios, i.e. 316L on 316L, 316L on Fe, Fe on 316L, Fe on Fe (**Chapter 4**); the effects of mixing powders on the cold spray characteristics of bimodal size 316L/Fe powder mixtures and the associated deposition mechanisms (**Chapter 5**); the effects of feedstock particle size on the DEs of 316L/Fe mixed powders (**Chapter 6**). Based on the findings, some generic conclusions can be summarized:

- The splat deposition behavior onto as-polished coatings can be indicative of the feedstock deposition behavior during composite coating formation. The orders of particle impacts (i.e. 316L on Fe, Fe on 316L) play an important role in final particle deposition/adhesion behavior. In the case of "soft on hard" impact scenario, due to the reluctance of the substrate deformation, the particle deformation is more effective in generating better particle deposition/adhesion. The native oxide layer on metallic powder surfaces is a significant concern of the particle deposition/adhesion. Specifically, the Fe powder with thick/porous

native oxides can more evidently inhibit the particle deposition/adhesion compared with the 316L powder whose surface oxides are thin/tenacious.

- During cold spray of bimodal size powder mixtures (hard + soft), there are various deposition mechanisms at play, e.g. mixed impact interfaces, feedstock size difference and tamping. The mixed powders should be considered as an entity instead of separate components during deposition in cold spray. The multiple subsequently incoming particles could interact and inhibit the rebounding particles during deposition (i.e. retention effect). A 50-50% large/small mixture could generate enhanced particle contact between the feedstock components and lead to reduced porosity.
- Adding a larger powder into the smaller one of the same species cannot further stimulate the DE. Adding a hard component into the soft can improve the DE due to the particle-particle interactions (i.e. tamping and retention). The occurrence of particle-particle interactions during cold spray is mainly affected by the feedstock particle size. Small size mixtures (e.g. in this study a median size < 30 μm) can exhibit particle-particle interactions due to the high particle number density. Changing the process parameters in high-pressure cold spray does not further enhance the particle-particle interactions.

7.2 Future work

- The effects of tamping by mixing 316L powders in Fe on the mechanical and functional properties (e.g. corrosion) of the cold sprayed coatings are recommended to be studied.
- Effects of heat treatment on the corrosion performances of different sizes of 316L/Fe mixed coatings are suggested to be studied.
- Quantitative evaluations of the effectiveness of tamping on deposition efficiency (DE) with regards to the characteristics of second component (SC) powders (e.g. relative hardness, density) are recommended to be studied.
- The characteristics of particle-particle interactions are suggested to be studied in more types of powder mixtures and cold spray systems.

Chapter 8

-

Contributions to Original Knowledge

To the best knowledge of the authors, the following points have been addressed for the first time, and are therefore deemed to be contributions to original knowledge:

- The single particle deposition behavior onto as-polished coatings could indicate the coating deposition behavior in cold spray.
- The sequence of particle impacts (e.g. 316L on Fe, Fe on 316L) can significantly affect the particle deposition/adhesion in cold spray.
- The mixed powders should be considered as an entity instead of separate components during cold spray deposition.
- The characteristics of particle-particle interactions in cold spray were found from deposition efficiency (DE) observations to exhibit a particle-size-dependence.

Appendix A

-

Supplementary File to Chapter 6

In this study, different commercially available Fe powders are used. In particular, Fe1 is a gas atomized powder and provided from Sandvik Osprey (Neath-Port Talbot, UK) and Fe2 is a water atomized powder and a different batch provided from Goodfellow (Cambridge, UK). SEM images and characteristics of the Fe powders are presented in Fig. A1 and Table A1, respectively.

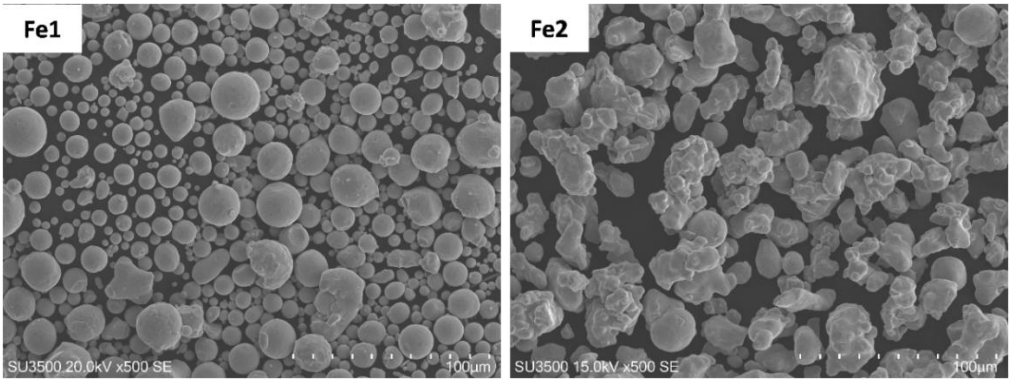

Fig. A1 SEM images of different Fe powders.

Table A1 Characteristics of different Fe powders.

Feedstock	Microhardness, $HV_{0.01}$	d50, μm
Fe1	297 ± 28	27
Fe2	115 ± 12	29

The cold spray experimental setups are the same as mentioned in the main text. The objective of this experiment is to investigate the effects of the process parameters on deposition

efficiency (DE) of a powder or relative DE between the two powders. The process details of this campaign are presented in Table A2. Note that the "Fe small" and "316 large" powders in Table A2 are the same as the ones shown in the main text.

Table A2 Process details of the cold spray campaign.

Feedstock	Gas pressure, MPa	Gas temperature, °C	Stand-off distance, mm	Gun speed, mm/s	Feed rate, g/min
20SS (Fe1/316L large)	4	700	80	300	0-30
10SS (Fe small/316L large)	3	600	80	300	30-125
Fe2, 10SS (Fe2/316L large)	3	600	80	300	40-60
	3	600	80	60	
	2	500	80	300	

The first parameter varied is the feed rate. In Section 6.3, the DE at "medium" feed rate range (20-60 g/min) has been validated to be stable (relative DE difference < 5%); thus, DE at "low" feed rate (e.g. 0-20 g/min) and "high" feed rate ranges (e.g. > 60 g/min) were mainly studied in this Section. Due to limitations of the powder feeder, generating incremental feed rate values covering both the "low" and "high" feed rate regions using a single powder is difficult. Thus, two powders with different feeding characteristics were selected to study the different interest regions and for each powder the DE at "medium" feed rate (20-60 g/min) was also recorded as a reference, as shown in Fig. A2 (a). Results show that increasing the feed rate from "low" to "medium" range (for 20SS) does not improve DE; further increase from "medium" feed rate to "high" feed rate (for 10SS) also does not increase DE except for a 10% DE reduction at very high feed rate of 122 g/min. Microhardness examination of the high feed rate coating reveals a relatively low value. This result,

combined with the reduced DE, implies that at this high feed rate the particles might have deceleration due to overloading of gas flow.

The effects of the process parameters on the relative DE between the single component Fe and mixed 10SS powders were also studied and are shown in Fig. A2 (b). The DEs of Fe and 10SS were firstly measured at the reference conditions (same as in Section 6.3) and no difference in DE between the two can be seen. Then DEs of two powders were measured at different conditions by changing one (or two) parameters at one time (i.e. 60 mm/s: reduced gun travel speed; 2 MPa, 500 °C: reduced gas temperature/pressure). These efforts were made based on speculations to enhance particle-particle interactions by increasing particle number density above the substrate (reduced gun travel speed) or reducing inter-particle in-flight separations (gas temperature/pressure) in order to obtain improved DE of 10SS compared with Fe. However, none of these efforts performed in this study can further improve DE (10SS vs Fe) and thus the numbers of SS/Fe interactions.

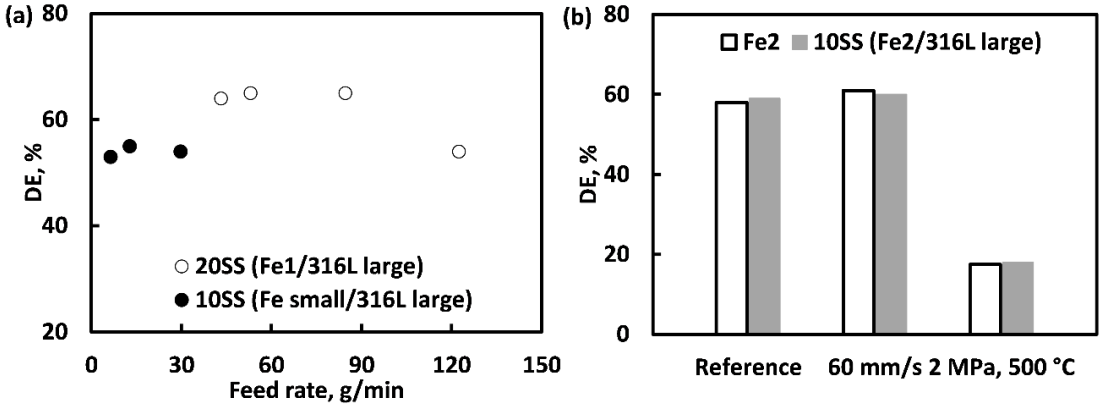

Fig. A2 (a) DEs of 20SS and 10SS mixtures at different powder feed rates; (b) DEs of Fe and 10SS at varied spray conditions. 60 mm/s: reduced gun travel speed; 2 MPa, 500 °C: reduced gas temperature/pressure.

Appendix B

-

Abstract of Unpublished Article

Title: Effects of Powder Characteristics and Mixing Powders on Cold Sprayability and Corrosion Properties of Tantalum Coatings

Abstract: Tantalum is an expensive 'exotic' metal and it is of particular interest in terms of extreme corrosion resistance and bio-compatibility. Previous studies on cold spray of tantalum show that it can be successfully deposited; whereas, limited effort has been performed to investigate and optimize powder characteristics for improved cold sprayability and corrosion properties. In this study, two spherical (P1: hard, P3: soft) and one angular (P2) tantalum powders were used as the feedstock. Two mixed powders (P1+20 wt.% P2, P1+20 wt.% P3) were also prepared and were deposited as well as the three single component powders. After cold spray, coating microstructure (as-polished and etched cross-sections, top surfaces) was characterized via optical and electron microscopy. Several industrial coating metrics, i.e. cold sprayability (porosity, deposition efficiency (DE), cohesion strength) and electrochemical corrosion properties were evaluated. Results show that: i) angular P2 powder is most preferred for industrial productions due to its lower cost and it exhibits the highest DE, corrosion resistance, and high cohesion strength than other two spherical ones (P1, P3); ii) mixing P2 and P3 powders into P1 both generate benefits and the mixed coatings exhibit much improved metrics than single component P1.